SWECLIM
SWEDISH REGIONAL CLIMATE MODELLING PROGRAMME

SMHI

No. 28, 2000

Reports Oceanography

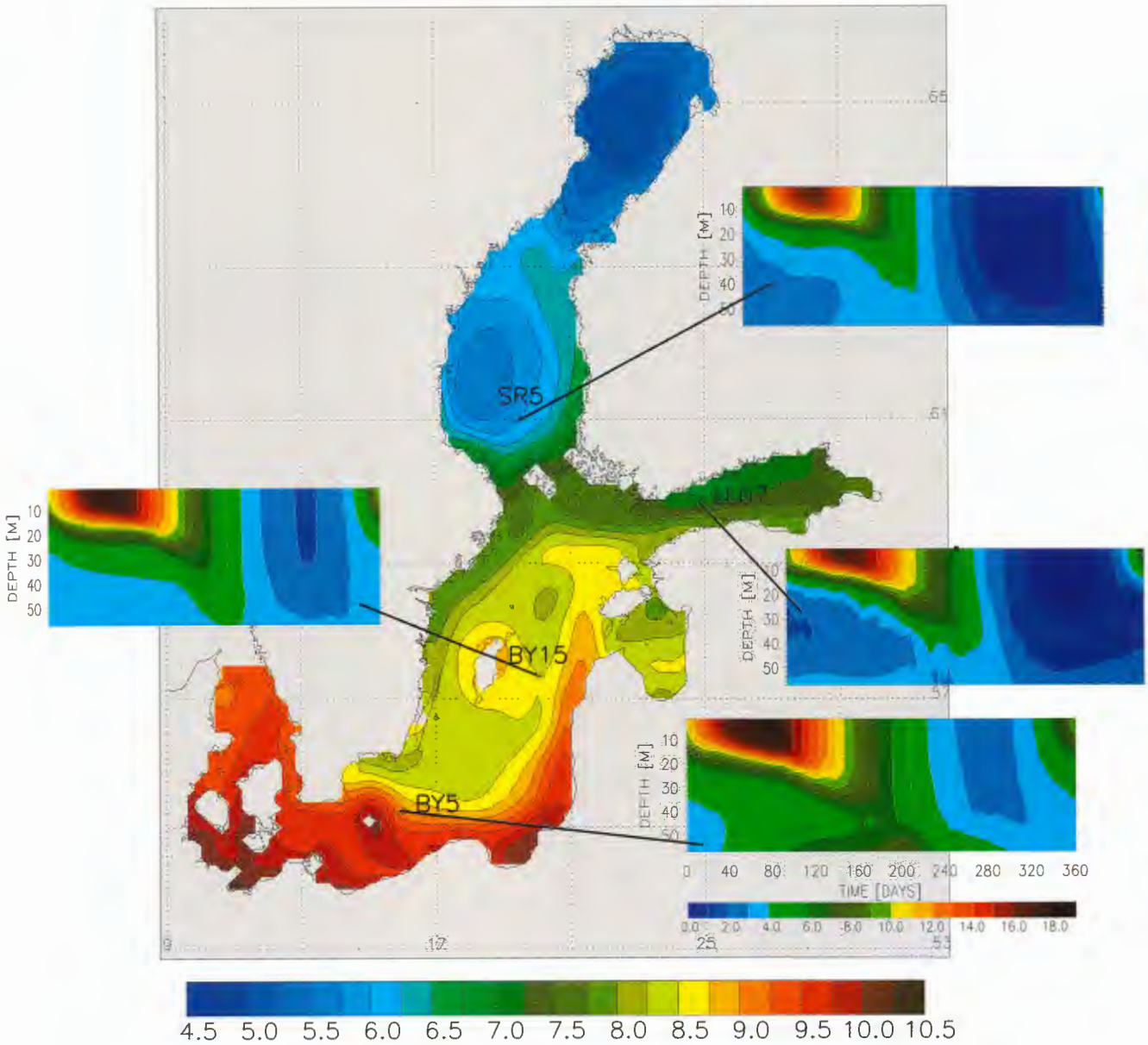

The use of the $k-\varepsilon$ turbulence model within the Rossby Centre regional ocean climate model: parameterization development and results

H.E. Markus Meier
Rossby Centre

Cover illustration: Simulated 13-year mean sea surface temperature (in ^{o}C) for the period May 1980 until May 1993 using the Rossby Centre regional ocean climate model (RCO). In addition, the 13-year mean seasonal cycles of isotherm depths (in ^{o}C) at selected monitoring positions simulated with embedded $k - \epsilon$ turbulence model are shown. These positions are from North to South SR5 in the Bothnian Sea, LL07 in the Gulf of Finland, BY15 (Gotland Deep) in the Eastern Gotland Basin and BY5 (Bornholm Deep) in the Bornholm Basin.

RO
No. 28, 2000

The use of the $k-\varepsilon$ turbulence model within the Rossby Centre regional ocean climate model: parameterization development and results

H.E. Markus Meier
Rossby Centre

Report Summary / Rapportsammanfattning

Issuing Agency/Utgivare	Report number/Publikation
Swedish Meteorological and Hydrological Institute S-601 76 NORRKÖPING Sweden	RO No. 28
	Report date/Utgivningsdatum September 2000

Author (s)/Författare

H. E. Markus Meier

Title (and Subtitle/Titel

The use of the $k-\varepsilon$ turbulence model within the Rossby Centre regional ocean climate model: parameterization development and results

Abstract/Sammandrag

As mixing plays a dominant role for the physics of an estuary like the Baltic Sea (seasonal heat storage, mixing in channels, deep water mixing), different mixing parameterizations for use in 3D Baltic Sea models are discussed and compared. For this purpose two different OGCMs of the Baltic Sea are utilized.

Within the Swedish regional climate modeling program, SWECLIM, a 3D coupled ice-ocean model for the Baltic Sea has been coupled with an improved version of the two-equation $k-\varepsilon$ turbulence model with corrected dissipation term, flux boundary conditions to include the effect of a turbulence enhanced layer due to breaking surface gravity waves and a parameterization for breaking internal waves. Results of multi-year simulations are compared with observations. The seasonal thermocline is simulated satisfactory and erosion of the halocline is avoided. Unsolved problems are discussed.

To replace the controversial equation for dissipation the performance of a hierarchy of k-models has been tested and compared with the $k-\varepsilon$ model. In addition, it is shown that the results of the mixing parameterization depend very much on the choice of the ocean model. Finally, the impact of two mixing parameterizations on Baltic Sea climate is investigated. In this case the sensitivity of mean SST, vertical temperature and salinity profiles, ice season and seasonal cycle of heat fluxes is quite large.

Key words/sök-, nyckelord

Baltic Sea, modelling, mixing parameterization, turbulence model, $k-\varepsilon$ model

Supplementary notes/Tillägg	Number of pages/Antal sidor	Language/Språk
This work is a part of the SWECLIM program.	81	English

ISSN and title/ISSN och titel

0283-1112 SMHI Reports Oceanography

Report available from/Rapporten kan köpas från:

SMHI
S-601 76 NORRKÖPING
Sweden

Contents

1 Introduction

Mixing plays a dominant role for the physics of an estuary like the Baltic Sea due to three reasons:

- the seasonal heat storage is determined by the mixed layer depth,
- mixing in the Danish Straits affects the water exchange between North and Baltic Sea,
- the longest internal timescale of the system is related to deep water mixing.

Wind stirring and cooling at the sea surface generates turbulence and a well mixed layer is formed which has in summer a depth of about 20 - 30 m and reaches in winter the permanent halocline. Stratification limits the direct influence of the atmosphere to the homogeneous upper layer. As the upper ocean heat content is determined by the depths of the well mixed layer, sea surface temperature (SST) depends very sensitive on mixing. Thus, heat fluxes at the sea surface which are functions of the air-water temperature difference are affected by mixing as well.

The Baltic Sea hydrography depends on the water exchange with the world ocean which is restricted by the narrows and sills of the Danish Straits (Fig.1) and on river runoff into the Baltic. The atmosphere forces transports through the Danish Straits with high variability in time. In the long-term mean high saline water from the Kattegat enters the Baltic proper and low saline water leaves the estuary due to the fresh water surplus. Mixing in the Danish Straits and in the western Baltic basins affects vertical current profiles in general and bottom currents in special. Thus, mixing must have an impact on total water exchange.

Diffusion controls the vertical salt flux across the halocline and causes a permanent inflow of Kattegat water into the bottom layer of the Baltic Sea. This longest time scale of the system is of the order of 30 years.

Already Welander (1974) included in his Baltic Sea model, consisting of only two boxes, two mixing coefficients, one representing entrance mixing and the other one representing deep water mixing. The timescales of his analytical solution, which describes the relaxation of the system to the equilibrium state after small perturbations, are dependent on these two mixing processes.

Due to the outlined importance of mixing for atmosphere-ocean interaction and for the climate of the Baltic Sea, different mixing parameterizations have been tested, embedded within two different OGCMs for the Baltic Sea. The first one is a regional high-resolution model of the western Baltic Sea with open boundary conditions in the Kattegat and Bornholm Basin (Meier, 1996). This model has a resolution of 1 nautical mile in horizontal and 3 m in vertical direction, respectively. Simulations with realistic initial, boundary and atmospheric forcing fields have been carried out for the BALTEX (Baltic Sea Experiment) test year 1992/93 and the results have been compared to observations. These simulations have the advantage to be performed using a high

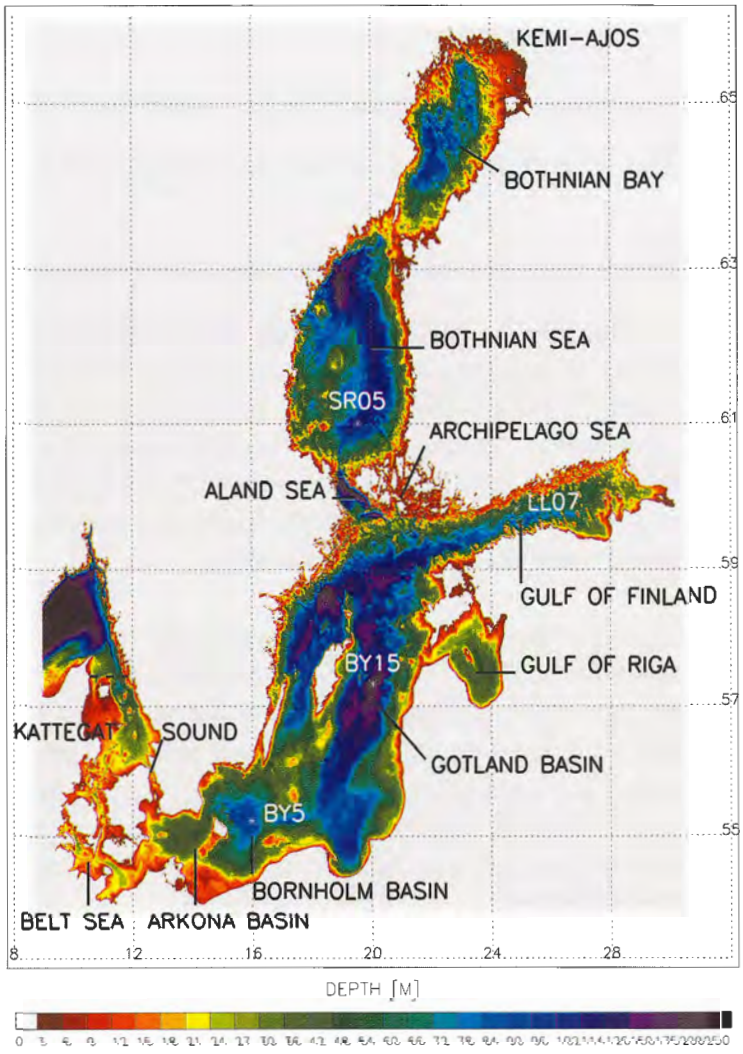

Figure 1: *Bottom topography of the Baltic Sea including Kattegat and Skagerrak (data from Seifert and Kayser, 1995). The model domain of RCO is limited with open boundaries in the northern Kattegat (dashed line). Selected monitoring positions (see text) are depicted additionally.*

resolution model grid and using forcing data of high quality. However, the model domain is restricted including only one deep basin (Bornholm Basin) and only one year could be integrated due to limited computer resources and due to the restricted data base.

To extend the model domain and to investigate also parameterizations for deep water mixing, a second 3D model has been used to perform multi-year simulations for the whole Baltic Sea. Apart from the deep water mixing aspect, long-term integrations are useful to eliminate the uncertainty of interannual variability and to reduce artificial trends as result of inaccuracies of mixed layer models, which have been tested during

one seasonal cycle only. Usually these trends show up clearly in multi-year simulations.

The second model is the Rossby Centre Ocean model (RCO), a 3D coupled ice-ocean model for the Baltic Sea, which has been developed within the Swedish regional climate modelling programme (SWECLIM) to simulate long-term changes and natural variability of the Baltic Sea (cf. Meier et al., 1999; Meier, 1999a; Meier and Faxén, 2000; Meier et al., 2000). A code adapted to massively parallel processor architectures makes it possible to overcome computational limits. So far, two horizontal resolutions (2 and 6 nautical miles) and 41 vertical levels with layer thicknesses between 3 and 12 m have been used to perform sensitivity and process studies for the period May 1980 until December 1993. RCO is started from realistic initial conditions and forced with observed atmospheric fields from the Swedish Meteorological and Hydrological Institute (SMHI) data base (Lars Meuller, pers.comm.).

In this report the investigations are focussed mainly on the widely used, so called $k-\epsilon$ model, a second-moment turbulence model, where k and ϵ denote turbulent kinetic energy (TKE) and dissipation of TKE, respectively. To introduce the $k-\epsilon$ model only four selected publications are mentioned here briefly. The pioneering work of Rodi (1980) introduces the $k-\epsilon$ model thoroughly with applications mainly in engineering and to the channel flow in Öresund. Svensson (1978) was the first to apply the $k-\epsilon$ turbulence model to a lake in Sweden (Lake Velen) and Omstedt et al. (1983) were the first to apply the $k-\epsilon$ turbulence model to the Baltic Sea for 1D process studies. Within the EU funded project BASYS (Baltic Sea System Study, 1996-1999) the 1D $k-\epsilon$ model has been embedded into the 3D regional high-resolution model of the western Baltic Sea (Meier, 1997).

The report is organized as followed: In Section 2 the two OGCMs for the Baltic Sea are described briefly. Different simplified mixed layer models are discussed with respect to Baltic Sea application in Section 3. In Section 4 the so-called standard $k-\epsilon$ turbulence model is introduced and compared to data. As a transport equation for dissipation might be questionable, a k-model with algebraic relationship for the turbulent macro length scale is developed in Section 5 which gives similar results compared to the standard $k-\epsilon$ model. New surface flux boundary conditions for turbulent kinetic energy and dissipation are discussed in Section 6. As the standard $k-\epsilon$ model underestimates mixed layer depths, a correction is tested in Section 7 based on reduced dissipation in stratified fluids. The turbulence model is further modified in Section 8 by considering more complex stability functions. Two different parameterizations for deep water mixing have been added in multi-year simulations as shown in Section 9. In Section 10 the impact of turbulence modeling under sea ice are discussed. To explore, if the performance of the embedded 1D turbulence model depends on the circulation model calculating stratification and velocity shear, the results of 1D and 3D models as well as the results of different horizontal grid resolutions in 3D models are compared in Section 11. The sensitivity of Baltic Sea climate on the mixed layer parameterization is shown in Section 12. In this comparison the results of the $k-\epsilon$ turbulence model have been compared to the widely used Richardson number dependent friction. The report ends with summary and conclusions. Figures depicted in section 3 to 6 (except

Fig.9) are drawn from results of the regional Baltic Sea model. Otherwise RCO is used.

2 The ocean circulation models

Both Baltic Sea models, utilized within this report, are based on the Bryan–Cox–Semtner model which is one of the most widely used general circulation models of the ocean (Bryan, 1969; Semtner, 1974; Cox, 1984). The conservation equations of momentum, mass, potential temperature and salinity are discretized in spherical coordinates on the Arakawa–B–grid (Mesinger and Arakawa, 1976) horizontally and in geopotential levels vertically.

The code of the regional model is based on the former GFDL (Geophysical Fluid Dynamics Laboratory, Princeton University) version with an explicit free surface (Killworth et al., 1991), whereas the climate model (RCO) is a further development of the more recent, multiprocessor-optimized version for the global ocean of the Ocean Circulation Climate Advanced Modelling Project, OCCAM (Webb et al., 1997). In the latter model a free surface is considered too.

2.1 The regional high-resolution model

For the regional model a grid resolution of 1 nautical mile (nm) in horizontal ($\Delta\varphi = 1'$, $\Delta\lambda = 2'$ with latitude φ and longitude λ) and 3 m in vertical direction has been chosen. Due to the computational burden the model domain is restricted to Kattegat, Belt Sea, Arkona Basin and Bornholm Basin (Fig.2). This implies a maximum number of 32 model layers in the center of the Bornholm Basin. Model depths are calculated from realistic bottom topography data (Seifert and Kayser, 1995).

A realistic initial temperature and salinity distribution is calculated by applying an objective analysis to measurements from October 1992. About 229 profiles are available between October 2 and November 6.

As the length of the integration period is much longer than the advective time scale for a water particle to cross the model domain, it is important to implement time and space dependent active open boundary conditions for temperature, salinity and surface elevation. Temperature and salinity values at the boundaries, in case of inflow, are prescribed by observed profiles from the BALTEX data base (Meier, 1996). In case of outflow, a modified Orlanski radiation condition is implemented (Stevens, 1990; 1991). Surface elevation as given by tide gauge data is prescribed at the boundaries. At the northern boundary hourly sea level data from Frederikshavn (Denmark) and Ringhals (Sweden) and at the eastern boundary data from Kungsholmsfort (Sweden) and Ustka (Poland) are used. The diurnal and semi-diurnal tides are removed by spectral filtering. The mean sea level of every record is subtracted and replaced by geodetic results according to Ekman and Mäkinen (1996).

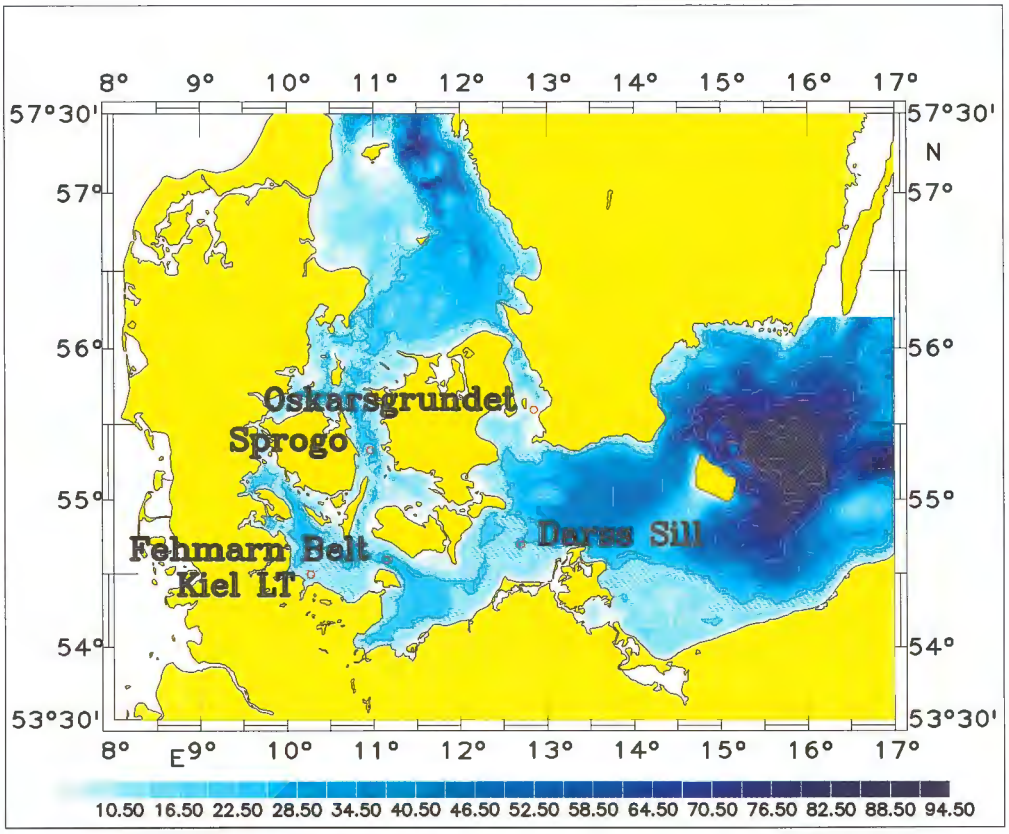

Figure 2: *Model domain of the regional western Baltic Sea model with bottom topography (data from Seifert and Kayser, 1995).*

The regional model is forced by 6 hourly wind fields and surface pressure gradients from the German weather forecast model for Europe. The wind stress is calculated using the drag coefficient from Large and Pond (1981). Based on the synoptical data, sea surface temperature charts were calculated (Bumke 1995, pers. comm.). The temperature of the first model layer is restored to these maps with a time constant of 6 hours. Precipitation and evaporation are neglected, which seems to be a good approximation to the western Baltic Sea. By using in situ measurements instead of climatological data for the initial fields and the heat flux, the results of the model are improved.

Density in the regional model is calculated from the equation of state given by Millero and Kremling (1976).

According to Cox (1984), a second order law for bottom friction is used, parameterizing the bottom drag due to the roughness of topography, which is not resolved by the model. As the accumulated transport into the Baltic Sea during the major inflow event in January 1993 is known quite well from observations (288 km^3 calculated by Jakobsen (1995) or 310 km^3 estimated by Matthäus et al. (1993)), the coefficient of the bottom friction c_b has been adjusted to yield these values ($c_b = 0.5 \times 10^{-3}$).

Horizontal eddy viscosity A_M and diffusivity A_T are used to parameterize subscale processes not resolved by the model grid. A biharmonic law is used because the high resolution of the model makes scale selective friction necessary ($A_M = -1.3 \times 10^{16}\, cm^4 s^{-1}$ and $A_T = -0.65 \times 10^{16} cm^4 s^{-1}$). Under calm and moderate wind conditions the contributions from the horizontal friction in the tracer and momentum equations are rather small compared to other terms. However, in case of strong forcing (e.g., during January 1993) horizontal friction is important to stabilize the numerical solution. In this model, higher resolution implies steeper topographic slopes which were found to be responsible for an increased amount of grid-scale noise (Beckmann et al., 1994). To reduce this noise higher explicit smoothing has to be prescribed on grid-scale. However, on larger scales friction should be smaller in order to not suppress eddy dynamics and the development of fronts. As frictional zones are necessary to stabilize the results at the open boundaries, we add to the biharmonic friction a common Laplacian operator. The harmonic viscosity and diffusivity in the inner model domain are small compared to the corresponding biharmonic terms and are increasing towards the open boundaries. Experiments with biharmonic boundary zones got instable.

2.2 The coupled ice-ocean climate model

OCCAM includes improved vertical and horizontal advection schemes (Webb, 1995; Webb et al., 1998), harmonic horizontal viscosity and diffusivity and a third order polynomial approximation (Bryan and Cox, 1972) of the equation of state as set by the Joint Panel on Oceanographic Tables and Standards (UNESCO, 1981) and as described by Gill (1982).

RCO is a further development of the OCCAM code applied to the Baltic Sea. Here, RCO version 1.3 is used with improved heat flux package, mixing parameterization and snow ice model (Meier et al., 2000).

The model depths are based on the same topography data from Seifert and Kayser (1995) as the regional model which are depicted in Fig.1. RCO is making use of 41 levels with layer thicknesses from 3 m close to the surface to 12 m near the bottom. The maximum depth in RCO is 250 m. Two different horizontal resolutions are used: 2 and 6 nm corresponding to $\Delta\varphi = 2'$, $\Delta\lambda = 4'$ and $\Delta\varphi = 6'$, $\Delta\lambda = 12'$, respectively.

For the calculation of initial temperature and salinity fields the model domain has been divided into 14 boxes filled with horizontal homogeneous profiles. The borders have been chosen according to topographic features which determine the hydrography of the sub-basins. Profiles from the SHARK (Svenskt HavsARKiv) data base (Swedish Oceanographic Data Centre at SMHI, http://www.smhi.se/sgn0102/nodc/nodc.html) have been selected to compile initial conditions for May 26 1980. A spin-up period of 3 months is sufficient to smooth out artificial horizontal gradients from the initialization procedure and to turn in basin wide volume changes correctly. This initialization method with emphasis on a realistic vertical structure gives more adequate results than

starting from too smooth 3D fields if not enough data are available.

Open boundary conditions as developed by Stevens (1990, 1991) for the GFDL version of the Bryan–Cox–Semtner model and as used within the regional model has been re–introduced because the model domain of RCO is limited (contrary to the global OCCAM) with open boundaries in the northern Kattegat (Fig.1). Due to the lack of data resolving the northern Kattegat hydrography mean temperature and salinity profiles from observations at the open sea monitoring station P2 in the northern Kattegat ($57^o N\, 52'$, $11^o E\, 18'$) are used as open boundary conditions.

Standard bulk formulae are used to calculate sea surface fluxes of wind stress, sensible and latent heat, longwave and shortwave incoming radiation (see Appendix A for the open water case and Appendix B for the sea ice case). The albedo for the open water surface is calculated from Fresnel's formula. The earlier used heat flux package by Meier et al. (1999), which followed mainly Omstedt and Nyberg (1995), resulted systematically in too low winter SSTs over the whole model domain and has been replaced consequently.

The atmospheric forcing data are three hourly maps for sea level pressure, geostrophic wind components, 2 m air temperature, 2 m relative humidity and total cloud cover from the SMHI data base (Lars Meuller, pers. comm.). In addition, at 06 and 18 UTC also 12 hourly accumulated precipitation is used. If no precipitation data are available, climatological areal estimates (1951-1970) from Dahlström (1986) have been used. The SMHI data base is available from 1979 onwards and is updated regularly. The horizontal resolution is one degree and the maps cover the latitudinal range $49.5^o N - 71.5^o N$ and the longitudinal range $7.5^o E - 39.5^o E$.

As only geostrophic wind fields are available a boundary layer parameterization has to be used to calculate wind speeds in 10 m height. According to Karger (1995) and Bumke (1997, pers.comm.) the dependence of the reduction coefficient from the distance to the coast is taken into account.

The river runoff data have been taken from the BALTEX Hydrological Data Centre at SMHI. The monthly data do not only represent the inflow by major rivers, but the runoff through coastal segments including also estimated smaller runoff ways (Bergström and Carlsson, 1994). In RCO the 29 most important coastal segments are considered. Contrary to Meier et al. (1999), river volume and freshwater transports are considered via surface flux boundary conditions. It is necessary to smooth the freshwater signal over river mouth surrounding grid boxes.

The ocean model in RCO is coupled with a Hibler-type (Hibler, 1979) two-level (open water and ice) dynamic-thermodynamic sea ice model. An extension of the widely used viscous-plastic rheology with an elastic component (Hunke and Dukowicz, 1997) leads to a fully explicit numerical scheme that improves computational efficiency, particularly on high resolution grids, and adapts easily to parallel computer architectures. A first version of the sea ice model of the OCCAM project has been adopted and signifi-

cantly modified to simulate seasonal ice in the Baltic (Meier et al., 1999). Within each time step, the dynamic component needs to be subcycled several times to damp elastic waves. As described in Hunke and Zhang (1999), the elastic term initially makes a prediction for the ice stress, which is then 'corrected' towards the viscous-plastic solution by means of subcycling. By choosing the number of subcycles (N), a compromise has to be made between an energetic solution that quickly adjust during rapidly changing forcing conditions (small N) and a solution which not significantly differs from the viscous-plastic one on longer timescales (high N). The equations of the ice model are discretized on the same Arakawa–B–grid used for the ocean.

The ice thermodynamics are based on Semtner's layer models (Semtner, 1976) for thick ice/snow (multiple layers) and thin ice/snow ('zero'-layer) using characteristic discrimination thicknesses for ice and snow. In RCO thick ice consists of one or two ice layers and thick snow consists of one snow layer. The reason for the discrimination between thick and thin ice/snow is numerical stability. The 'zero'-layer models for ice and snow are based on simple heat budgets.

Snow is converted to snow ice if flooding as calculated from Archimedes' law occurs. According to Saloranta (2000) negative freeboard conditions in the Baltic fast ice area last up to months. Hence, a negative freeboard of up to 5 cm is allowed.

For a more detailed model description of RCO the reader is referred to Meier et al. (1999) and Meier et al. (2000).

3 Comparison of different mixed layer models

In a first step two 'local' parameterizations of mixing in 3D models have been studied, the Richardson number dependent friction according to Pacanowski and Philander (1981) and the scheme according to Kochergin (1987).

The first scheme has been developed based on observations by Munk and Anderson (1948) and has been applied within a 3D circulation model for the tropical Atlantic by Pacanowski and Philander (1981). Within Baltic Sea models it has been employed for example by Lehmann (1992, 1995), Meier and Krauss (1994) or Schmidt et al. (1998). Using an empirical function eddy viscosity ν_t and diffusivity ν_t' are related to the gradient Richardson number Ri according to

$$\nu_t = \frac{\nu_{t,0}}{\left(1+\frac{Ri}{Ri_0}\right)^n} + \nu_{t,min} \quad \text{with} \quad Ri = \frac{N^2}{\left(\frac{\partial u}{\partial z}\right)^2 + \left(\frac{\partial v}{\partial z}\right)^2}. \tag{1}$$

N is the Brunt-Väisälä frequency

$$N^2 = -\frac{g}{\rho_0}\frac{\partial \rho}{\partial z}, \tag{2}$$

and $\nu_{t,0}$, $\nu_{t,min}$, n and Ri_0 are constants which have to be fitted to available data. The vertical coordinate z is positive upward and zero at the sea surface. u and v are horizontal velocity components, g is acceleration of gravity and ρ_0 is a reference density of water. A corresponding second equation is used for ν_t'. Here, the values in Tab.1 are used for positive Richardson numbers.

	$\nu_{t,0}$ $(cm^2\,s^{-1})$	$\nu_{t,min}$ $(cm^2\,s^{-1})$	n	Ri_0
ν_t	175	1	2/3	0.1
ν_t'	20	0.01	3/2	0.1

Table 1: *Constants of the Richardson number dependent mixing parameterization.*

In case of negative Richardson numbers, eddy viscosity and diffusivity are set to the maximum values, i.e., $\nu_t = 175\,cm^2\,s^{-1}$ and $\nu_t' = 20\,cm^2\,s^{-1}$. Results of the Richardson number dependent parameterization are shown in Figures 3 and 4. Mixed layer depths are underestimated systematically compared to observations and compared to more realistic results of a second-order moment turbulent closure model, the standard $k-\epsilon$ model, which is presented in the next section. More results of the Richardson number dependent parameterization are discussed with respect to sensitivity of the Baltic Sea climate in Section 12.

The mixing scheme from Kochergin (1987) is based on the reduced TKE equation without advection and diffusion and an empirical relation for the turbulent length scale. It is assumed that the length scale is proportional to the thickness of the mixed layer which is calculated diagnosticly (cf. Pohlmann, 1996). Kochergin's scheme has been used for the Baltic Sea for example by Schrum et al. (2000) within the Hamburg Shelf Sea Model, HAMSOM. The results of this approach depend very much on the choice of the characteristic length scale. As the assumption that the length scale is proportional to the mixed layer thickness within the whole water column is not valid, an alternative scheme is derived in Section 5 using the distance to the sea surface or bottom to calculate the turbulent length scale. Mixed layer depths calculated with this modified Kochergin scheme are underestimated as with the Richardson number dependent parameterization because both local schemes neglect the diffusion of TKE. To proof the last statement an experiment with the standard $k-\epsilon$ model without diffusion of TKE and dissipation has been performed with the result that mixed layer depths are underestimated as well.

In a second step a reduced Kraus-Turner type model (Niiler and Kraus, 1977) has been embedded into the regional Baltic Sea model. The change of potential energy PE within the water column, which is available for mixing, is calculated directly from the supplied wind work at the sea surface:

$$-\frac{\partial PE}{\partial t} = m_0\, u_\star^3 \tag{3}$$

with the friction velocity in the ocean $u_\star$. (3) is derived from the vertical integrated TKE equation (cf. Dengg, 1995; Meier, 1996). Dissipation within the mixed layer is

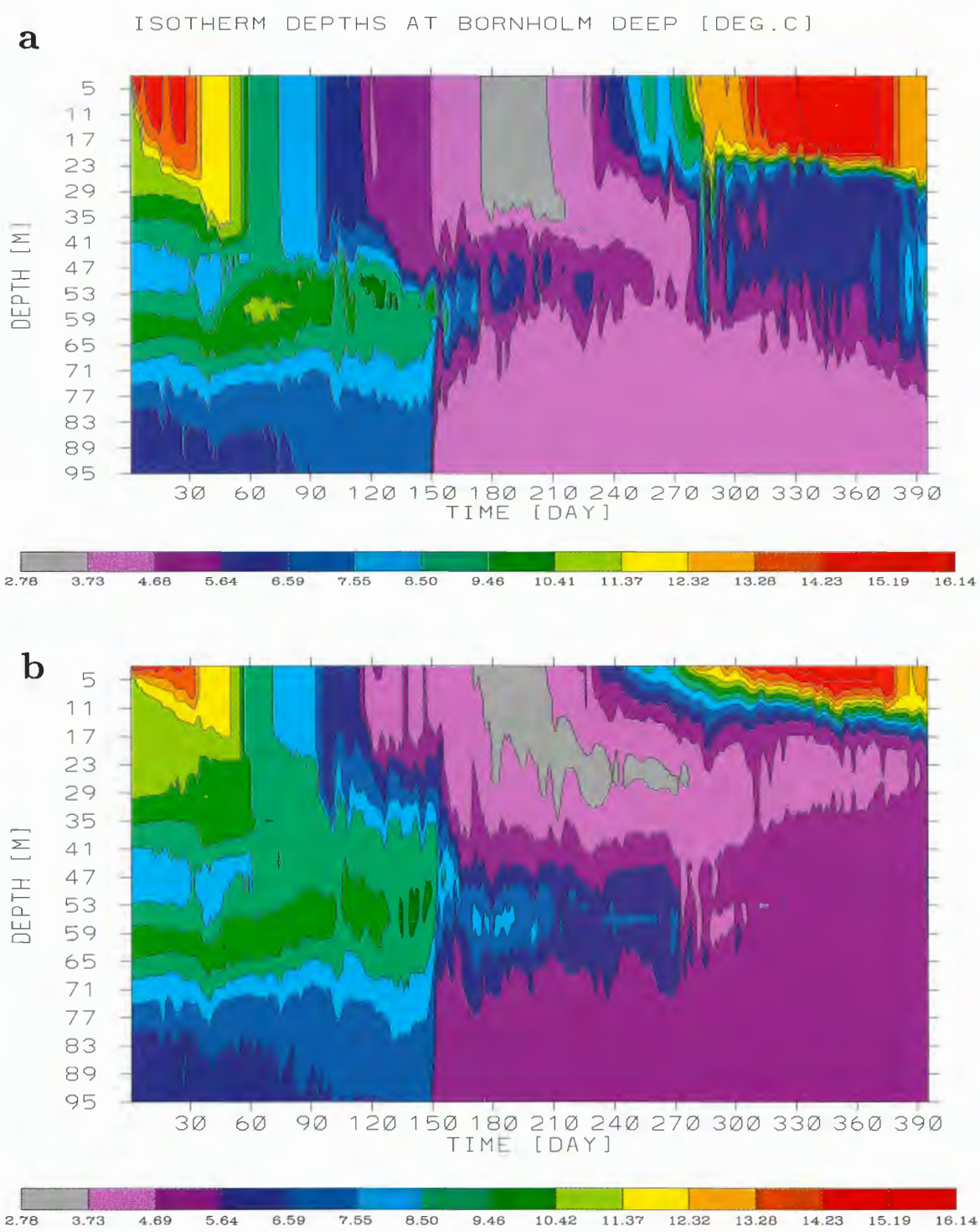

Figure 3: *Isotherm depths (in °C) from September 1992 until September 1993 at Bornholm Deep (BY5): $k-\epsilon$ turbulence model (a), Richardson number dependent friction (b).*

considered by using the Ekman length scale λ as decay length (Wells, 1979):

$$m_0 = m\, e^{-\frac{h}{\lambda}} \quad \text{with} \quad m = 4.2,\ \lambda = 20\, m\,. \tag{4}$$

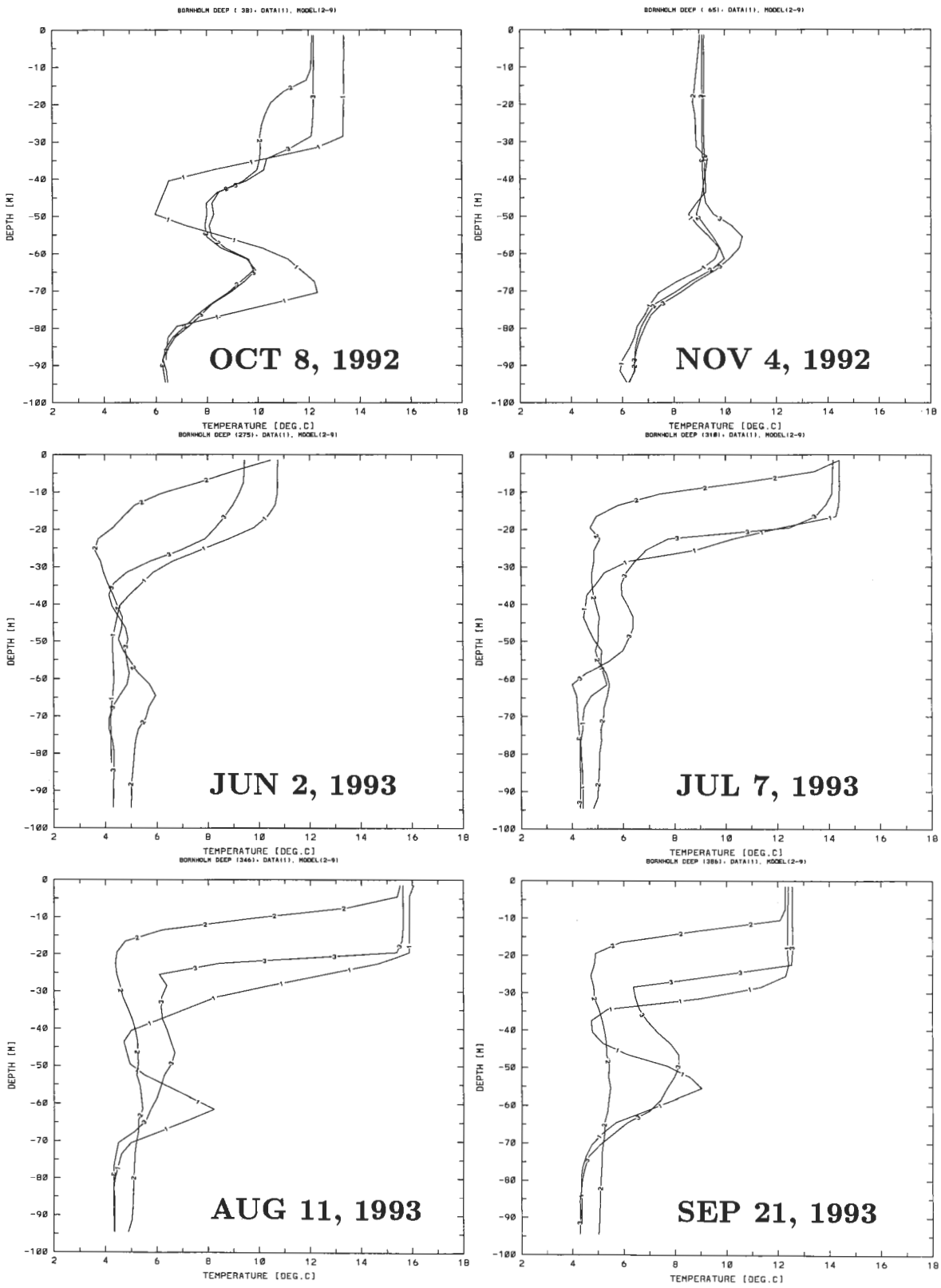

Figure 4: *Selected temperature profiles at Bornholm Deep: (1) observations, (2) Richardson number dependent friction, (3) $k-\epsilon$ turbulence model.*

h is the depth of the mixed layer. An overview about other approaches is given by Gaspar (1988). The simulations lead to surface mixed layers which are too homogeneous (Meier, 1996). In addition, the turbulent bottom layer is missing completely and the problem whether momentum should be mixed as tracers or not can not be solved satisfactory. In fact, these results are not surprising because of the philosophy of vertical integrated slab models. As the Baltic is a quite shallow sea with a mean depth of 56 m, surface and bottom mixed layer may overlap and may affect the whole water column as shown in Figure 5. In the two records TKE calculated with the standard $k-\epsilon$ model is depicted at two different sites, i.e., Bornholm Deep (BY5) in the Bornholm Basin with a water depth of about 100 m (Fig.1) and Sprogø in the Great Belt with a water depth of about 20 m (Fig.2). In the deeper Bornholm Basin the turbulent bottom layer is much thinner than the turbulent surface layer which extends in winter time down to about 50 m water depth. Contrary, turbulent surface and bottom layer overlap at Sprogø during strong wind events. Thus, transports through the Danish Straits are affected by mixing. In coastal waters mixed layer models are needed which are able to simulate turbulent properties of the whole water column correctly. This is impossible with the reduced Kraus-Turner type model.

In a third step a turbulence model has been tested consisting of the prognostic equation for TKE and a diagnostic equation for the turbulent length scale (k-model) according to Gaspar et al. (1990). The length scale is calculated from the square root of TKE divided by the Brunt-Väisälä frequency. Again the mixed layer depth is underestimated so that the vertical diffusion of TKE has to be enhanced unphysically to get adequate results (see Blanke and Delecluse, 1993; Meier, 1996). The reason for the underestimation in the untuned model version is that the model parameters in the TKE equation as used by Gaspar et al. (1990) have values resulting in too high dissipation and too low mixing coefficients. In addition, vertical shear of velocity is not included into the length scale formulation, although it is important as shown in Section 5. In that section an improved approach for the turbulent length scale is derived which gives similar results compared to the standard $k-\epsilon$ model with realistic mixed layer depths. That means, more complex two-equation turbulence models are not necessarily preferable to k-models. If model parameters and length scales are chosen correctly, also k-models can perform well.

Simplified mixing parameterizations as discussed in this section have serious shortcomings and can not predict the seasonal thermocline in 3D circulation models of the Baltic Sea accurately. Thus, a two-equation turbulence model, the $k-\epsilon$ model, is tested in the next section.

4 The standard $k-\epsilon$ turbulence model

In this section the so-called standard $k-\epsilon$ turbulence model is presented. As shown by Baumert and Peters (2000), the two commonly used two-equation turbulence closures, the $k-\epsilon$ (Svensson, 1978; Rodi, 1980) and the Mellor-Yamada level 2.5 model (Mellor

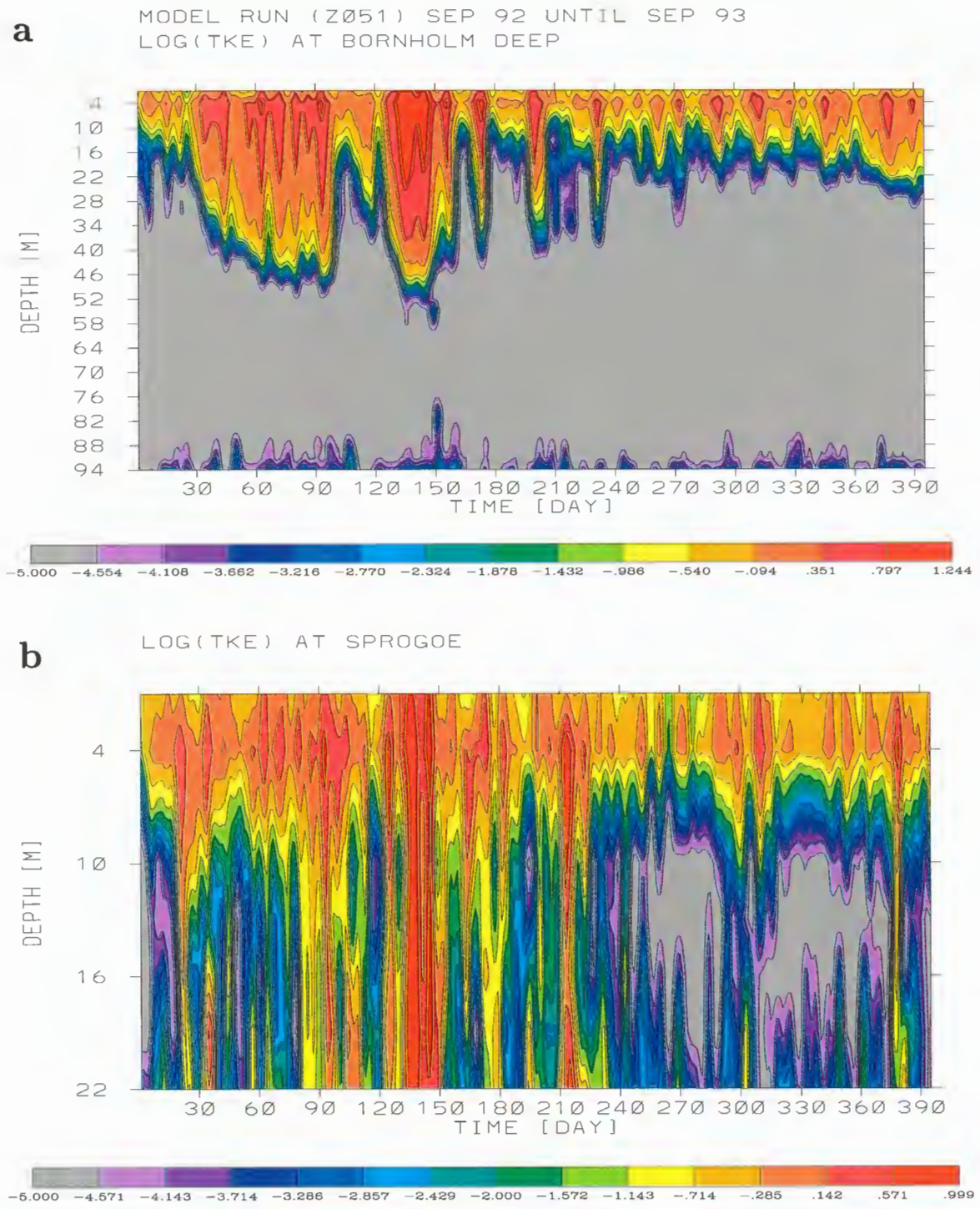

Figure 5: *Depths of logarithmic smoothed turbulent kinetic energy isolines calculated with the standard $k-\epsilon$ model from September 1992 until September 1993: (a) Bornholm Deep, (b) Sprogø/Great Belt.*

and Yamada, 1974; 1982), can be written in a joint form with different parameters. Burchard and Petersen (1999) have shown that the two model types perform similarly. In both Baltic Sea models discussed here, the regional high-resolution model and RCO,

the $k-\epsilon$ model is embedded, i.e., two prognostic equations for TKE and for dissipation of TKE have to be solved at every grid point of the 3D model additionally:

$$\frac{\partial k}{\partial t} - \frac{\partial}{\partial z}\left(\frac{\nu_t}{\sigma_k}\frac{\partial k}{\partial z}\right) = P + G - \epsilon\,, \tag{5}$$

$$\frac{\partial \epsilon}{\partial t} - \frac{\partial}{\partial z}\left(\frac{\nu_t}{\sigma_\epsilon}\frac{\partial \epsilon}{\partial z}\right) = c_{\epsilon 1}\,\frac{\epsilon}{k}\,(P + c_{\epsilon 3}\,G) - c_{\epsilon 2}\,\frac{\epsilon^2}{k}\,, \tag{6}$$

$$\text{with} \quad P = \nu_t\left[\left(\frac{\partial u}{\partial z}\right)^2 + \left(\frac{\partial v}{\partial z}\right)^2\right], \quad G = -\frac{\nu_t}{\sigma_t}\,N^2\,, \tag{7}$$

$$\nu_t = c_\mu\,\frac{k^2}{\epsilon}\,. \tag{8}$$

Here, k denotes TKE, ϵ dissipation of TKE and t time. The constants c_μ, $c_{\epsilon 1}$, $c_{\epsilon 2}$, $c_{\epsilon 3}$, σ_k and σ_ϵ are given in Table 2 according to Rodi (1980).

c_μ	$c_{\epsilon 1}$	$c_{\epsilon 2}$	$c_{\epsilon 3}$	σ_k	σ_ϵ
0.09	1.44	1.92	0/1	1	1.3

Table 2: *Constants of the $k-\epsilon$ model (Rodi, 1980).*

In case of unstable stratification the constant $c_{\epsilon 3}$ is set equal to 1 to ensure complete mixing between adjacent grid boxes. Otherwise $c_{\epsilon 3}$ is zero.

The turbulence model gives no information about the turbulent Prandtl number σ_t so that an empirical formula has to be used to complete the mixing scheme. In several experiments the best results are obtained using a Richardson number dependent Prandtl number (Blanke and Delecluse, 1993):

$$\sigma_t = \begin{cases} 1 & : \quad Ri \le 0.2 \\ 5\,Ri & : \quad 0.2 < Ri \le 2 \\ 10 & : \quad 2 < Ri \end{cases}\,. \tag{9}$$

With (9) diffusivity of tracers is calculated according to $\nu_t' = \nu_t/\sigma_t$. Other approaches for the turbulent Prandtl number have been tested as well, e.g., the empirical formula from Munk and Anderson (1948) which has been used by Burchard and Baumert (1995) in their standard version of the $k-\epsilon$ model. Here, this approach results in shallower mixed layer depths during early summer than those calculated with the Richardson number dependent Prandtl number (not shown). Omstedt et al. (1983) used a constant Prandtl number equal to 1.0. In Figures 6 and 7 temperature and salinity simulated at Bornholm Deep employing constant and Richardson number dependent Prandtl numbers are compared. The temperature evolution looks rather similar in both experiments (Fig.6) but the halocline is eroded much stronger with constant Prandtl number (Fig.7) because diffusivities are 10 times larger if $Ri > 2$ than in case of using (9). Thus, (9) is used for the standard $k-\epsilon$ model.

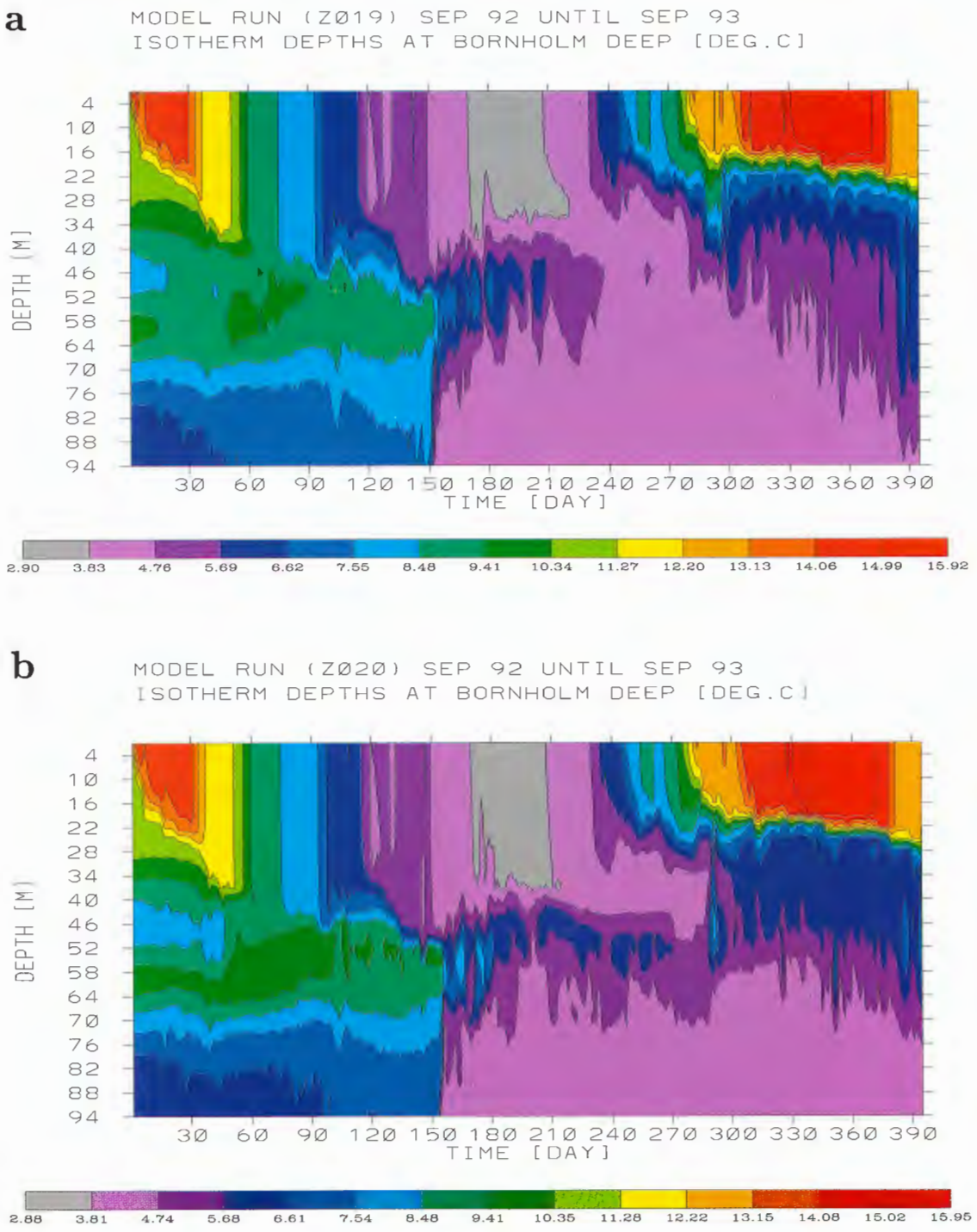

Figure 6: *Isotherm depths (in °C) from September 1992 until September 1993 at Bornholm Deep: (a) constant Prandtl number ($\sigma_t = 1$) and (b) Richardson number dependent Prandtl number (Blanke and Delecluse, 1993; cf. Equation 9).*

Additional heating of the water column occurs due to penetration of shortwave radiation, which can not be neglected and has to be considered too because it is not part of the turbulence model. Conservation of potential temperature T is given in the

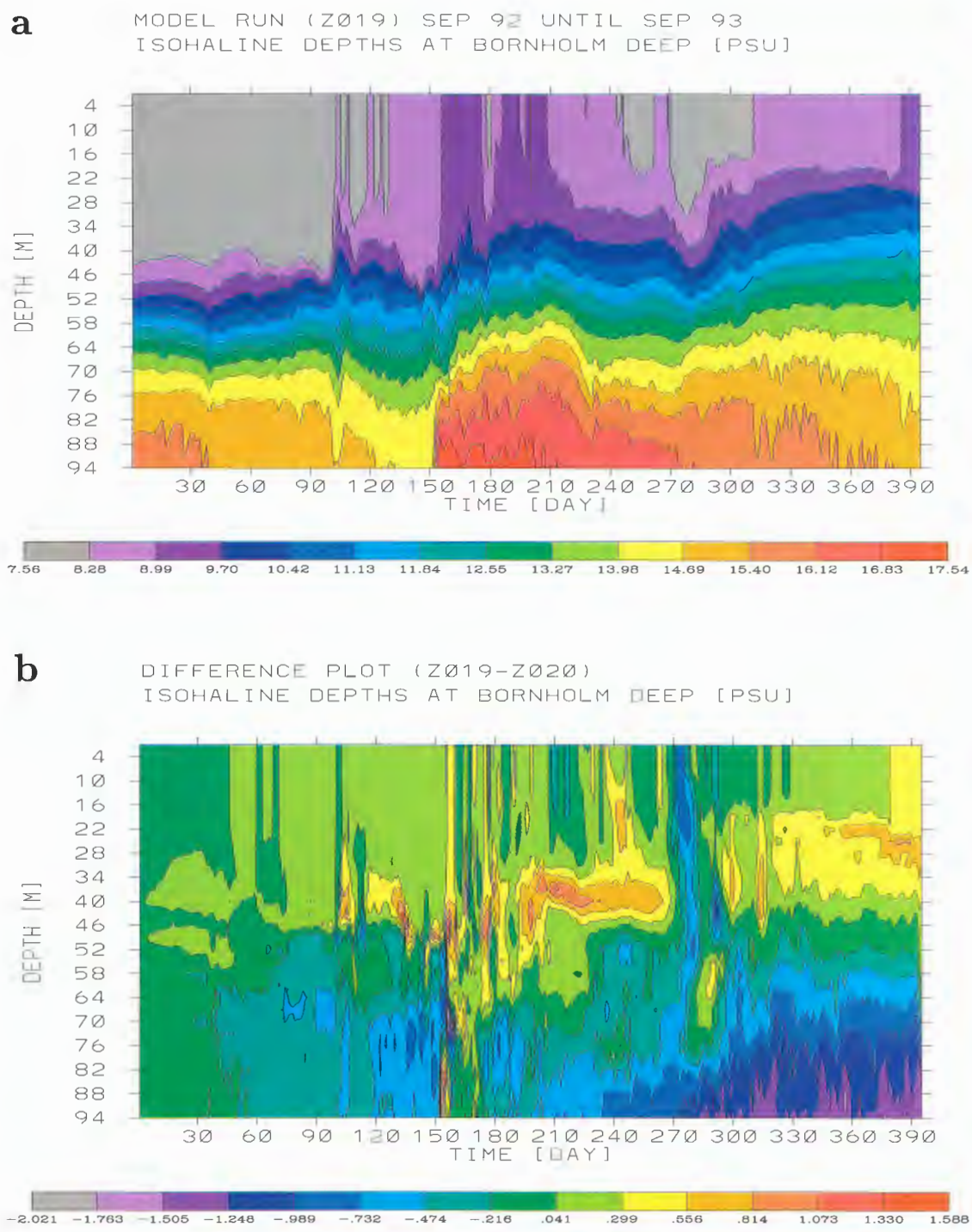

Figure 7: *Isohaline depths (in psu) from September 1992 until September 1993 at Bornholm Deep: (a) constant Prandtl number ($\sigma_t = 1$) and (b) difference between simulations with constant Prandtl number and Richardson number dependent Prandtl number (Blanke and Delecluse, 1993; cf. Equation 9).*

circulation model by

$$\frac{\partial T}{\partial t} + \Gamma(T) = \frac{\partial}{\partial z}\left(\frac{\nu_t}{\sigma_t}(z)\,\frac{\partial T}{\partial z}\right) + A_T\,\nabla^2 T + \frac{1}{\rho_0\,c_{pw}}\,\frac{\partial I}{\partial z} \qquad (10)$$

with the advection operator

$$\Gamma(T) = \frac{1}{R\cos\phi}\left[\frac{\partial}{\partial\lambda}(uT) + \frac{\partial}{\partial\phi}(vT\cos\phi)\right] + \frac{\partial}{\partial z}(wT)\,, \tag{11}$$

earth radius R, specific heat capacity of water c_{pw}, horizontal austausch coefficient A_T and solar insolation I. The divergence of absorbed intensity of the penetrated shortwave radiation is heating the water column. The solar intensity is parameterized according to Paulson and Simpson (1977) with two extinction lengths

$$I = Q_{SW}\left[R_{SW}\,e^{\frac{z}{\zeta_1}} + (1 - R_{SW})\,e^{\frac{z}{\zeta_2}}\right] \tag{12}$$

with $R_{SW} = 0.64$, $\zeta_1 = 1.78\,m$ and $\zeta_2 = 3.26\,m$. Q_{SW} is the shortwave energy flux. Usually optical water types are classified according to Jerlov (1968) but not very detailed information is available for the Baltic Sea. Jerlov classified the Skagerrak water as coastal water type 1 and the Baltic proper as coastal water type 3 without giving the corresponding extinction lengths. Hence, climatology data from Dera (1992, see his Tab. 5.3.1) has been used to optimize the unknown constant R_{SW} and the extinction lengths ζ_1 and ζ_2 utilizing a least-squares fit. The available data are average monthly means of solar energy over the entire spectrum reaching particular depths in the southern Baltic. The optimization procedure has been done as described by Paulson and Simpson (1977). For comparison, the most turbid optical water type III for oceans according to Jerlov (1968) uses the values $R_{SW} = 0.78$, $\zeta_1 = 1.4\,m$ and $\zeta_2 = 7.9\,m$.

The impact of solar insolation is illustrated in Figure 8. Shown is the temperature difference between two simulations with and without penetrating short wave radiation. Warming of about $1 - 2°C$ occurs in 10 to 20 m depth at Bornholm Deep during summer. The difference is zero at the sea surface because simulated sea surface temperatures are restored in both cases towards observed SST maps with a time constant of 6 hours as mentioned in Section 2.

Results of the standard $k - \epsilon$ model are compared to temperature and salinity profiles with satisfactory agreement. In Figure 4 selected temperature profiles at Bornholm Deep are shown. Especially in summer the seasonal thermocline is simulated correctly whereas the Richardson number dependent parameterization underestimates mixed layer depths drastically. Hence, the successful coupling of the turbulence model with the circulation model is regarded as important progress in 3D Baltic Sea modeling. In autumn the standard $k - \epsilon$ model shows a tendency to overestimate temperature gradients within the thermocline. The differences between standard $k - \epsilon$ model and Richardson number dependent friction are smallest in winter.

In the following a list of problems of the standard $k - \epsilon$ model are presented summarizing the author's experience with the $k - \epsilon$ model. Some of the problems have been solved yet, others not. Improvements of the standard $k - \epsilon$ model are discussed in the following sections.

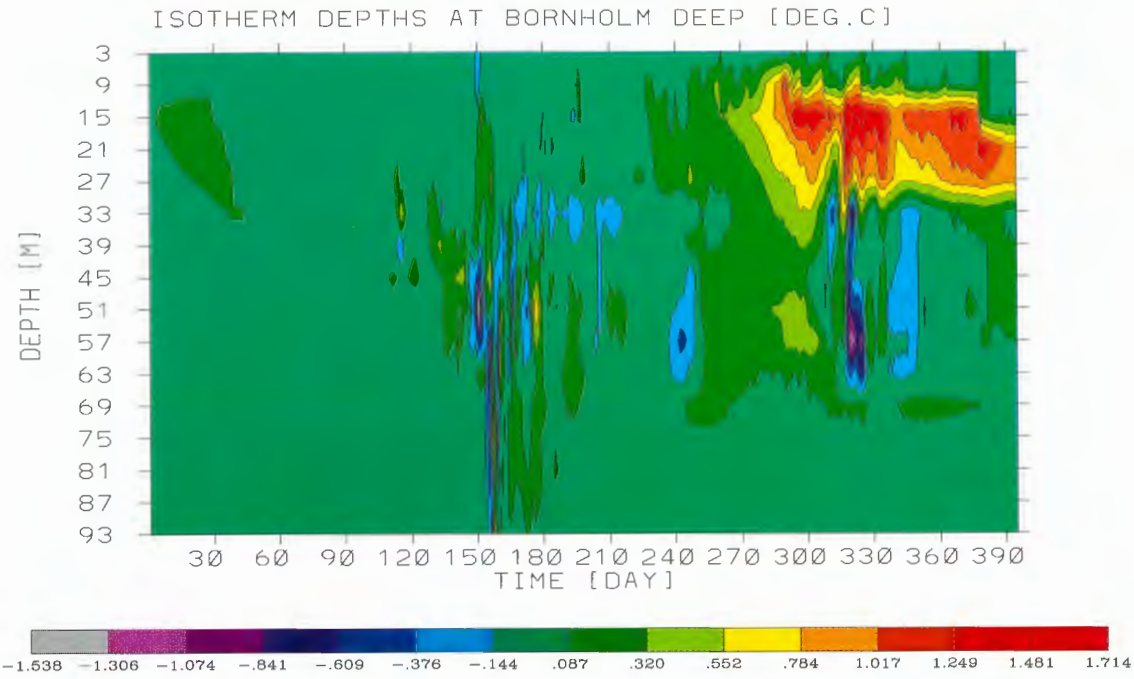

Figure 8: *Isotherm depths (in °C) of the difference between simulations with and without solar insolation from September 1992 until September 1993 at Bornholm Deep (adopted from Meier, 1996).*

1. The ϵ-equation is discussed controversial in the literature:
   As pointed out by Hasse (1977, 1993) dissipation is a process, not a conserved property. According to Kolmogorov's hypothesis, dissipation in the proper sense (conversion of turbulent kinetic energy into internal energy) is dependent only on the input into the energy cascade in case of high Reynolds numbers. Hence, dissipation measures the energy transfer rate rather than the dissipation proper. Therefore, a conservation equation for ϵ is not justified necessarily.
   $\Longrightarrow$ As a consequence, in Section 5 so-called k-models are compared with the $k-\epsilon$ model with the aim to replace the dissipation equation by a length scale formulation so that the results of both models are identical.

2. The sea surface could be an artificial sink for k and ϵ due to the widely used Dirichlet boundary conditions. Observations show a turbulence enhanced surface layer due to breaking surface gravity waves (Craig and Banner, 1994) which is not considered by Dirichlet boundary conditions.
   $\Longrightarrow$ Flux boundary conditions have been added to the standard $k-\epsilon$ model in Section 6.

3. Usually $k-\epsilon$ and Mellor-Yamada turbulence models overestimate temperature gradients in the thermocline (e.g., temperature profile on August 11 1993 in Fig.4 or Fig.8 by Burchard and Baumert, 1995) and underestimate mixed layer depths (Mellor, 2000; Ezer, 2000).

$\Longrightarrow$ In Section 7 a correction to reduce dissipation in stratified fluids as proposed by Mellor (2000) is tested. In addition to this modification, Mellor (2000) suggested that in 1D simulations an additional sink parameterization should be included to account for energy flux divergence. A comparison between 1D and 3D results is shown in Section 11.

4. The interaction of turbulence with stratification is not very well understood as indicated by the wide spread of values for $c_{\epsilon 3}$ (Tab.3). Indications for a negative $c_{\epsilon 3}$ have been given by Burchard and Baumert (1995), but the actual value is sensitive to the stability functions c_μ, $c'_\mu = c_\mu/\sigma_t$.
   $\Longrightarrow$ Experiments with the standard $k-\epsilon$ model with different values for $c_{\epsilon 3}$ have been performed indicating that mixed layer depths decrease if smaller values of $c_{\epsilon 3}$ than zero are used (not shown). As in that case the results get worse compared to observations, the problem might be related to the proper choice of stability functions which has to be solved first. Modified stability functions have been tested in Section 8. Another explanation is given by Baumert (2000, pers.comm.) who pointed out that the problem of $c_{\epsilon 3}$ might be related to the proper parameterization of internal waves. A consistent parameter choice should include negative $c_{\epsilon 3}$ (because otherwise no stationary solution exists for the $k-\epsilon$ model) together with wind dependent deep water mixing parameterization. Here, only two rather crude approaches without wind effect are discussed in Section 9.

5. The constant c_μ might be a complex function of TKE, dissipation, vertical velocity shear and stratification as discussed in the literature. The relation for the turbulent Prandtl number σ_t is only empirically derived.
   $\Longrightarrow$ One advanced version of the $k-\epsilon$ model with modified stability functions c_μ, c'_μ is tested in Section 8.

6. For multi-year simulations deep water mixing has to be considered.
   $\Longrightarrow$ Two approaches to add a parameterization for breaking of internal waves to the $k-\epsilon$ model are presented in Section 9.

$c_{\epsilon 3}$	author(s)
-1.9	Burchard and Baumert (1995), advanced
-1.4	Burchard and Baumert (1995), standard
0...0.2	Rodi (1980)
0.56	Omstedt (1996, pers.comm.)
0.8	Omstedt et al. (1983)

Table 3: *Different values of $c_{\epsilon 3}$ used by a couple of authors in case of stable stratification.*

5 The k-turbulence model

In this section so-called k-models are compared with the standard $k-\epsilon$ model. Instead of the equation for dissipation an algebraic relationship for the turbulent length scale is used in k-models. Such a model intercomparison have been performed already by Luyten et al. (1996) using the Blackadar (1962) formula of the turbulent length scale for neutral stratification in their k-model. They applied their version of the k- and $k-\epsilon$ model to the Rhine outflow region. A somewhat more general family of turbulence closures for stratified shallow water flows is presented here and has been applied to the Baltic Sea.

Using Kolmogorov's hypothesis (1942) for the dissipation of TKE

$$\epsilon = c_d \frac{k^{\frac{3}{2}}}{l} \tag{13}$$

with the empirical constant c_d, the equation for TKE results in

$$\frac{\partial k}{\partial t} - \frac{\partial}{\partial z}\left(\frac{\nu_t}{\sigma_k}\frac{\partial k}{\partial z}\right) = P + G - c_d \frac{k^{\frac{3}{2}}}{l} \tag{14}$$

with

$$\nu_t = \frac{c_\mu}{c_d}\, l\, \sqrt{k}\,. \tag{15}$$

The value of the empirical constant c_d is related to the applied stability function c_μ. Following Burchard et al. (1998) or Burchard and Bolding (2000) c_d can be calculated from the quasi-equilibrium momentum stability function for neutral flow for example from Galperin et al. (1988) resulting in $c_d = 0.17$ or from Canuto et al. (2000) resulting in $c_d = 0.15$. Here, the value $c_d = 0.1618$ is used. In addition, $\sigma_k = 1$ and the turbulent Prandtl number in (9) are adopted from the $k-\epsilon$ model.

According to Willebrand (1994) the equation for TKE (14) can be scaled using the following length scales

$$l_b = \frac{\sqrt{2\,k}}{N}\,, \tag{16}$$

$$l_u = \frac{\sqrt{k}}{\sqrt{\left(\frac{\partial u}{\partial z}\right)^2 + \left(\frac{\partial v}{\partial z}\right)^2}} \tag{17}$$

and l_d, the distance to the sea surface or bottom. Neglecting time tendency and assuming stable stratification (14) can be written for scale analysis as

$$\frac{l^2}{l_d^2} + \frac{l^2}{l_u^2} - \frac{l^2}{l_b^2} - 1 = 0\,. \tag{18}$$

The only relevant length scales contained in (14) which determine the turbulent length scale l are l_d, l_u and l_b. Further, it follows from (18) that physically sound solutions of the TKE equation (14) have to consider always dissipation.

As $\sqrt{2\,k}$ is the velocity of the turbulent eddies, l_u can be interpreted as characteristic length scale for the background shear of mean velocity. If the turbulent length scale l is larger than l_u the classical hypothesis from Prandtl is violated. Thus, the austausch ansatz applied to the TKE equation makes only sense if always $l \leq l_u$ is fulfilled.

Further, l_b is the characteristic length scale of a turbulent eddy in stratified fluid which is elevated from equilibrium position z_0 so that its change of potential energy equals its TKE:

$$k(z_0) = \frac{g}{\rho_0} \int_{z_0}^{z_0+l_b} (\rho(z_0) - \rho(z))\, dz\,. \tag{19}$$

Expanding density into a Taylor series

$$\rho(z) = \rho(z_0) + \left.\frac{\partial \rho}{\partial z}\right|_{z_0} (z - z_0) + \ldots \tag{20}$$

the integral can be solved analytically

$$k = \frac{1}{2} N^2 l_b^2\,, \tag{21}$$

which is equivalent to (16). As for turbulent eddies it is assumed that potential energy is smaller than kinetic energy (TKE), the turbulent length scale is limited by $l \leq l_b$.

A third limitation, $l \leq l_d$, follows from simple geometrical arguments. As the turbulent length scale is limited by 3 characteristic length scales simultaneously, the most simple model for l would be to choose just the minimum:

$$l = \min[l_d, l_u, l_b]\,. \tag{22}$$

However, there is still a degree of freedom for the choice of the proportionality constants of the 3 characteristic length scales (with magnitude of the order of 1). To consider roughness lengths z_0 and z_{0H} at the sea surface and bottom, respectively, and to use only one length scale l_d for the whole water column, the following expression for l_d is used here:

$$l_d = \kappa\,(z_0 - z)\left(1 + \frac{(z_{0H} + z)}{H}\right) \tag{23}$$

with von Kármán's constant $\kappa = 0.4$ and water depth H (recall that z is positive upward and zero at the sea surface).

To ensure that in the shear layer the balance $P = \epsilon$ replaces the full equation (14), the following k-model is proposed:

$$l = \min\left[\kappa\,(z_0 - z)\left(1 + \frac{(z_{0H} + z)}{H}\right)\,,\quad \frac{c_d}{\sqrt{c_\mu}}\,\frac{\sqrt{k}}{\sqrt{\left(\frac{\partial u}{\partial z}\right)^2 + \left(\frac{\partial v}{\partial z}\right)^2}}\,,\quad \frac{\sqrt{2\,k}}{N}\right]. \tag{24}$$

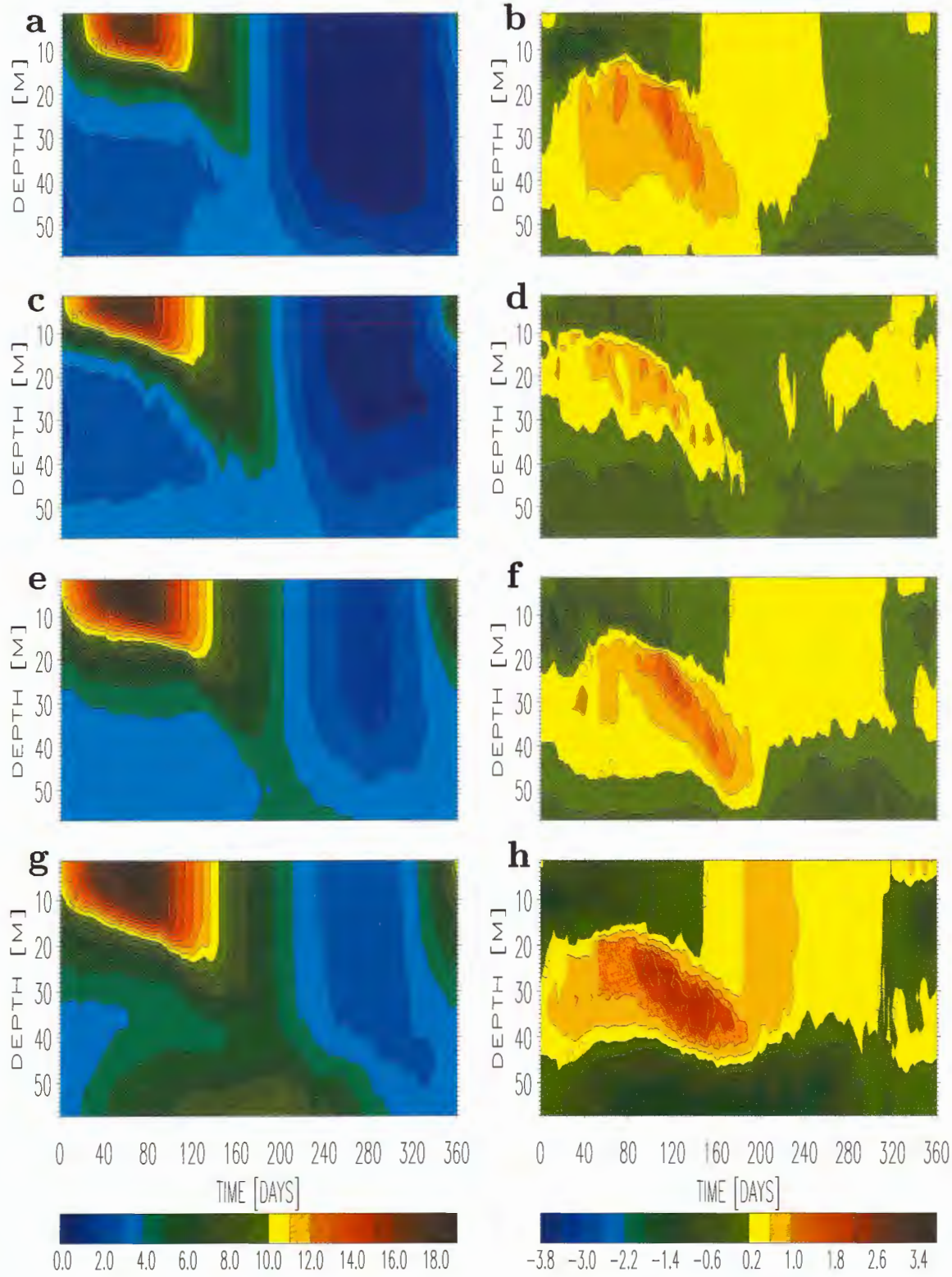

Figure 9: *13-year mean seasonal cycle of isotherm depths (in °C) of the k-model with* $l = \min(l_d, l_u, l_b)$ *(left column) and difference between standard* $k-\epsilon$ *and k-model (right column) at positions SR5 (a,b), LL07 (c,d), BY15 (e,f) and BY5 (g,h) (cf. Fig.1).*

Results of the k-model with (24) at four stations are shown in Fig.9, left column. These are from North to South SR5 in the Bothnian Sea, LL07 in the Gulf of Finland, BY15 (Gotland Deep) in the Eastern Gotland Basin and BY5 (Bornholm Deep) in the Bornholm Basin (Fig.1). Time axis starts with May 27 and only the upper 60 m are shown. The 13-year mean mixed layer of the k-model is only slightly shallower in all basins than of the standard $k-\epsilon$ model (right column).

Thus, it is in principal possible to replace the prognostic equation for dissipation by a diagnostic equation for the mixing length scale which should by a function of l_d, l_u and l_b. As this function is unknown and as using simply the minimum of l_d, l_u and l_b tends to cause numerical instabilities, the ϵ-equation is preferred, satisfying condition (24) approximately as shown in the next section. The computational performance (cpu time) of a k-model using (24) is only slightly better than that of the standard $k-\epsilon$ model.

If only the characteristic length scales l_d and l_b in (24) are used, the k-model is of the type as used by Gaspar et al. (1990) or Blanke and Delecluse (1993). The latter authors used the parameters $c_\mu = 0.07$, $c_d = 0.7$ and $\sigma_k = 0.033$. When the density profile is unstable, the turbulent length scale is taken equal to the local depth ($l_d = |z|$). It is not obvious why diffusion of TKE is 30 times larger than diffusion of momentum. However, as mentioned in Section 3, mixed layer depths are underestimated if $\sigma_k = 1$ is used. The artificial enhancement of vertical diffusion of TKE is necessary to make the k-model of Blanke and Delecluse (1993) performing well. Indeed, a factor of 30 is not enough to get the same results as with the standard $k-\epsilon$ model embedded in the here presented Baltic Sea models. If the constants of the standard $k-\epsilon$ model are kept in a k-model with $l = \min(l_d, l_b)$ (i.e., $c_\mu = 0.09$, $c_d = 0.1618$ and $\sigma_k = 1$), there is overestimation of mixed layer depth because l_u has been neglected which is an important length scale. A k-model with turbulent length scale $l = \min(l_d, l_u)$ gives almost the same results as with $l = \min(l_d, l_u, l_b)$. Compared to the $k-\epsilon$ model or compared to the k-model with $l = \min(l_d, l_u, l_b)$ the mixed layer depth is overestimated only slightly (Fig.10). The length scale l_b is adding only minor information to the here presented model hierarchy.

If in (14) diffusion is neglected (time tendency is always small), a Kochergin (1987) type model is obtained:

$$P + G = c_d \frac{k^{\frac{3}{2}}}{l} \,. \tag{25}$$

With (15) follows

$$\nu_t \left[\left(\frac{\partial u}{\partial z} \right)^2 + \left(\frac{\partial v}{\partial z} \right)^2 - \frac{N^2}{\sigma_t} \right] = \frac{\nu_t^3 \, c_d^4}{l^4 \, c_\mu^3} \tag{26}$$

or

$$\nu_t = (l\,c)^2 \sqrt{\left(\frac{\partial u}{\partial z} \right)^2 + \left(\frac{\partial v}{\partial z} \right)^2 - \frac{N^2}{\sigma_t}} \tag{27}$$

with $c = c_\mu^{\frac{3}{4}} / c_d \cong 1.0$. If in (27) $l = l_d$ is used, the corresponding mixed layer model results in underestimated mixed layer depths because diffusion is neglected.

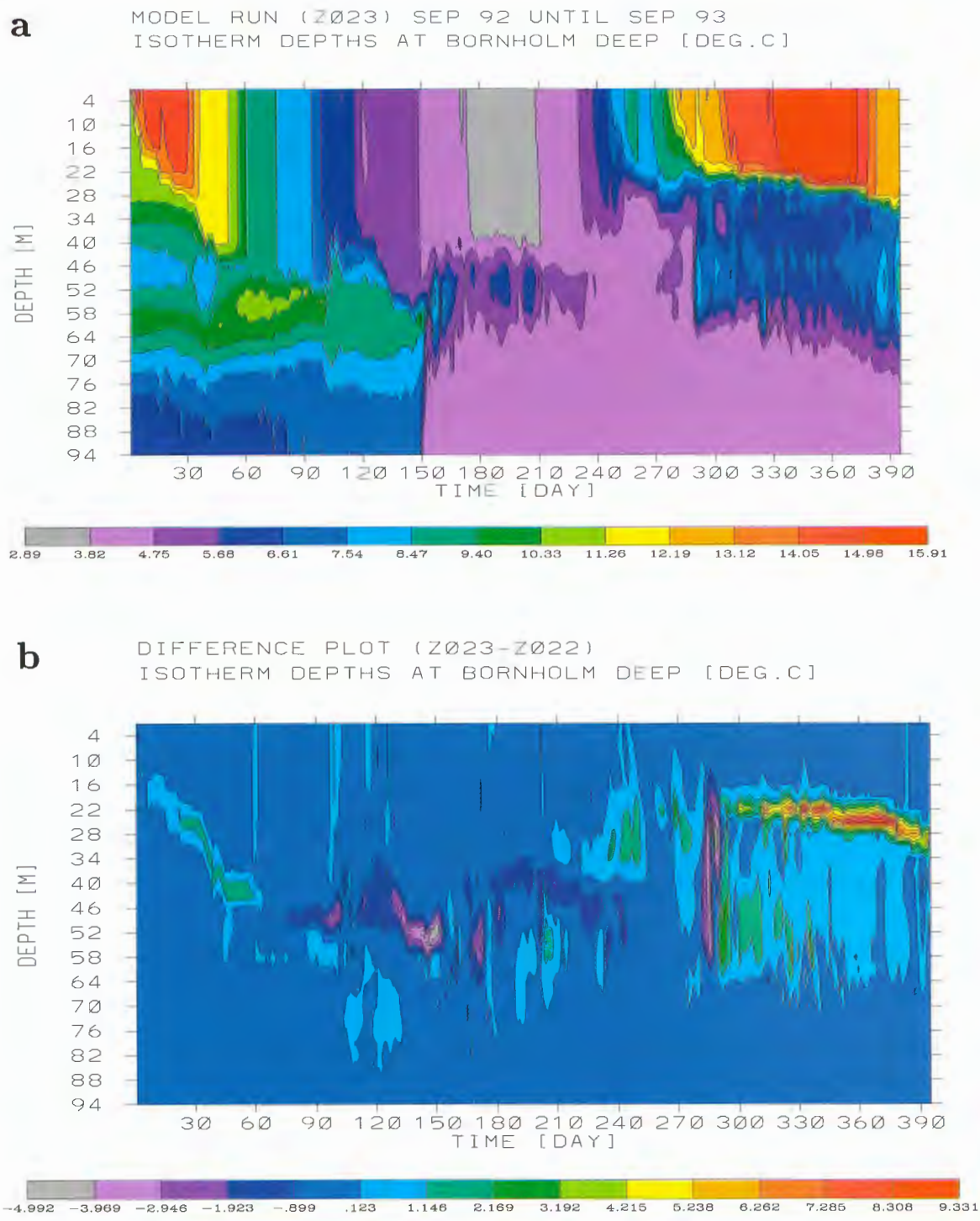

Figure 10: *Isotherm depths (in °C) from September 1992 until September 1993 at Bornholm Deep: k-model with* $l = \min(l_d, l_u)$ *(a), k minus* $k - \epsilon$ *model (b).*

6 Surface flux boundary conditions for the $k-\epsilon$ model

Commonly, Dirichlet boundary conditions are used for the $k-\epsilon$ turbulence model. At the surface a logarithmic boundary layer is assumed with balance between shear production P, interaction with stratification G and dissipation ϵ (Svensson, 1978):

$$P + G = \epsilon, \quad l = \kappa\,(z_0 - z)\,. \tag{28}$$

In case of high vertical resolution these boundary conditions are only slightly dependent on the surface roughness length. Within the boundary layer dissipation decays inversely proportional with the distance from the surface. Contrary, measurements show that dissipation decays much faster with the second or third power (Craig and Banner, 1994; Craig, 1996). Due to breaking surface gravity waves a turbulence enhanced layer is developed which controls the vertical flux of TKE from the wave field to the mixed layer interior. Therefore, flux boundary conditions (Neumann boundary conditions) are included which are calculated from an analytical solution of the TKE equation based on the assumption of a balance of TKE diffusion and dissipation (Craig and Banner, 1994):

$$\frac{\partial}{\partial z}\left(\frac{\nu_t}{\sigma_k}\frac{\partial k}{\partial z}\right) = \epsilon, \quad l = \kappa\,(z_0 - z) \tag{29}$$

Neglecting the term which represents reflected energy from the bottom, the solution of (29) within the turbulence enhanced layer is

$$\sqrt{k} = C\,(z_0 - z)^{-\frac{n}{3}} \tag{30}$$

with

$$n = \sqrt{\frac{3}{2}\,\frac{\sigma_k}{c_\mu}}\,\frac{c_d}{\kappa} = 1.65\,. \tag{31}$$

The constant C is determined by the boundary condition at the surface

$$\left.\frac{\nu_t}{\sigma_k}\,\frac{\partial k}{\partial z}\right|_{z=0} = m\,u_\star^3 + \kappa\,z_0\,B_0 \tag{32}$$

with friction velocity in the ocean $u_\star$, surface buoyancy flux B_0 and a constant $m = 100$ given by Craig and Banner (1994) or estimated by Lueck and Reid (1984). From (30) and (32) follows

$$C = \left(\frac{3\,\sigma_k}{2\,c_\mu}\right)^{\frac{1}{6}}\; z_0^{\frac{n}{3}}\; \left(m\,u_\star^3 + \kappa\,z_0\,B_0\right)^{\frac{1}{3}} \tag{33}$$

Using (30), (31) and (33) one can calculate dissipation within the boundary layer

$$\epsilon = C^3\,\frac{c_d}{\kappa}\,(z_0 - z)^{-n-1} \tag{34}$$

or fluxes of k and ϵ

$$\frac{\nu_t}{\sigma_k}\,\frac{\partial k}{\partial z} = C^3\,\sqrt{\frac{2\,c_\mu}{3\,\sigma_k}}\,(z_0 - z)^{-n} \tag{35}$$

and

$$\frac{\nu_t}{\sigma_\epsilon}\frac{\partial \epsilon}{\partial z} = C^4 \frac{c_\mu}{\sigma_\epsilon}(n+1)(z_0 - z)^{-\frac{4n}{3}-1}, \tag{36}$$

respectively.

For the discretization of the $k-\epsilon$ model a staggered grid is used in vertical direction with ν_t, k and ϵ at edges of the grid boxes of thickness Δz. Contrary, the prognostic variables of the circulation model u, v, T, S are located in box centers. Hence, fluxes of k and ϵ have to be prescribed at $z = -\Delta z/2$. Assuming that this depth is within the turbulence enhanced boundary layer, the following flux boundary conditions are derived from (35) and (36):

$$\frac{\nu_t}{\sigma_k}\frac{\partial k}{\partial z}\bigg|_{z=-\frac{\Delta z}{2}} = \frac{m\, u_\star^3 + \kappa\, z_0\, B_0}{\left(1+\frac{\Delta z}{2\, z_0}\right)^n} \tag{37}$$

$$\frac{\nu_t}{\sigma_\epsilon}\frac{\partial \epsilon}{\partial z}\bigg|_{z=-\frac{\Delta z}{2}} = a_\epsilon \frac{(m\, u_\star^3 + \kappa\, z_0\, B_0)^{\frac{4}{3}}}{z_0\left(1+\frac{\Delta z}{2\, z_0}\right)^{\frac{4n}{3}+1}} \tag{38}$$

The value of the constant a_ϵ is given by

$$a_\epsilon = \frac{c_\mu^{\frac{1}{3}}}{\sigma_\epsilon}\left(\frac{3\,\sigma_k}{2}\right)^{\frac{2}{3}}\left(\sqrt{\frac{3\,\sigma_k}{2\,c_\mu}}\,\frac{c_d}{\kappa}+1\right) \tag{39}$$

The surface roughness length is calculated from Charnock's formula (Charnock, 1955) in analogy with the atmosphere:

$$z_0 = \alpha\,\frac{u_\star^2}{g} \tag{40}$$

with $\alpha = 1400$ (Ly, 1990). Using $z_0 = 10\,cm$ and $\Delta z = 3\,m$ the denominator in (37) reduces the TKE flux in $\Delta z/2 = 1.5\,m$ depth to 1 percent of the corresponding surface flux. Most of the TKE generated by breaking surface gravity waves is dissipated within the uppermost grid box of the circulation model.

The depth z_{crit} of the transition from the turbulence enhanced surface layer to the shear layer ($P = \epsilon$) can be estimated as follows. Assuming that z_{crit} is smaller than the Ekman depth, rotation can be neglected in the steady Ekman equations for momentum:

$$\rho_0\,\nu_t\frac{\partial \vec{u}}{\partial z} = \vec{\tau} = \text{const} \tag{41}$$

with $|\vec{\tau}| = \rho_0\, u_\star^2$. Thus, $P = \epsilon$ is transformed to

$$\frac{u_\star^4}{\nu_t} = \epsilon \tag{42}$$

and with (8)

$$k = \frac{u_\star^2}{\sqrt{c_\mu}} = \text{const}\,. \tag{43}$$

If the surface buoyancy flux B_0 is considered too according to Svensson (1978), (43) has to be modified to

$$k = \frac{1}{\sqrt{c_\mu}} \left(u_\star^3 + \kappa\, z_0\, B_0\right)^{\frac{2}{3}} . \tag{44}$$

Except the case of convective boundary layers, the buoyancy flux is smaller than the momentum flux. By equating (30) and (43), the critical depth results in

$$z_{crit} = z_0 \left(1 - \left[m\, c_\mu^{\frac{1}{4}} \sqrt{\frac{3}{2}\sigma_k}\right]^{\frac{1}{n}}\right) = -11.8\, z_0 . \tag{45}$$

The depth of the turbulence enhanced surface layer depends only from the roughness length.

The boundary conditions (37) and (38) for $z = -\Delta z/2$ make sense if $|z_{crit}| \geq \Delta z/2 = 1.5\, m$ or if $z_0 \geq 13\, cm$. If the roughness length z_0 is less than $13\, cm$, the turbulence enhanced surface layer does not influence the uppermost level of the turbulence model and can be neglected. In that case Dirichlet and Neumann boundary conditions give the same results. According to (40) a roughness length of $z_0 = 13\, cm$ corresponds to a wind speed of about $U_{10} = 20\, m/s$. Thus, only in case of strong gale and storm the modification of the $k - \epsilon$ model using Neumann boundary conditions is important resulting in higher vertical TKE flux than calculated with Dirichlet boundary conditions. It should be noted that the low sensitivity of the turbulence model from the boundary conditions in case of moderate wind speeds is due to the fact that the turbulence enhanced surface layer is not resolved by the coarse vertical model grid. However, additional sensitivity experiments with higher grid resolution show that the choice of boundary conditions is unimportant for the whole mixed layer also in general, if wind speed is less than $20\, m/s$ (see Fig.13 and discussion below).

Stacey and Pond (1997) compared Dirichlet and Neumann surface boundary condition within the Mellor-Yamada turbulence scheme with data from Knight Inlet, British Columbia. The two boundary conditions produced simulations that are different down to a depth of at least $5\, m$. Somewhat more accurate simulations were produced by the flux boundary condition.

The analytical solution from Craig and Banner (1994) is an approximate solution of the whole $k - \epsilon$ model if diffusion and dissipation in the ϵ-equation (6) is balanced too:

$$\frac{\partial}{\partial z}\left(\frac{\nu_t}{\sigma_\epsilon}\frac{\partial \epsilon}{\partial z}\right) = c_{\epsilon 2}\frac{\epsilon^2}{k} . \tag{46}$$

With (30), (34) and (36) one obtain the following equation for the constant σ_ϵ

$$\sigma_\epsilon = \frac{c_\mu}{c_{\epsilon 2}\, c_d^2}\left(\sqrt{\frac{3}{2}\frac{\sigma_k}{c_\mu}}\, c_d + \kappa\right)\left(\frac{4}{3}\sqrt{\frac{3}{2}\frac{\sigma_k}{c_\mu}}\, c_d + \kappa\right) . \tag{47}$$

With the values of Table 2 the result is $\sigma_\epsilon = 2.43$ instead of $\sigma_\epsilon = 1.3$ from Rodi (1980). If σ_ϵ is altered according to (47), the solution of the $k - \epsilon$ model converge towards the

approximate solution from which the flux boundary conditions are calculated.

Using the new flux boundary conditions, Figure 11 shows the budget of the TKE equation in a modified Kato-Phillips experiment with rotation after 5 days of integration (Kato and Phillips, 1969; see also Deleersnijder and Luyten, 1994). Here, a

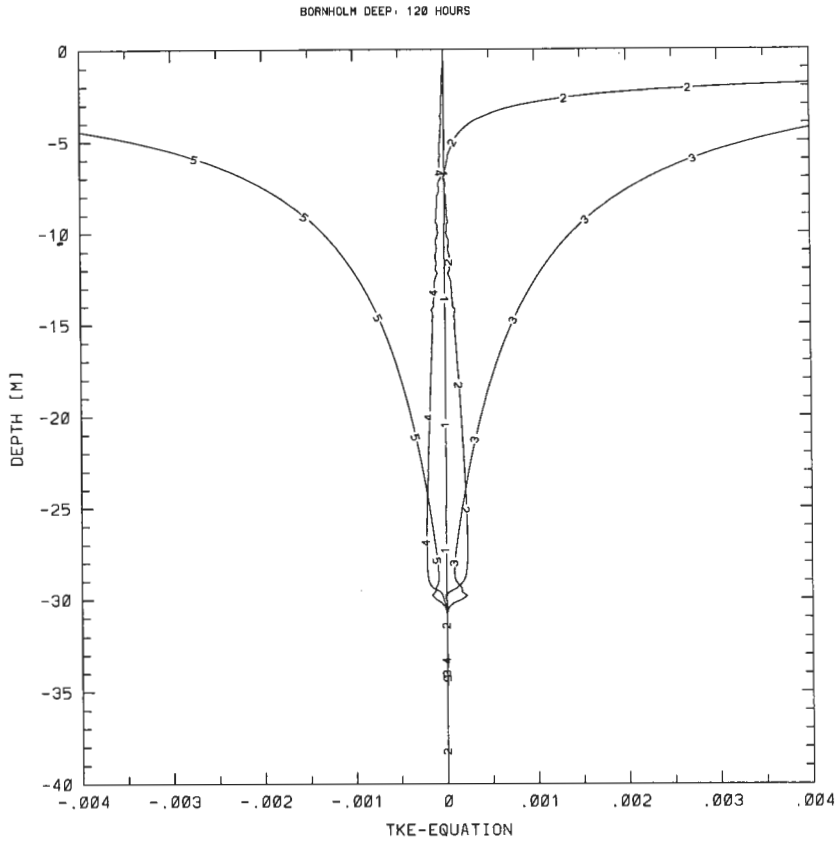

Figure 11: *Budget of the TKE equation in a Kato-Phillips experiment with rotation after 5 days of integration: (1) time tendency, (2) diffusion, (3) turbulence generation due to vertical shear of velocity P, (4) interaction of turbulence with stratification G, (5) dissipation ϵ.*

rectangular basin with dimensions 290 km times 190 km and with 99 m depth is used (which corresponds to the Bornholm Basin). The grid resolution is about 5.4 nm in horizontal ($\Delta\varphi = 5.4'$, $\Delta\lambda = 10.8'$) and 0.2 m in vertical direction. The time step is $\Delta t = 120\,s$. In the simulations initial density profiles with constant Brunt-Väisälä frequency ($N_0 = 10^{-2}\,1/s$) and constant wind forcing ($u_\star = 1\,cm/s$) are used. The results are analyzed after 5 days of integration when the system is in quasi-equilibrium. Contrary to the laboratory experiment of Kato and Phillips (1969) rotation is taken into account. Thus, existing analytical formulae for the mixed layer height (see Deleersnijder and Luyten, 1994) can not be used for comparison. However, well defined conditions of the 3D box model make analysis of the turbulence model easier than using data from the Baltic Sea models.

In Figure 12 corresponding, diagnosticly calculated mixing lengths are depicted and

compared with the turbulent length scale of the standard $k-\epsilon$ model with flux boundary conditions (curve 6). To ensure the convergence to the analytical solution of Craig

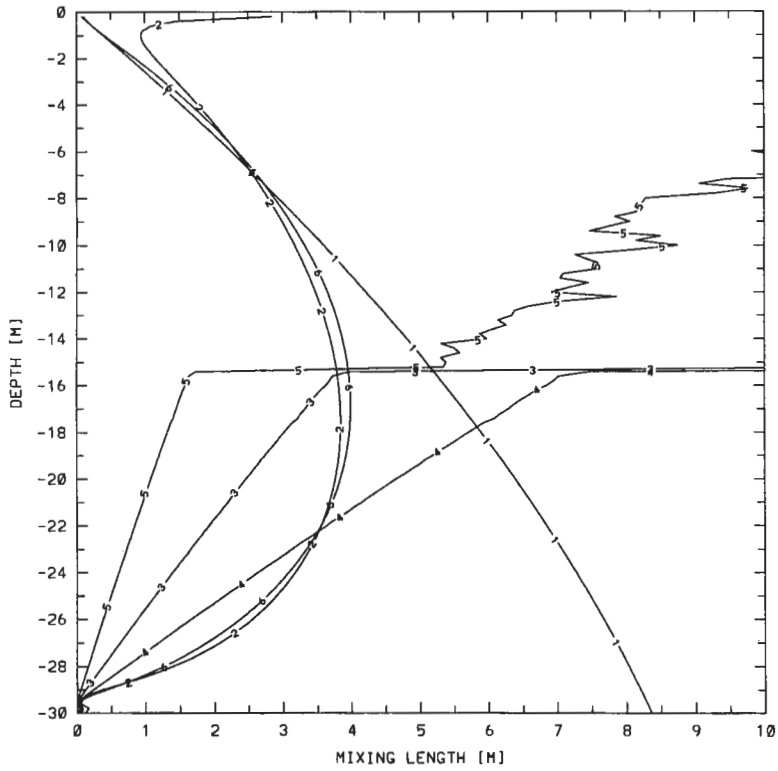

Figure 12: *Different mixing lengths in a Kato-Phillips experiment with rotation after 5 days of integration: (1)* $l = \kappa|z|\left(1-\frac{|z|}{H}\right)$, *(2)* $l = \frac{c_d}{\sqrt{c_\mu}}\frac{\sqrt{k}}{\left|\frac{\partial \vec{u}}{\partial z}\right|}$, *(3)* $l = \frac{\sqrt{0.56\,k}}{N}$, *(4)* $l = \frac{\sqrt{2\,k}}{N}$, *(5)* $l = 0.23\frac{\sqrt{2\,k}}{N}$, *(6)* $l = c_d\frac{k^{\frac{3}{2}}}{\epsilon}$.

and Banner (1994) at the surface, $\sigma_\epsilon = 2.43$ is used.

From both Figures 11 and 12 it is evident that the mixed layer can be divided into three different sublayers. Near the surface diffusion and dissipation balance each other as assumed when calculating the flux boundary conditions (curve 2 and 5 outside the depicted range in Fig.11). Hence, the limiting length scale of the largest eddies is proportional to the distance to the surface (l_d, curve 1 in Fig.12). In the interior of the mixed layer there is a balance of turbulence generation due to vertical shear of the mean velocity and dissipation (curve 3 and 5 in Fig.11). The accompanying length scale is proportional to the square root of TKE divided by the vertical velocity shear (l_u, curve 2 in Fig.12). At the bottom of the mixed layer all terms of the TKE equation become important. Especially, the interaction of turbulence with the stratification is described by the length scale which is proportional to the square root of TKE divided by the Brunt-Väisälä frequency (l_b, curve 4 in Fig.12). Due to this length scale the mixed layer is restricted in depth if a corresponding k-model is utilized. Indeed, l_b is slightly smaller than the turbulent length scale of the $k-\epsilon$ model

(curve 6) indicating that the proportionality factor $\sqrt{2}$ is too small. For comparison two more curves are shown in Fig.12 with other proportionality factors. For example, $l \leq \sqrt{0.56\,k}\,/\,N$ has been proposed by Galperin et al. (1988) as limiting length scale (curve 3). More tangential behavior of curve 4 to curve 6 is obtained if the original choice of $\sigma_\epsilon = 1.3$ is used. As the curves 4 and 2 are so close to each other at the mixed layer bottom, the results of the previous section become an explanation, i.e., that a k-model with turbulent length scale $l = \min(l_d, l_u)$ gives almost the same results as with $l = \min(l_d, l_u, l_b)$ or with the $k - \epsilon$ model (Fig.10). The main result of Fig.12 is that the turbulent length scale of the $k-\epsilon$ model fulfill condition (24) approximately.

As shown in Figure 13 the main difference between Dirichlet and Neumann (or flux) boundary conditions is the dependence on the surface roughness length in the range between $10\,cm$ up to $1\,m$ (larger roughness lengths are unrealistic). In case of flux boundary conditions the friction coefficients are much more sensitive against changes of the roughness length than in case of Dirichlet boundary conditions. As in these simulations high vertical resolution is used ($\Delta z = 0.2\,m$), the low sensitivity by roughness lengths smaller than 10 cm can not be the result of an unresolved surface enhanced turbulence layer as discussed above.

7 Reduced dissipation in stratified fluids

In this section a modification to the standard $k - \epsilon$ model is tested which has been proposed originally by Mellor (2000) for the Mellor-Yamada turbulence scheme (Mellor and Yamada, 1974; 1982). Mellor (2000) and Ezer (2000) have tested the modification within a 1D model and within a 3D basin-scale ocean model, respectively. The modification should help to overcome the common problem of insufficient surface mixing and too shallow summer thermocline in 3D models which is observed in the Baltic Sea too (cf. Fig.4).

Contrary to results of basin-scale 3D ocean models (Ezer, 2000), the problem here is less severe and can not be traced back to the lack of high frequency variability in the wind stress or to the lack of short wave radiation penetration into the upper layers because both are included. 3 hourly surface wind fields based on observations are used here as forcing (SMHI data base; Lars Meuller, pers.comm.) instead of monthly climatological data utilized in many large-scale ocean models. The insolation of short wave radiation is considered as well with two extinction lengths calculated from available data of monthly mean radiation reaching particular depths in the southern Baltic (Dera, 1992). In Section 4 the important impact of solar insolation has been illustrated (Fig.8). Baltic Sea models have the advantage compared to large-scale ocean models that high-quality data sets are available and that horizontal and vertical resolution are much higher.

Guided by laboratory data, a Richardson number dependent dissipation has been added to the standard $k-\epsilon$ model to study the source of shortcomings in the Baltic Sea models

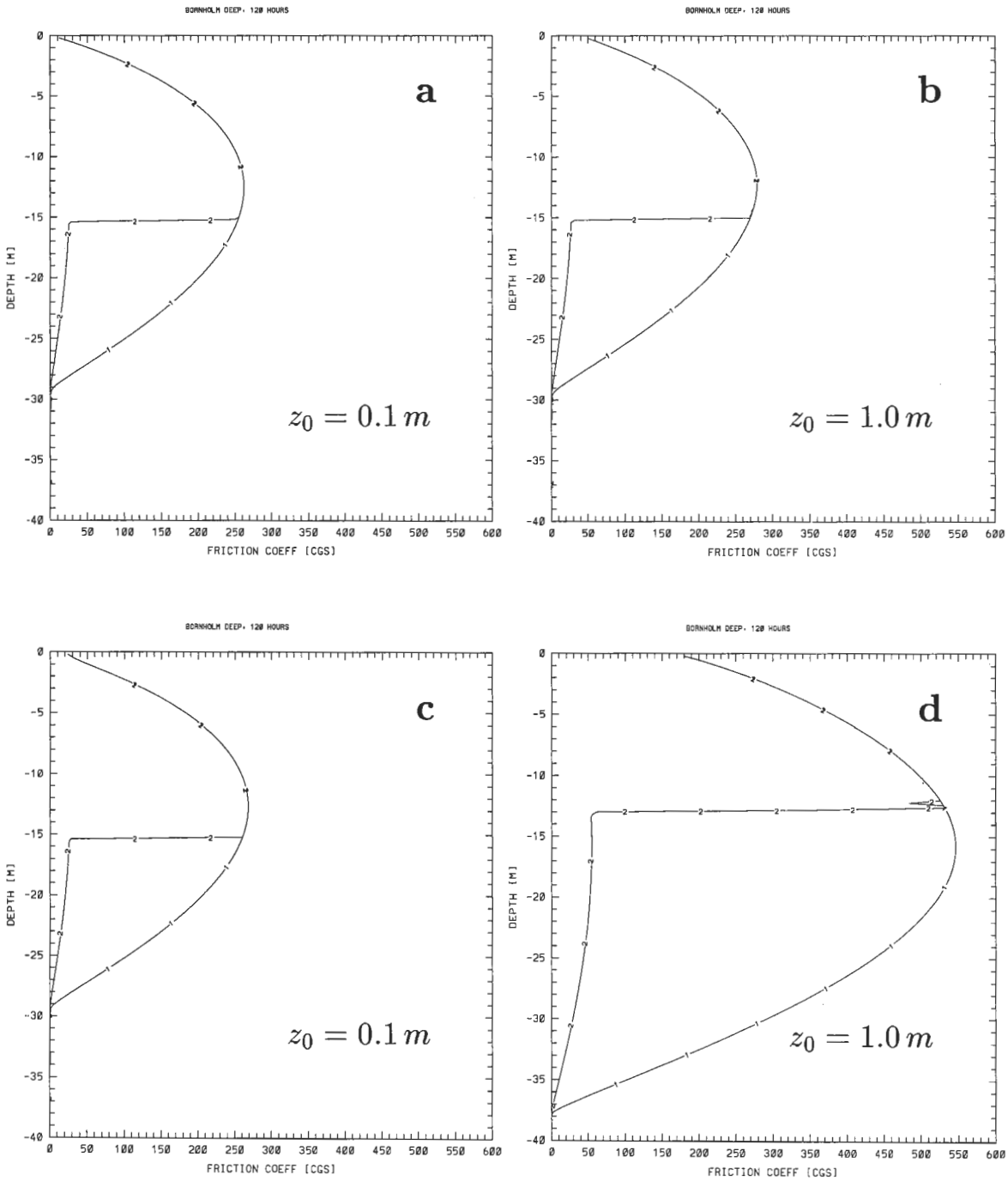

Figure 13: *Friction coefficients in cm^2/s for viscosity (1) and diffusivity (2) in a Kato-Phillips experiment with rotation after 5 days of integration: Dirichlet boundary conditions (a, b), Neumann boundary conditions (c, d).*

of this report:

$$\frac{\partial k}{\partial t} - \frac{\partial}{\partial z}\left(\frac{\nu_t}{\sigma_k}\,\frac{\partial k}{\partial z}\right) = P + G - c_m\,\epsilon\,, \tag{48}$$

$$\frac{\partial \epsilon}{\partial t} - \frac{\partial}{\partial z}\left(\frac{\nu_t}{\sigma_\epsilon}\,\frac{\partial \epsilon}{\partial z}\right) = c_{\epsilon 1}\,\frac{\epsilon}{k}\,\left(P + c_{\epsilon 3}\,G\right) - c_{\epsilon 2}\,c_m\,\frac{\epsilon^2}{k}\,, \tag{49}$$

c_m is a Richardson number dependent correction function proposed by Mellor (2000). The correction is suggested by an experiment by Dickey and Mellor (1980) showing that the turbulence in stratified fluid decays as in the unstratified case until a critical Richardson number is reached. The decay process nearly ceases for higher than critical Richardson number. What had been non-linearly interacting, turbulent eddies becomes nearly linear internal waves with approximately constant TKE. The transition is rather abruptly:

$$c_m = \begin{cases} 1 & : \quad Ri \leq 0 \\ 1 - 0.9 \left(\frac{Ri}{Ri_c}\right)^{1.5} & : \quad 0 < Ri < Ri_c \\ 0.1 & : \quad Ri_c \leq Ri \end{cases} \tag{50}$$

Here Ri denotes the gradient Richardson number and $Ri_c = 1$ a critical value which is obtained from tuning to get the best fit to observations.

Results are shown in Figure 14 for 4 different basins in the Baltic. Mellor's modification, which has shown a significant improvement in 1D calculations, has positive, but relatively smaller influence on 3D results in the Baltic in agreement with the results by Ezer (2000). The correction c_m affects the thermocline during spring and summer continuously in the depth range from 5 to 15 m in all basins. The surface layer in that range is more than $1^o\,C$ warmer in the mean. It should be noted that the results depend strongly on the tuning parameter Ri_c. Smaller values for Ri_c result in larger mixed layer depths. In a sensitivity experiment using $Ri_c = 0.2$ perfect agreement of median and quartile simulated and observed temperature profiles were obtained (not shown). However, simultaneously serious erosion destroyed the stratification in the 13-year long simulation. Obviously, it is impossible to simulate the seasonal summer thermocline correctly without negative side effects on long-term evolution of stratification. This generic problem is discussed further in Section 11.

8 Modified stability functions

Burchard et al. (1998) concluded from their results that the choice of the stability functions, which are used as proportionality factors for calculating eddy viscosity and diffusivity, has a stronger influence on the performance of the turbulence model than does the choice of the length scale related equation. In a comparative study of four different approaches for second-moment algebraic Reynolds stress closures Burchard and Bolding (2000) found that the stability functions of Canuto et al. (2000) fulfill the following requirements best compared to the other models of their study:

1. derivation from second-moment transport equations,
2. physical soundness,
3. high predictability,
4. computational economy and
5. numerical robustness.

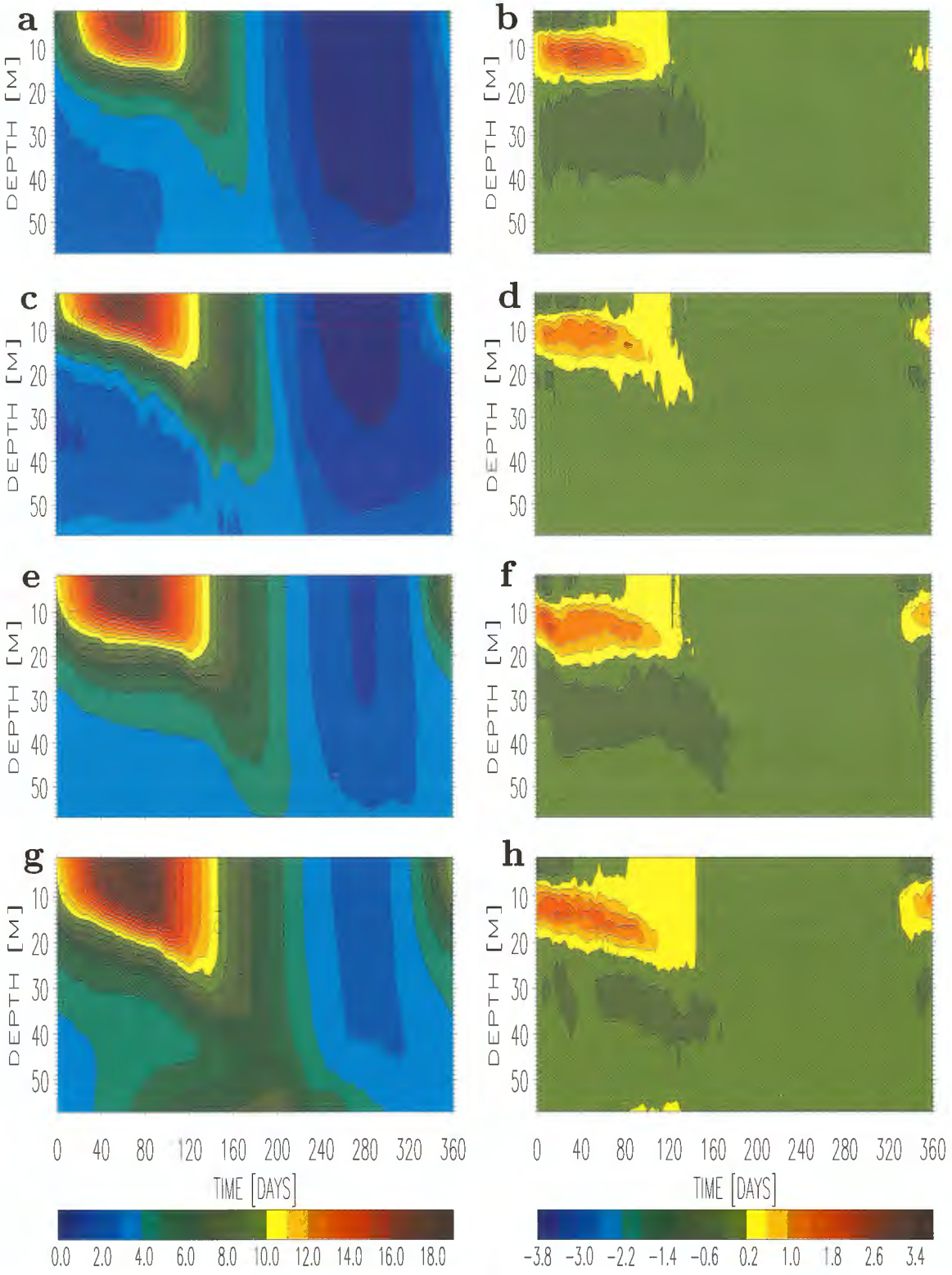

Figure 14: *As Fig.9 but for the standard $k - \epsilon$ model (left column) and difference between simulations with and without reduced dissipation (right column) at positions SR5 (a,b), LL07 (c,d), BY15 (e,f) and BY5 (g,h) (cf. Fig.1).*

Hence, the stability functions of Canuto et al. (2000) are embedded into the standard $k-\epsilon$ model:

$$c_\mu = \frac{0.1070 + 0.0174\,\alpha_N - 0.00012\,\alpha_M}{1 + 0.2555\,\alpha_N + 0.02872\,\alpha_M + 0.008677\,\alpha_N^2 + 0.005222\,\alpha_N\,\alpha_M - 0.0000337\,\alpha_M^2} \quad (51)$$

$$c'_\mu = \frac{0.1120 + 0.004519\,\alpha_N + 0.00088\,\alpha_M}{1 + 0.2555\,\alpha_N + 0.02872\,\alpha_M + 0.008677\,\alpha_N^2 + 0.005222\,\alpha_N\,\alpha_M - 0.0000337\,\alpha_M^2} \quad (52)$$

with

$$\alpha_M = \frac{k^2}{\epsilon^2}\left[\left(\frac{\partial u}{\partial z}\right)^2 + \left(\frac{\partial v}{\partial z}\right)^2\right], \quad \alpha_N = \frac{k^2}{\epsilon^2}\,N^2. \quad (53)$$

The range of α_N has to be limited because the stability functions get infinity for sufficient negative values of α_N. Galperin et al. (1988) recommended the following limitations

$$-1.7800 \leq \alpha_N \leq 21.391 \quad (54)$$

which are used here. Contrary, Burchard and Bolding (2000) used $-3.0675 \leq \alpha_N$ (Burchard, pers.comm.). The latter inequality in (54) corresponds to $l \leq \sqrt{0.56\,k}\,/\,N$. The Prandtl number of Blanke and Delecluse (1993) is replaced by $\sigma_t = c_\mu/c'_\mu$. According to Burchard and Bolding (2000) the parameters $\sigma_\epsilon = 1.02$ (instead of 1.3/2.43) and $c_{\epsilon 3} = -0.629$ in case of stable stratification (instead of 0) are used.

Results of 6-year mean seasonal cycle of temperature profiles are shown in Figure 15. Mixed layer depth is underestimated in summer and winter using the improved stability functions and modifications from Burchard and Bolding (2000) compared to the standard $k-\epsilon$ model. Mean SSTs are higher than $19°C$ in summer in Bornholm and Gotland Basin and colder than $0°C$ in winter in the Bothnian Sea and Gulf of Finland because of the shallower mixing depths (left column). The differences between simulations with improved stability functions and the standard $k-\epsilon$ model are quite large with more than $-1.4°C$ in the depth range between 10 and 40 m in summer in Bornholm and Gotland Basin (right column). In the Bothnian Sea the differences are larger than $-3.8°C$ in 10 m depth in August. SSTs differs in early summer by more than $1°C$ and in winter in Bornholm and Gotland Basin by about $-0.5°C$. Using the theoretical improved stability functions results are worse compared to observations than in the standard simulation.

9 Deep water mixing

For multi-year integrations deep water mixing needs to be taken into account. The $k-\epsilon$ model is extended to include a parameterization for breaking internal waves (Stigebrandt, 1987):

$$\nu = \nu_t + \sigma_t \min\left(\frac{\alpha}{N}, \nu_{0,max}\right) \quad (55)$$

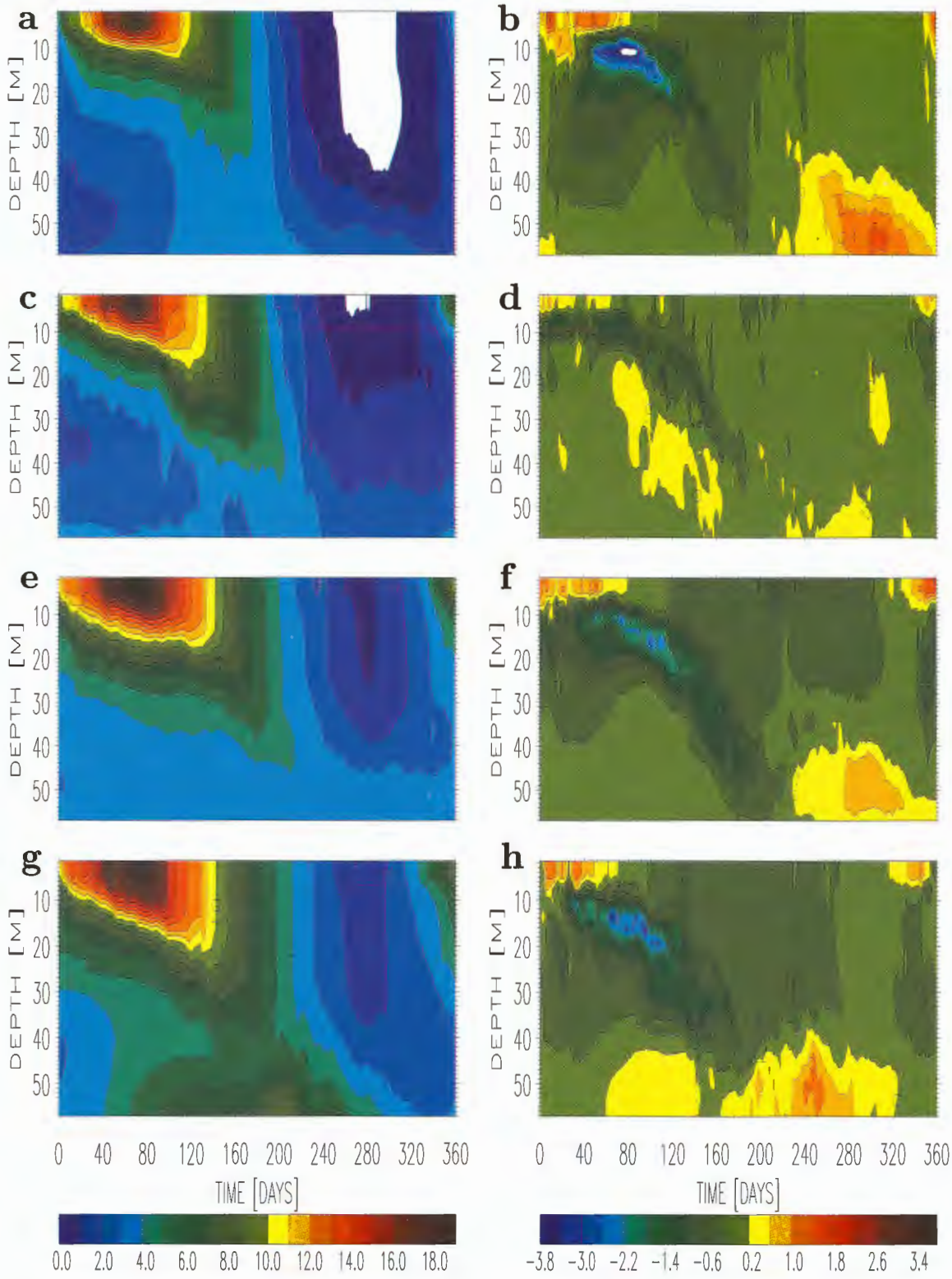

Figure 15: *6-year mean seasonal cycle of isotherm depths (in °C) using improved stability functions (left) and difference between simulations with improved stability functions and the standard $k-\epsilon$ model (right): (a,b) SR5, (c,d) LL07, (e,f) BY15, (g,h) BY5.*

with $\alpha = 0.5 \cdot 10^{-3}\, cm^2\, s^{-2}$, $\nu_{0,max} = 0.5\, cm^2\, s^{-1}$. The inverse proportionality between the deep mixing and the Brunt-Väisälä frequency is in accordance with ocean observations (Gargett, 1984).

Figure 16 shows records of observed and simulated salinity profiles from May 1980 until December 1993 at Gotland Deep. The 16 year stagnation period between 1976 and 1992 serves as an excellent test for deep water parameterization because the Baltic proper has not been affected by horizontal advection of salt water. Only vertical diffusion across the halocline alters salinity in the deeper layer. During the stagnation period salinity in the deeper layer of the Baltic Sea decreases remarkably. No high-salinity water from the North Sea is advected horizontally into the Gotland Deep until the major salt water inflow in January 1993. However, the influence of this latest event was mainly restricted to the Bornholm Basin. Only a small increase of bottom water salinity of about 0.5 psu occurred at Gotland Deep after January 1993 (about 4700 days after start of the depicted record, cf. Fig.16a).

The correspondence of observed and simulated isohaline depths is satisfactory indicating a proper choice of deep water parameterization (cf. Fig.16b and c). Different values for the mixing parameter α have been tested in the range $\alpha = 0.5 - 2 \cdot 10^{-3}\, cm^2\, s^{-2}$. Correspondingly, the maximum background mixing has been chosen to $\nu_{0,max} = 0.5 - 2\, cm^2\, s^{-1}$. The optimized value for the constant α at Gotland Deep is somewhere between 0.5 and $1.0 \cdot 10^{-3}\, cm^2\, s^{-2}$ (Meier, 1999a) in agreement with results from the North Atlantic by Oschlies and Garçon (1999). In Figure 16 a value of $\alpha = 0.5 \cdot 10^{-3}\, cm^2\, s^{-2}$ is used which is much smaller than the values published by Axell (1998). He estimated from profile data of the Baltic Sea from the period 1964 until 1997 using a budget method an annual mean value of α for Gotland Deep of $1.5 \cdot 10^{-3}\, cm^2\, s^{-2}$ at two different depths. This is very close to the value obtained by Stigebrandt (1987) in his horizontally integrated model for the Baltic proper. In that model, Stigebrandt tuned α until the observed and computed evolutions of the stratification agreed ($\alpha = 2 \cdot 10^{-3}\, cm^2\, s^{-2}$). Further, Axell (1998) has shown that there was a seasonal variation of the vertical diffusion well below the pycnocline and that diffusion was higher at Landsort Deep (closer to the coast) than at Gotland Deep. Obviously, α depends on local fluxes from energy sources, such as wind-driven inertial currents, Kelvin waves and other coastal trapped waves. Therefore, it is assumed that mixing near the coasts and topographic slopes is larger than in the open sea. In the 3D Baltic Sea model some sorts of these waves are resolved completely, others only partly and some sorts are not resolved at all. Thus, deep water mixing is already included in parts in the standard $k - \epsilon$ model. Explicitly parameterized deep water mixing has to be smaller than the value obtained from budget methods for all kind of mixing. Indeed, 13-year mean vertical integrated simulated TKE, dissipation or viscosity show maxima close to topographic slopes in Bornholm Basin, Gotland Basin, Åland Sea and Bothnian Sea (in downwelling areas of eastern parts of the basins, but not at the coasts directly because small water depths limit viscosity and diffusivity).

In a sensitivity experiment explicit prescribed deep water mixing has been omitted. As shown in Figure 17 salinity decreases with time in the deeper layer of the Gotland

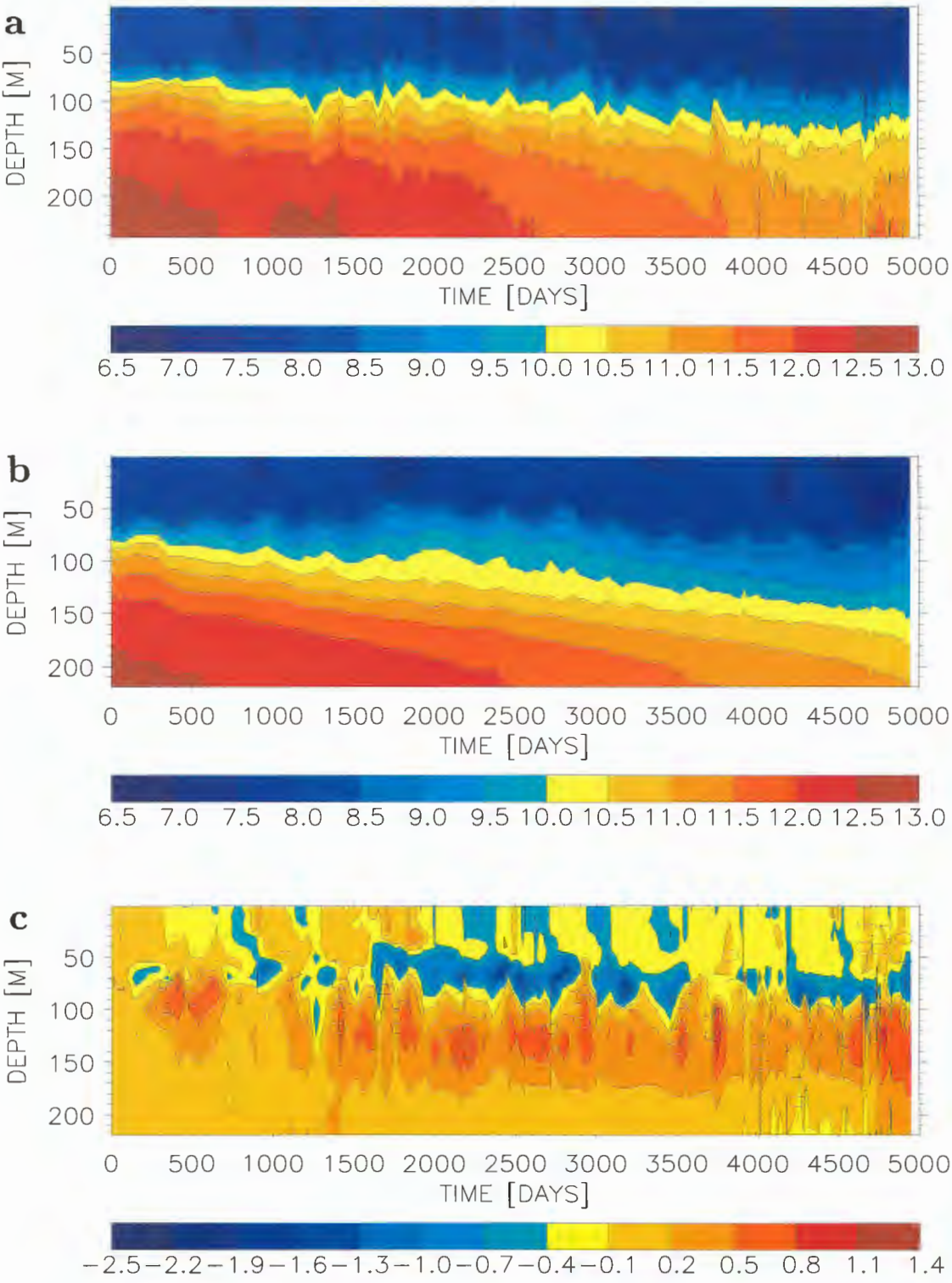

Figure 16: *Observed (a) and simulated (b) isohaline depths (in psu) from May 1980 until December 1993 at Gotland Deep (BY15). The difference between observations and model results is depicted in (c). The time axis starts at May 26 1980.*

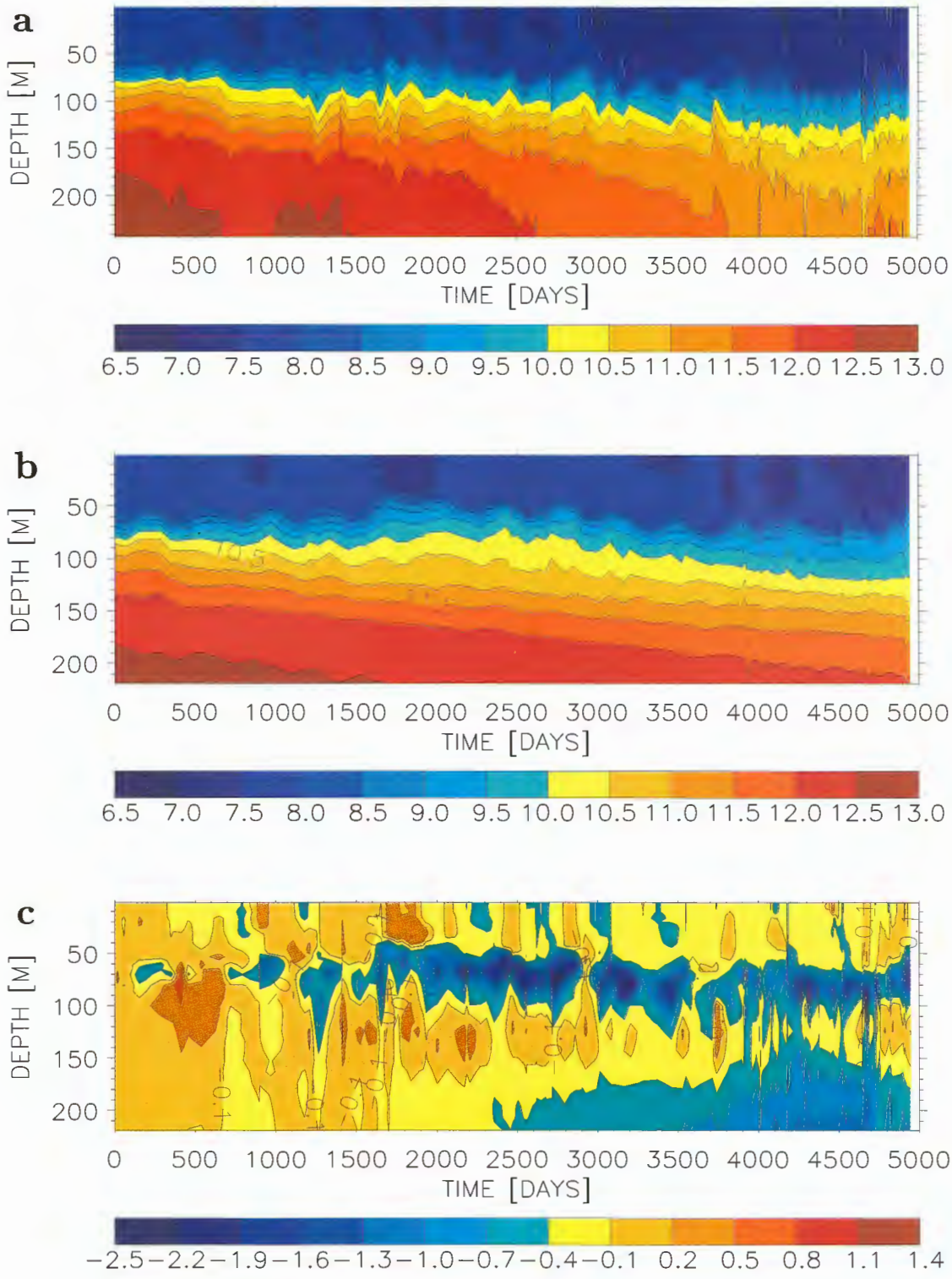

Figure 17: *As Fig.16 but in the simulation explicitly parameterized deep water mixing is negligible.*

Basin. However, the decrease is smaller than in case with explicit prescribed deep water mixing. For example, the 11.5 *psu* isohaline does not hit the bottom during the

integration period whereas in the observations that happens after about 3800 days. In Figures 16c and 17c the differences between the observations and the two simulations are depicted with the same color bars. In both experiments salinity in the surface layer ($0 \ldots 40\,m$) drifts slightly by less than $0.1 \ldots 0.4\,psu$ indicating that the horizontal transport of juvenile fresh water might be underestimated. In the depth range $40 \ldots 100\,m$ the simulated halocline is elevated stronger than observed with the consequence that differences are larger than $0.4\,psu$ (maximum $1.6\,psu$ with deep water mixing and maximum $2.1\,psu$ without deep water mixing). With deep water mixing salinity in the lower range of the halocline ($100 \ldots 170\,m$) is smaller by $0.2\,psu$ or more than observed. Contrary, without deep water mixing no differences or slightly higher salinities occur in this depth range. Obviously, the used parameterization for deep water mixing has also small but systematic negative side effects in the depth range $100 \ldots 170\,m$ and corrects salinity somewhat in $40 \ldots 100\,m$. In the deep layer ($150\,m$ to bottom) the differences are quite large if no deep water mixing is used. After 2400 days simulated bottom salinity is $> 0.7\,psu$ larger than observed and after 4100 days until the salt water inflow it is even $> 1\,psu$ larger.

Alternatively, it is possible to include the effect of breaking internal waves into the $k-\epsilon$ model directly. As in stable stratified layers the turbulent macro length scale l is limited by

$$l \leq \frac{\sqrt{2\,k}}{N}\,, \tag{56}$$

as shown in Section 5, a corresponding lower limit for the dissipation rate ϵ using Kolmogorov's equation can be derived:

$$\epsilon \geq \frac{c_d}{\sqrt{2}}\,k\,N\,. \tag{57}$$

Hence, a necessary condition to fulfill (56) is given by

$$\epsilon \geq \epsilon_{min} \cong 0.1144\,k_{min}\,N\,. \tag{58}$$

Using the relationship of Kolmogorov and Prandtl (8) the viscosity is limited by

$$\nu_t \geq \nu_{t,min} = c_\mu\,\frac{k_{min}^2}{\epsilon_{min}}\,. \tag{59}$$

Comparison with (55) gives a lower limit for TKE:

$$k \geq k_{min} = \frac{\alpha\,c_d\,\sigma_{t,max}}{c_\mu\,\sqrt{2}} \cong 6.356 \cdot 10^{-3}\,cm^2 s^{-2}\,. \tag{60}$$

The results of both approaches (Eq.(55) or Eq.(58) and (60) have been compared. The differences as depicted in Figure 18 for Bornholm and Gotland Basin are only small ($\leq 0.5\,psu$).

A similar approach to include the effect of breaking internal waves in stably stratified layers has been proposed by Burchard and Petersen (1999). They use an upper limit for the macro length scale according to Galperin et al. (1988)

$$l \leq \frac{\sqrt{0.56\,k}}{N} \tag{61}$$

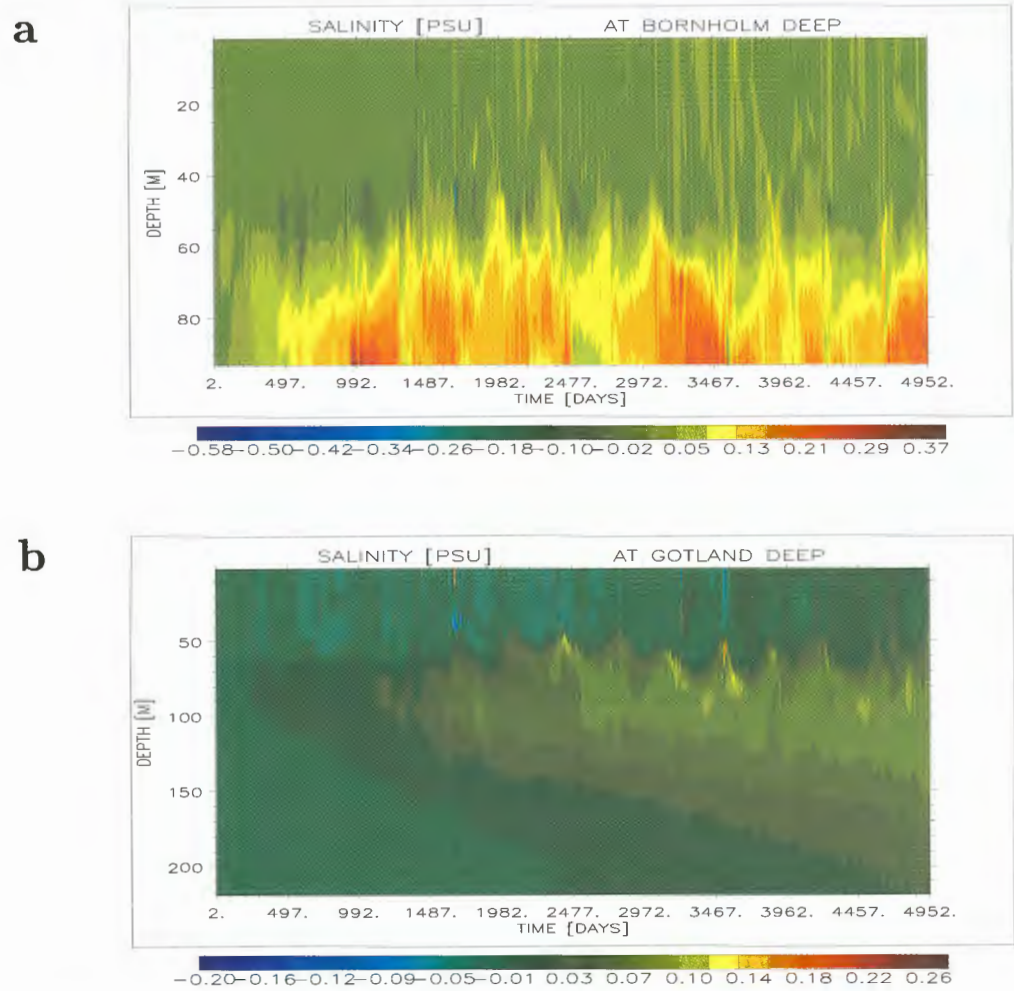

Figure 18: *Isohaline depths (in psu) of the difference between simulations using the two deep water mixing parameterizations from May 1980 until December 1993 at Bornholm Deep (a) and Gotland Deep (b).*

together with a minimum value for TKE of $k_{min} = 3 \cdot 10^{-2}\, cm^2 s^{-2}$. If the turbulent Prandtl number of Eq.(9) is used, this approach corresponds to $\alpha = 1.3 \cdot 10^{-3}\, cm^2\, s^{-2}$. This value is about a factor of 2 larger than the optimized value for the model presented here.

10 Modeling turbulence under sea ice

An essential feature of the Baltic is the seasonal sea ice cover. Sea ice acts as a relatively rigid insulating film between the air and the sea which modifies air-sea exchange of momentum, heat and matter and influences local meteorological conditions. With respect to the ocean sea ice influences the temperature and salinity characteristics of the water masses and the circulation of the Baltic Sea. Normally the ice season lasts 5-7 months, from November to May, with large interannual variability of ice extent.

During a mild winter ice occurs only in the Bothnian Bay, but in a cold winter the whole Baltic Sea becomes ice-covered.

Ice thickness is inter alia sensitive to the ice-ocean heat flux as shown already by Semtner (1979). In Figure 33c mean heat fluxes into the ice are depicted showing that the ice-ocean heat flux is quite important because it balances longwave radiation during the first half of the ice season whereas all other fluxes are smaller. The mean flux amounts to $5-8\,W\,m^{-2}$ during January and February. In RCO the heat flux between ice and ocean is parameterized by a bulk formula with bulk heat transfer coefficient according to Omstedt and Wettlaufer (1992) (see Appendix B, Eq.(83)). Measurements show that the ice-ocean heat flux vary tremendously on time scales of days and on space scales of kilometers (Wettlaufer, 1991). Further, McPhee et al. (1987) have shown from measurements in the marginal ice zone of the Greenland Sea that molecular effects are important for heat and mass transport at the hydraulically rough ice-ocean interface. In case of melting a fresh molecular surface layer develops and reduces interfacial salinity. As freezing point temperature depends on the interfacial salinity (Millero, 1978), the temperature difference determinant melting is reduced and melting ceases. This negative feedback mechanism is affected by mixing because increased mixing increases the interfacial salinity toward the far-field salinity and decreased mixing results in the extreme case of ice salinity (close to zero) near the surface. Thus, mixing might affect the evolution of ice thickness. Omstedt (1990) tried to include the molecular sublayer near the surface into his coupled one-dimensional sea ice-ocean model using wall functions without resolving the relevant processes. However, to the authors knowledge the impact of mixing on ice thickness under realistic Baltic Sea conditions have not been shown yet. The question is how much turbulence is generated under ice and how interfacial salinity is affected by TKE. According to the flux boundary conditions for the $k-\epsilon$ model, Eq.(37) and (38), the important quantity of the turbulence enhanced surface layer is the surface roughness length z_0 which is in the range between 1 and 10 cm (McPhee et al., 1987). Thus, Neumann boundary conditions give almost the same results as Dirichlet boundary conditions as shown in Section 6. If Charnock's formula (40) can also be used under ice is more than questionable because the roughness length depends on the corresponding ice class. Unfortunately, different ice classes are not implemented in RCO yet. Here, further investigations are necessary. For the time being, in RCO $u_\star$ is calculated in case of sea ice from the corresponding ice-ocean stress (see Appendix B, Eq.(80)) and z_0 from Charnock's formula (40). The argument for this strategy is that the boundary conditions for the $k-\epsilon$ model are not sensitive to surface roughness length in the range between 1 and 10 cm. As the flux of momentum τ_{ice} has the same order of magnitude than $\tau_{no\,ice}$ (assume $U_{10}=10\,m/s$ and free drift, i.e., $u_{ice}=20\,cm/s$, it follows from (80) $\tau_{ice}\cong\tau_{no\,ice}$), the same amount of TKE is generated under ice than in the open water case. Hence, only in strong gale and storm situations z_0 becomes important for the vertical flux of TKE. A sensitivity experiment with constant salinity in the Baltic Sea, i.e., the Baltic Sea is treated as a lake (Meier, 1999b), shows that ice extent and ice thickness change not very much compared to the standard experiment. This finding points towards a minor importance of the above mentioned negative feedback mechanism for the ice-ocean heat flux in case of melting. Probably the salinity in the seasonally ice covered areas of the Baltic Sea is too

low. However, for the time being it is impossible to decide whether the neglected fresh molecular sub-surface layer is important during melting in the Baltic or not.

11 The effect of horizontal resolution

Mellor (2000) discussed in his paper a generic problem of 1D ocean surface layer model comparison with ocean observations. He pointed out that 1D simulations should include an additional sink parameterization to account for energy flux divergence which is generally present in the real ocean and in 3D numerical ocean simulations. Without an energy sink, wind-driven surface layer velocities generated by a 1D model will inexorably increase and, in the course of a multi-month simulation, erroneously enhance mixed layer deepening and surface temperature cooling. Already Pollard and Millard (1970) incorporated a sink term in a simple model in order to match the model with current meter observations.

Of course, an additional sink term within the momentum equation is physically inconsistent and can be regarded as preliminary solution only. To test Mellor's ideas a comparison between 1D and 3D simulations has been performed. To avoid differences in discretization, for the 1D simulations RCO has been used without horizontal and vertical advection of momentum, temperature and salinity. In addition, sea level elevation and pressure gradient have been set to zero so that the momentum conservation is reduced to Ekman dynamics only which are included in 1D models usually. Sea ice is simulated in a thermodynamic mode. Net precipitation is considered as in the 3D model but river runoff has to be neglected consequently. Thus, the 3D model is reduced to a number of 1D column models. At every wet surface grid point of the RCO model domain a 1D simulation forced by the same atmospheric data than used in the 3D simulation has been performed.

In Figure 19 the evolution of salinity at Gotland Deep from May 1980 until December 1993 is shown. Deep water mixing parameterization is utilized as in the 3D simulation with $\epsilon_{min} = 0.1144\, k_{min} N$ and $k_{min} = 6.356 \cdot 10^{-3}\, cm^2 s^{-2}$ corresponding to $\alpha = 0.5 \cdot 10^{-3}\, cm^2\, s^{-2}$ in (55) as shown in Section 9. There is a decrease in salinity in the deeper layer but less than observed. As mentioned in Section 9 the here prescribed explicit deep water mixing is smaller than that one would obtain if in the 1D model α is tuned until the observed and computed evolutions of the stratification agree. The reason for the weaker decrease is that waves in the 3D model generate TKE contributing to deep water mixing implicitly. These horizontally propagating waves are missing in the 1D simulation of course. Figure 19 proofs that the additional amount of deep water mixing is not related to artificial numerical diffusion related to improper discretization of the governing equations.

In the upper layer salinity increases in the 1D simulation as shown in Figure 19b and c because horizontal advection of low saline surface water originating from fresh water of river runoff is not considered. The only source of fresh water in this model is net

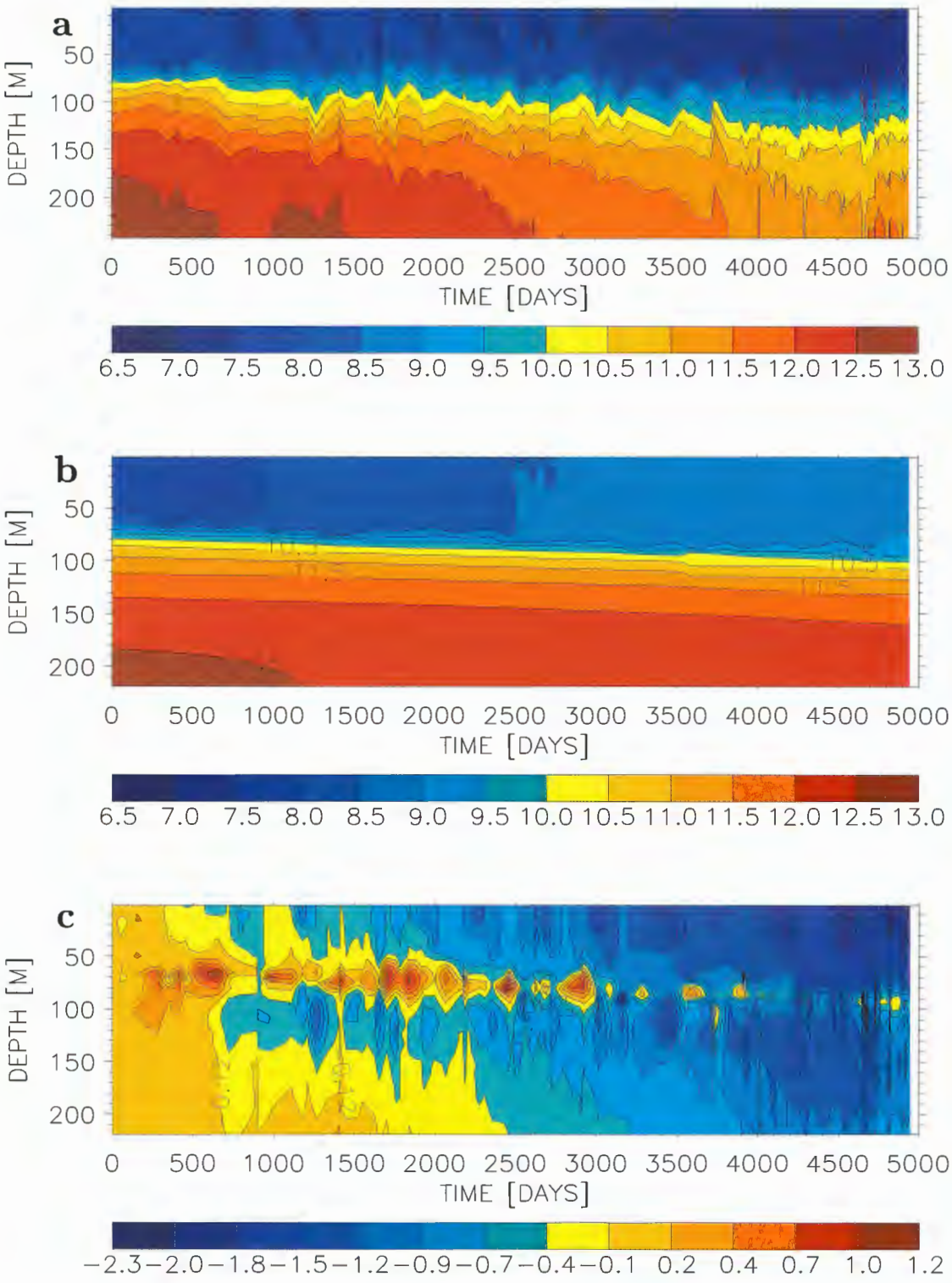

Figure 19: *As Figure 16 but the simulation (b,c) has been performed without advection.*

precipitation. Due to vertical diffusion across the halocline surface salinity increases by about $2\,psu$ after 5000 days.

Another effect of omission of horizontal and vertical advection is shown in Figure 20. 13-year mean SST fields of the 3D reference run and the sensitivity experiment without

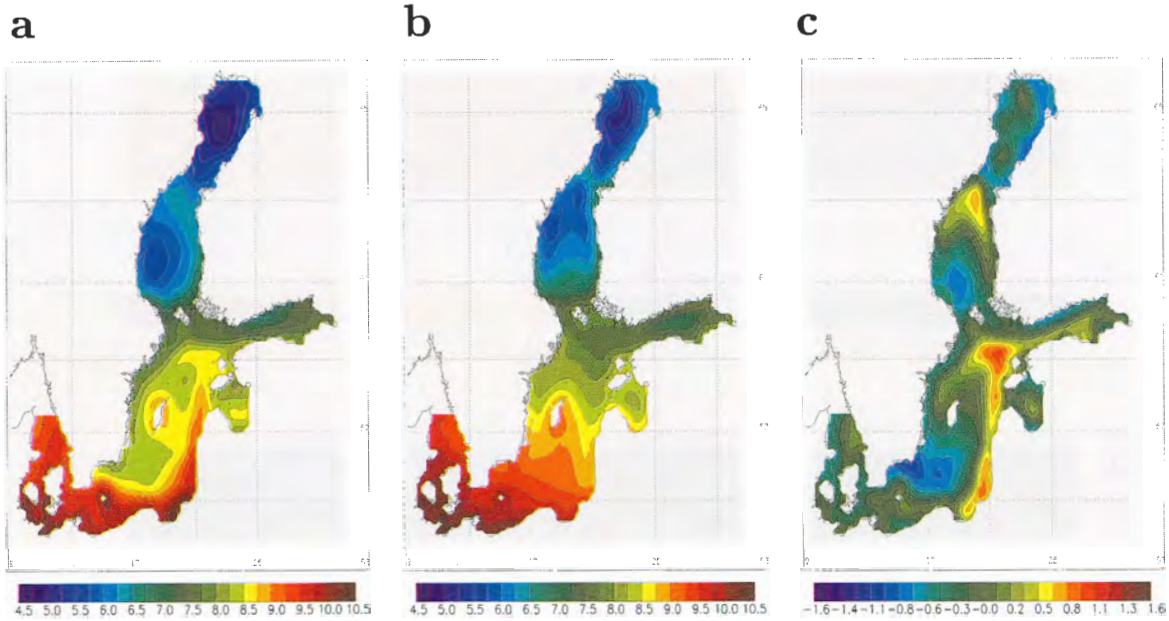

Figure 20: *Mean sea surface temperature (in °C) for the period May 27 1980 until May 26 1993: (a) reference run, (b) without advection and (c) the difference between (a) and (b).*

advection are compared. Without advection SSTs are mainly distributed in latitudinal direction. From the difference plot in Fig.20c it is evident that advection is warming the eastern coastal waters in the Baltic proper by more than $1\,°C$ and is cooling the western Swedish side by more than $-1\,°C$ correspondingly. Similar differences occur in the Bothnian Sea in a more North-South oriented pattern. There is no constant offset between the two SST fields and mean SST at Gotland Deep is almost identical in the two experiments. SSTs are even more zonally homogeneous if the wind forcing is switched off (see Fig.19 by Meier, 1999a). In case of omitted advection the signal of the coasts is still included in the wind field.

In Figure 21 mean seasonal cycles of vertical temperature evolution in Bornholm and Gotland Basin, Gulf of Finland and Bothnian Sea are shown for the simulation without advection (left column). A generally deeper mixed layer of the 1D experiment as suggested by Mellor (2000) is not observed. However, differences between simulations without and with advection (right column) are quite large, i.e., in the range between about -3 and $3\,°C$ in the whole surface layer $(0 \ldots 60\,m)$. In Bornholm and Gotland Basin the mixed layer depth of the 1D simulation is smaller in summer (July, August) and larger in autumn (September, October). In February the upper $20 - 30\,m$ of the water column are more than $1\,°C$ warmer in Bornholm Basin and more than $0.6\,°C$ warmer in Gotland Basin. Also the northern basins, Gulf of Finland and Bothnian Sea, are warmer in winter in the 1D simulation. In the Bothnian Sea the upper $0 - 45\,m$ of the water column are more than $1\,°C$ warmer than in the 3D simulation. In the Gulf of Finland the gradient of the summer thermocline is much smaller in the 1D

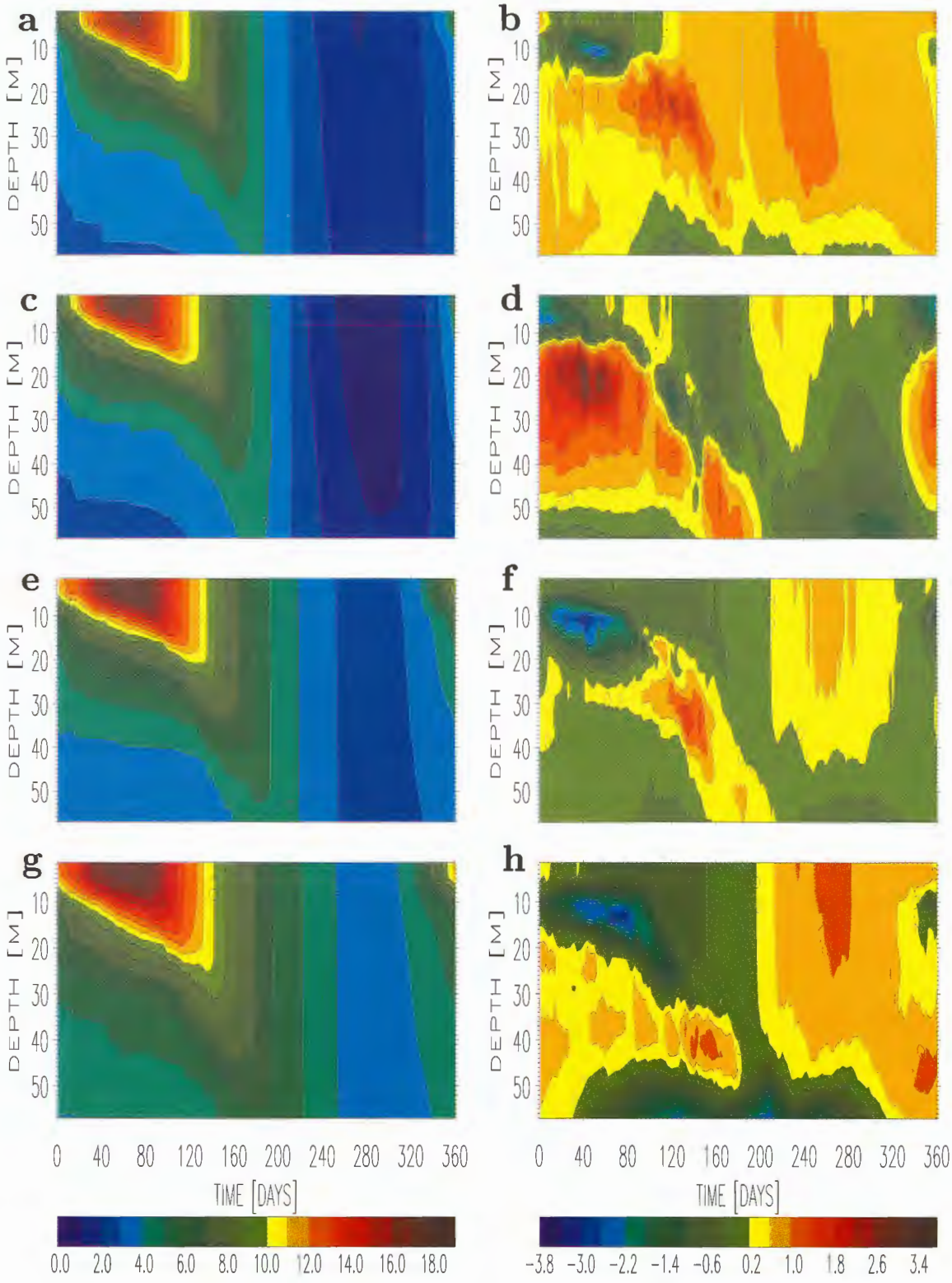

Figure 21: *13-year mean seasonal cycle of isotherm depths (in °C) calculated without advection (left column) and difference between simulations without and with advection (right column): (a,b) SR5, (c,d) LL07, (e,f) BY15, (g,h) BY5.*

experiment resulting in a warming of more than $1.8\,°C$ in the depths between 15 and $30\,m$ whereas in May the upper $10\,m$ are colder by about $2\,°C$. Although the picture is somewhat different in different basins depending on background stratification and atmospheric forcing, in all basins mixed layer depths in autumn are larger in 1D than in 3D simulations. In addition, the seasonal thermocline is much smoother.

The following theory might explain the situation at Gotland Deep for example. In the 3D simulation vertical velocities due to Ekman pumping/suction elevate the upper halocline (Fig.16b). In addition, horizontally advected intrusions of water masses into the halocline originating from the corresponding upstream basin (here the Bornholm Basin) are observed. These oscillations can be found in observations too (Fig.16a) but the 3D model tends to overestimate amplitudes and tends to smooth the halocline gradient resulting in an artificial re-stratification of the upper well mixed layer between 30 and 50 m depth. Thus, background stratification in this depth range is greater in the 3D model than in observations and in the 1D model more than ever. There are no vertical oscillations in the 1D simulation consequently (Fig.19b). Thus, TKE can penetrate deeper without being dissipated by the background stratification. A horizontal re-stratification mechanism is missing in 1D simulations and is overestimated in 3D simulations. Hence, viscosities and diffusivities in autumn and winter and the seasonal thermocline depth in autumn are larger in the sensitivity experiment without advection. In summer the analysis of model results shows that the Brunt-Väisälä frequency maximum is deeper in 3D than in 1D together with larger vertical velocity shear in the seasonal thermocline. Obviously, the shear production term P in (5) generates more TKE in 3D than in 1D resulting in a shallower seasonal thermocline in the 1D simulation.

To test the assumption that due to smaller stratification of the upper layer in the 1D simulation (compare Fig.16b and Fig.19b) TKE could penetrate deeper without being dissipated by the background stratification, two sensitivity experiments with constant salinity have been performed (no background stratification) for the 1D and 3D case, respectively (Fig.22). Indeed, the results are quite different compared to Fig.21 indicating that background stratification plays an important role generating differences between 1D and 3D simulation. However, more investigations are necessary to elucidate the mechanism further.

In Figure 23 two different horizontal resolutions of RCO are compared (2 and 6 nm). The overall differences in mixed layer depth are smaller than in Fig.21 but can not be neglected. In Gotland Basin the seasonal thermocline is simulated deeper in summer and autumn with increased horizontal resolution. Although 2 nm grid resolution is regarded as eddy permitting only (determined by the size of internal Rossby radii, cf. Fennel et al., 1991), horizontally propagating waves are partly better resolved generating more TKE than in case of the coarse resolution version. However, results are looking different in different basins making conclusions difficult.

In any case the experiments show that the depth of the seasonal thermocline depends not only on the used turbulence model but also on the used ocean circulation model.

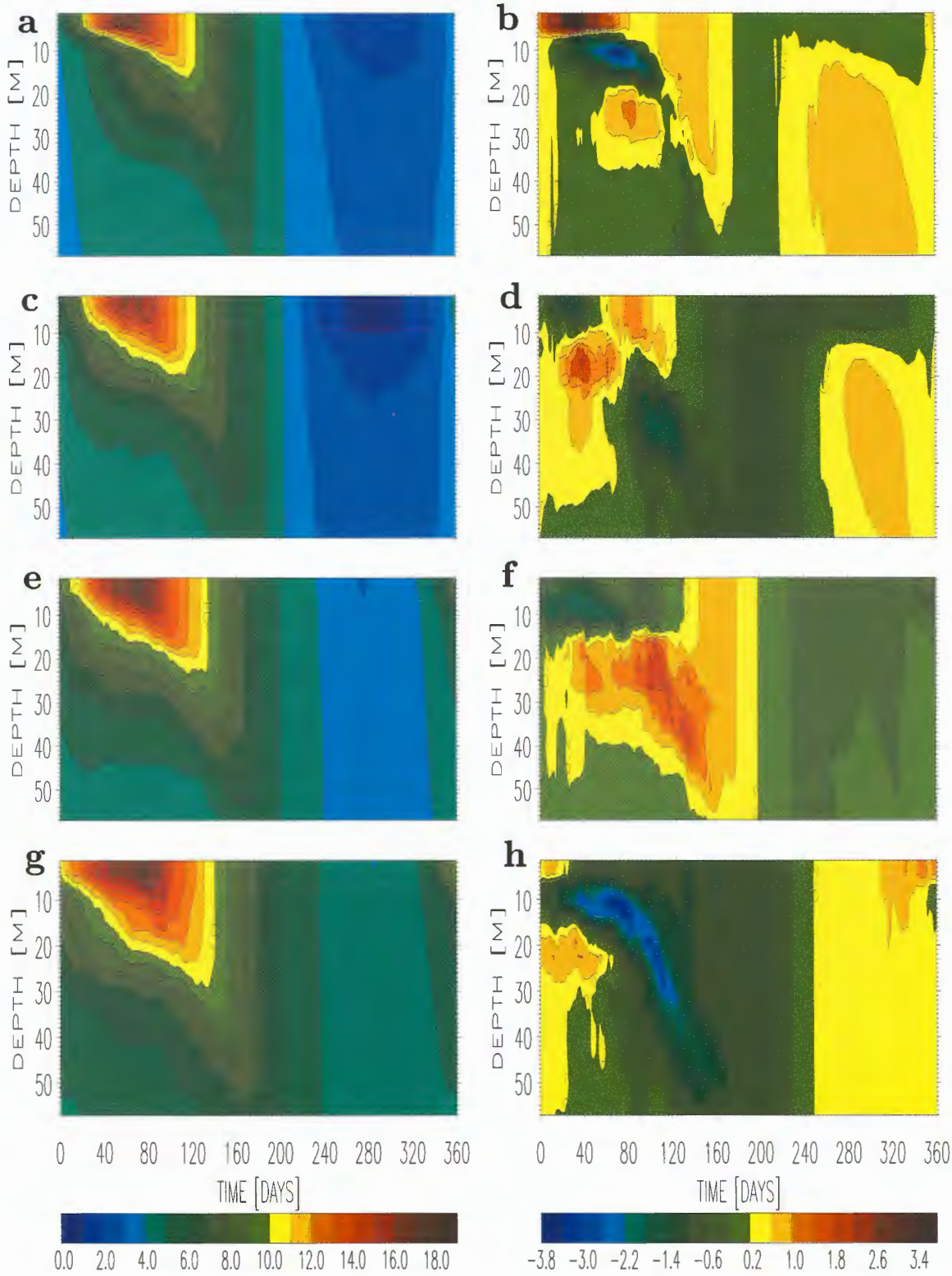

Figure 22: *As Fig.21 but calculated without advection and without salinity (left column) and difference between constant salinity simulations without and with advection (right column): (a,b) SR5, (c,d) LL07, (e,f) BY15, (g,h) BY5.*

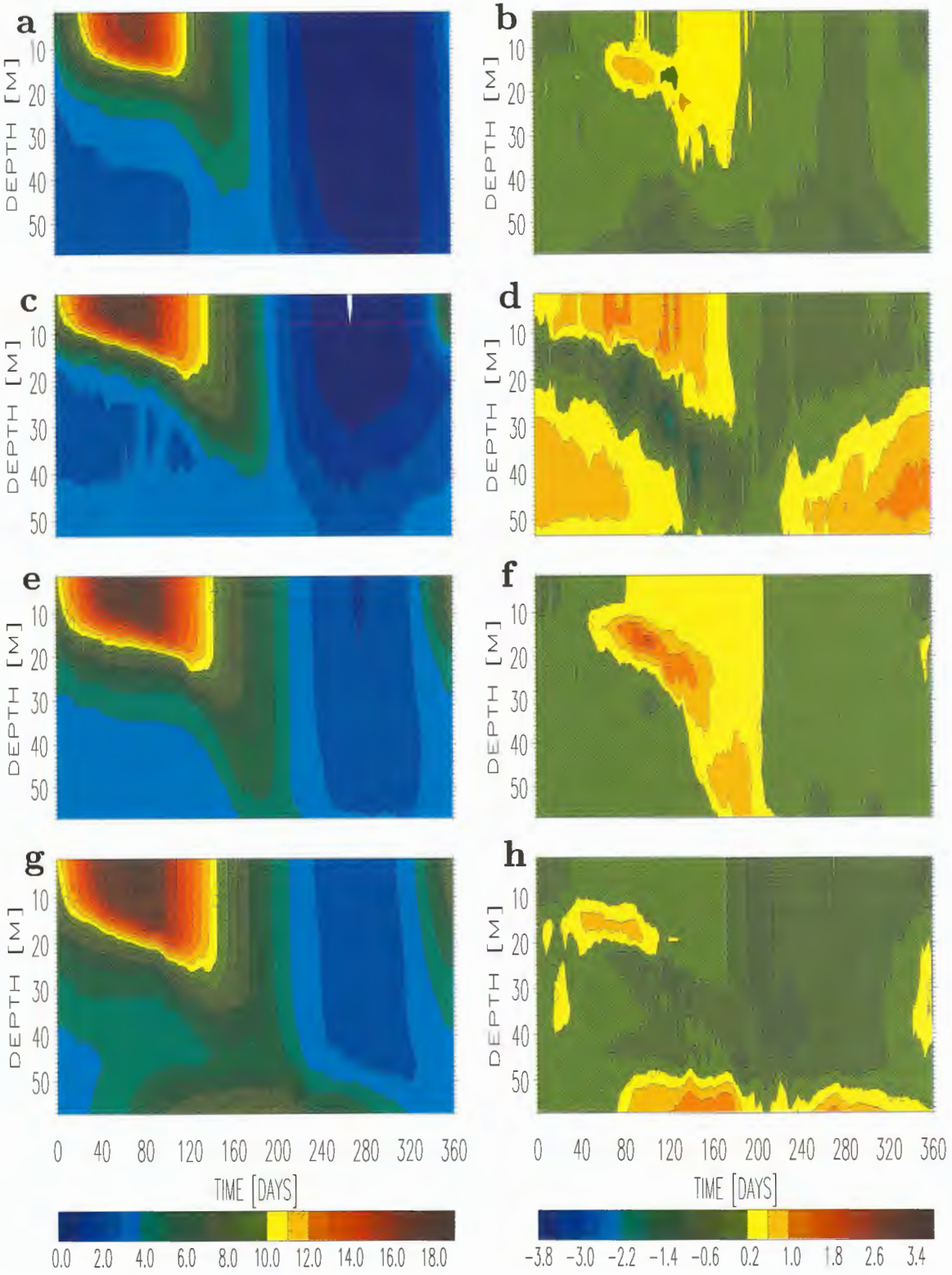

Figure 23: *As Fig.14 but using 2 nm horizontal resolution (left column) and difference between simulations using 2 and 6 nm horizontal resolution (right column): (a,b) SR5, (c,d) LL07, (e,f) BY15, (g,h) BY5.*

Regardless of performance the choice of the ocean circulation model (1D or 3D, horizontal grid resolution) is more important or comparatively important than including surface flux boundary conditions to the $k-\epsilon$ model, reducing dissipation in stratified fluid (with critical Richardson number $Ri_c = 1$), replacing the equation for dissipation by an appropriate algebraic equation for the turbulent length scale or introducing theoretically improved stability functions according to Canuto et al. (2000) (compare Fig.21 and Fig.23 with Fig.14, Fig.9 and Fig.15). Hence, improvements of the $k-\epsilon$ model tested in 1D studies can not be adopted automatically to the $k-\epsilon$ model embedded in the two 3D Baltic Sea models presented here.

12 Sensitivity of Baltic Sea climate

In Figures 3 and 4 standard $k-\epsilon$ model and Richardson number dependent friction have been compared utilizing the regional high-resolution model of the western Baltic. It is shown that the summer thermocline in Bornholm Basin is much too shallow compared to observations if in the simulation Richardson number dependent friction is used. As this local approach has been used in several models in the past, e.g., Lehmann (1992, 1995), Meier and Krauss (1994) or Schmidt et al. (1998), the model comparison have been extended to the other basins of the Baltic Sea and to multi-year integrations between May 1980 and December 1993 using RCO. In addition, the sensitivity of the mean state of the Baltic Sea (mean profiles, mean SST, mean heat fluxes, etc.) on the mixed layer depths has been analyzed. Especially, the impact on sea ice has been explored addressing the important question if a coupled ice-ocean model is really necessary to investigate the Baltic Sea ice season climatology. For example, a very sophisticated ice model for the Baltic with different ice classes has been presented by Haapala and Leppäranta (1996) and Haapala (2000) which is coupled to a less sophisticated ocean model consisting of a barotropic circulation model with 4-layer vertical thermodynamic evolution. The aim here is to find out the role of the ocean, in special the role of mixing in the ocean, for atmosphere-ice-ocean interaction and to find out how complex the ocean model has to be for climate investigations. The results are presented in this section.

12.1 Mean temperature and salinity profiles

In Figure 24 median profiles of temperature and salinity for the period May 1980 until December 1993 are shown at four stations. The model profiles have been selected at the same dates as the data to avoid a comparison between high-frequent model results and undersampled observations in time. With sufficient quality there are 121 profiles in the Bothnian Sea, 106 in the Gulf of Finland, 153 in the Gotland Basin and 253 in the Bornholm Basin available. There is a good agreement between observations and model results. The simulation has been performed with the improved $k-\epsilon$ model using reduced dissipation in stratified fluids (Mellor, 2000). The model reproduces salinity gradients from North to South as well as from the surface to the bottom. The halocline

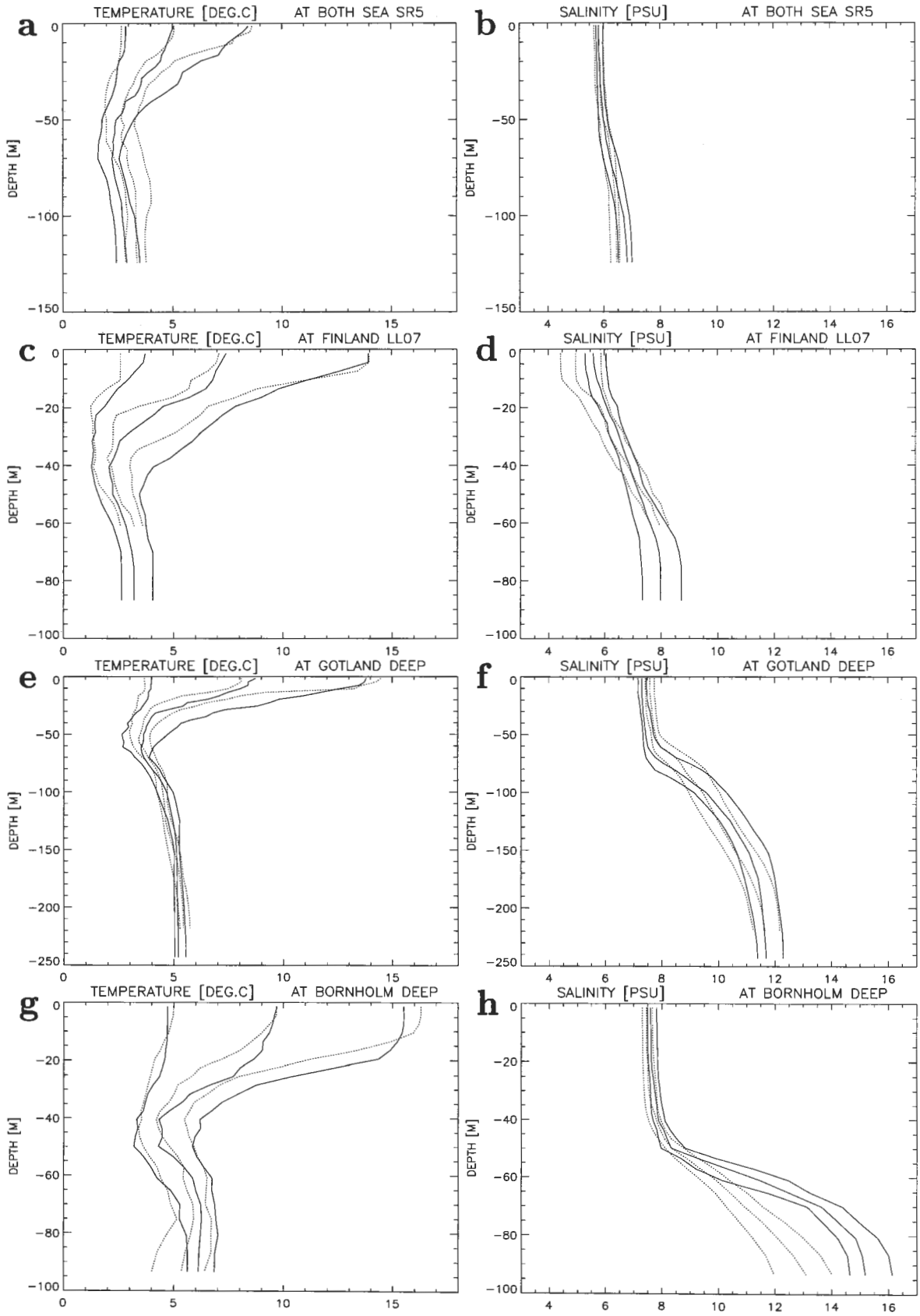
a
TEMPERATURE [DEG.C] AT BOTH SEA SR5
b
SALINITY [PSU] AT BOTH SEA SR5
c
TEMPERATURE [DEG.C] AT FINLAND LL07
d
SALINITY [PSU] AT FINLAND LL07
e
TEMPERATURE [DEG.C] AT GOTLAND DEEP
f
SALINITY [PSU] AT GOTLAND DEEP
g
TEMPERATURE [DEG.C] AT BORNHOLM DEEP
h
SALINITY [PSU] AT BORNHOLM DEEP
DEPTH [M]

Figure 24: *Previous page: Observed (solid) and with $k-\epsilon$ model simulated (dotted) median, first and third quartile profiles for temperature (in ^{o}C) and salinity (in psu) from the period May 1980 until December 1993 at SR5 (a,b), LL07 (c,d), BY15 (e,f) and BY5 (g,h).*

is not eroded during the almost 5000 days long integration. However, the problem of coarse resolution level models with overflow is visible in results from Bornholm Basin. The continuous inflow of salt water from Kattegat into the Baltic Sea is underestimated resulting in too strong decrease of bottom layer salinity visible after about 1000 days of integration (not shown). After 5000 days of integration the median of simulated bottom salinity is about 2 psu smaller than observed. As the bottom boundary layer is not resolved accurately, smaller inflows over the sills of the Danish Straits and through Bornholm Channel are not simulated satisfactory. Increased horizontal resolution or a bottom boundary layer model as described by Beckmann and Döscher (1997) will help to overcome these problems in the next RCO version.

In addition, Figure 24 shows that the seasonal heat cycle is simulated correctly. Especially, median sea surface temperatures reveal a very small error. The differences between simulated and observed median SSTs are smaller than $0.5^{o}C$. The revised heat flux package (see Appendix A and B) together with the improved $k-\epsilon$ turbulence model contribute to the good results. There is still slight underestimation of mixed layer depth as can be seen from the third quartiles in Fig.24.

In Figure 25 the same median profiles are shown but in the simulation Richardson number dependent friction is used. Model results are not satisfactory compared to observations. At the sea surface median temperatures are too high (about $1\,^{o}C$) except in the Gulf of Finland and the differences of the third quartiles are even higher (more than $3\,^{o}C$ in the Bothnian Sea). Median temperatures in deeper than $5\,m$ are much too cold because of the underestimated mixed layer depth. Simulated first quartiles are about $1\,^{o}C$ colder at the sea surface in Gotland Basin and Gulf of Finland, but slightly warmer in Bornholm Basin and identical in the Bothnian Sea.

Stratification has serious shortcomings too. The halocline in Gotland Basin is shifted by about $50\,m$ towards the surface and sea surface salinity is smaller in all 4 basins. The Richardson number dependent friction is not able to homogenize the upper layer in Bornholm and Gotland Basin. Only deep water in Bornholm Basin is simulated better with the Richardson number dependent approach than with the $k-\epsilon$ model indicating that shortcomings of the mixing scheme contribute to the overflow problem. Not only the coarse model resolution is responsible for the lack of high saline water flowing downhill into Bornholm Deep. Meier (1996) has shown that simulated model velocities in the western trench of the Great Belt near the Danish island Sprogø are in perfect agreement with current velocity data from different depths during November and December 1992, if Richardson number dependent friction is used (see his Fig.18). The position of Sprogø is shown in Fig.2. Obviously, it is possible to simulate current velocities in channels of good quality with the Richardson number approach although

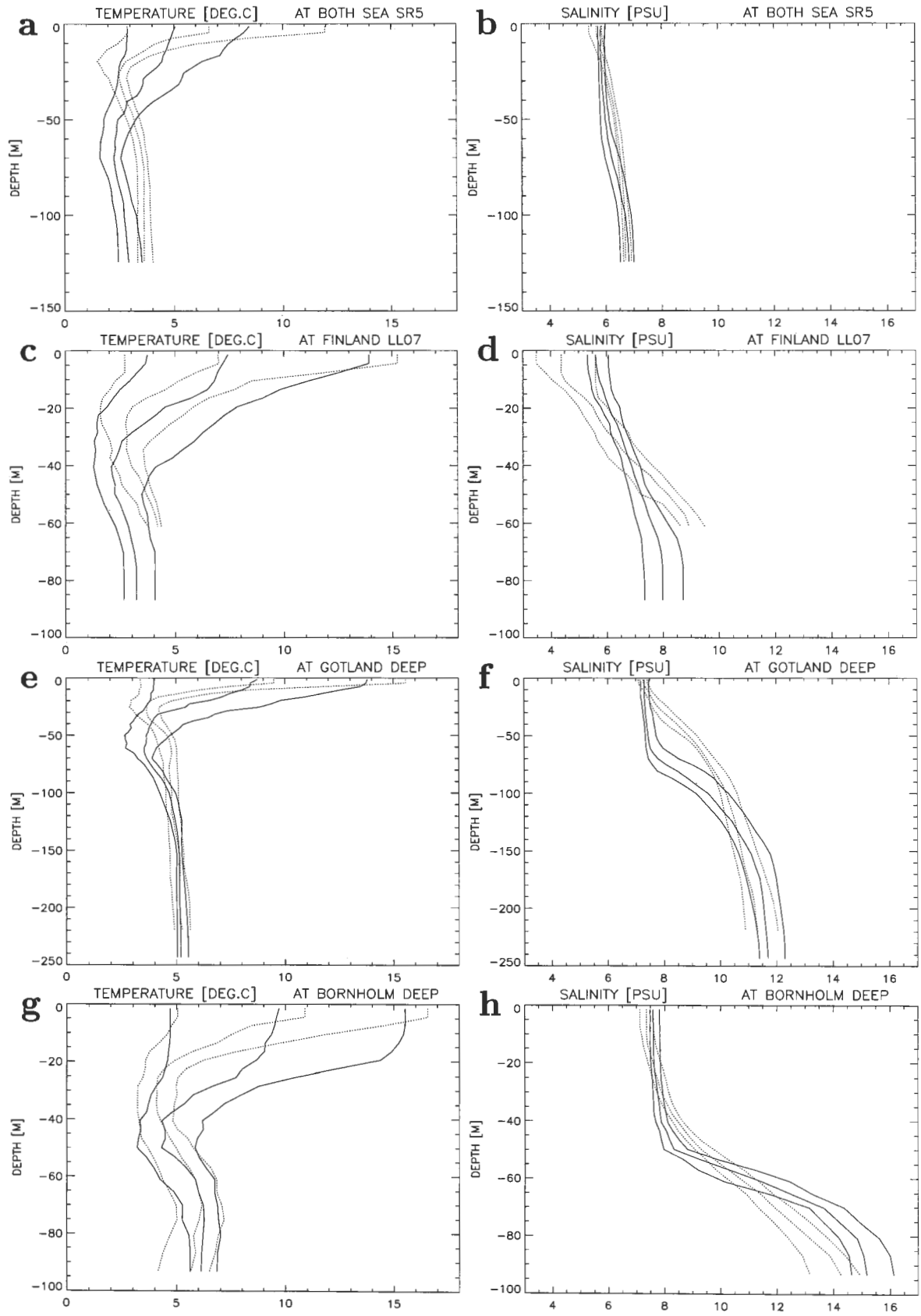
a
TEMPERATURE [DEG.C] AT BOTH SEA SR5
b
SALINITY [PSU] AT BOTH SEA SR5
c
TEMPERATURE [DEG.C] AT FINLAND LL07
d
SALINITY [PSU] AT FINLAND LL07
e
TEMPERATURE [DEG.C] AT GOTLAND DEEP
f
SALINITY [PSU] AT GOTLAND DEEP
g
TEMPERATURE [DEG.C] AT BORNHOLM DEEP
h
SALINITY [PSU] AT BORNHOLM DEEP
DEPTH [M]

Figure 25: *Previous page: As Fig.24 but in the simulation Richardson number dependent friction is used instead of the $k-\epsilon$ model.*

mixing at the surface is underestimated tremendously. Further investigations are necessary in context with the planned embedded bottom boundary layer model in RCO.

12.2 Mean seasonal cycle of temperature profiles

In Figure 26 the 13-year mean seasonal cycle of isotherm depths in 4 different basins using Richardson number dependent friction are shown (left column). The differences between $k-\epsilon$ model and this local approach are extremely large (right column). The reader should note the different color bar compared to Fig.9, Fig.14, Fig.15, Fig.21, Fig.22 and Fig.23 indicating that the differences discussed earlier are much smaller. Mixed layer depths in summer and winter are underestimated. SSTs in spring are warmer but in winter colder than in simulations using the $k-\epsilon$ model. The whole water column is affected by the mixing scheme with differences between $k-\epsilon$ model and Richardson approach of more than $6\,°C$ in summer and more than $-1\,°C$ in winter in most basins (except Gulf of Finland where the differences are slightly smaller).

12.3 Sea ice extent, ice and snow thickness

In Figure 27 ice extent, ice and snow thickness are shown for a 13-year simulation using the $k-\epsilon$ model. Figure 27a shows simulated total ice extent compared with the observed maximum ice extent. Ice extent is highly correlated with air temperature but represents also a sensitive measure of the coupled ice-ocean model performance. The model must cover the high variability of observed ice extent. Contrary, other variables like ice thickness of the Bothnian Bay have lower variability. Hence, the correspondence between model results and observations in Figure 27a is encouraging. In some mild winters maximum ice extent is somewhat overestimated. However, the overall agreement is good. That is also true for the date when the maximum ice extent occurred. There is only one exception (winter 1988/89) when the ice model predicted a higher ice extent much earlier than the observations.

In Figure 27b and c ice and snow thickness model results are compared to measurements at the coastal station Kemi-Ajos in the northern Bothnian Bay (cf. Fig.1). The data are published in reports of the Finnish Institute of Marine Research (Finnish Marine Research, 1982; Kalliosaari and Seinä, 1987; Seinä and Kalliosaari, 1991; Seinä and Peltola, 1991; Seinä et al., 1996). The agreement is regarded as very good although ice thickness during the severe winter 1985/86 is overestimated and although snow thickness is underestimated during some years (e.g., 1982/83). However, one has to keep in mind that the precipitation data from the SMHI data base might have a large error and that the utilized snow ice model is quite simple (cf. Meier et al., 2000). Ice and snow thicknesses are very sensitive against changes in the snow ice model.

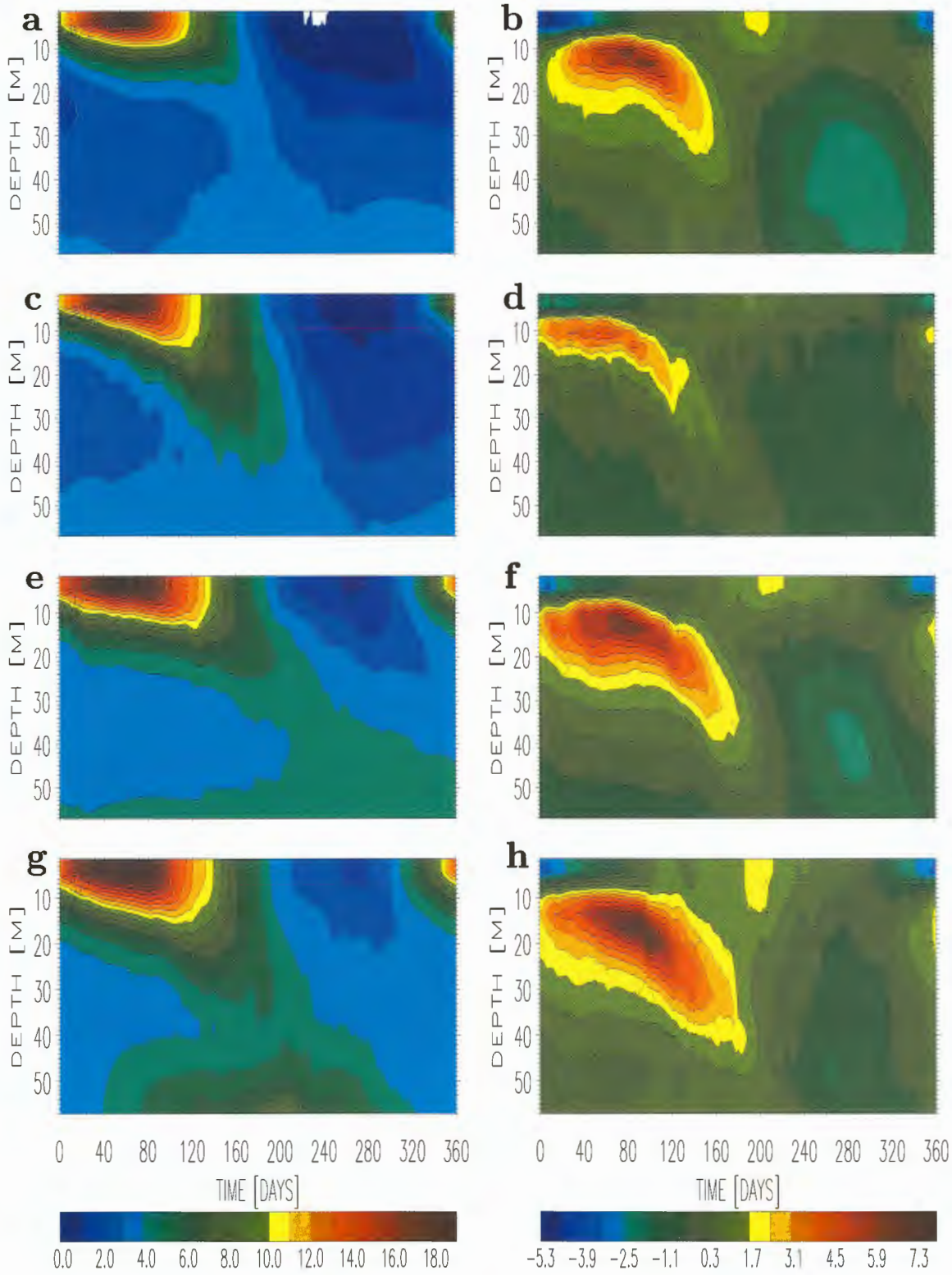

Figure 26: *As Fig.14 but using Richardson number dependent friction (left column) and difference between simulations with $k-\epsilon$ model and Richardson number dependent friction (right column): (a,b) SR5, (c,d) LL07, (e,f) BY15, (g,h) BY5.*

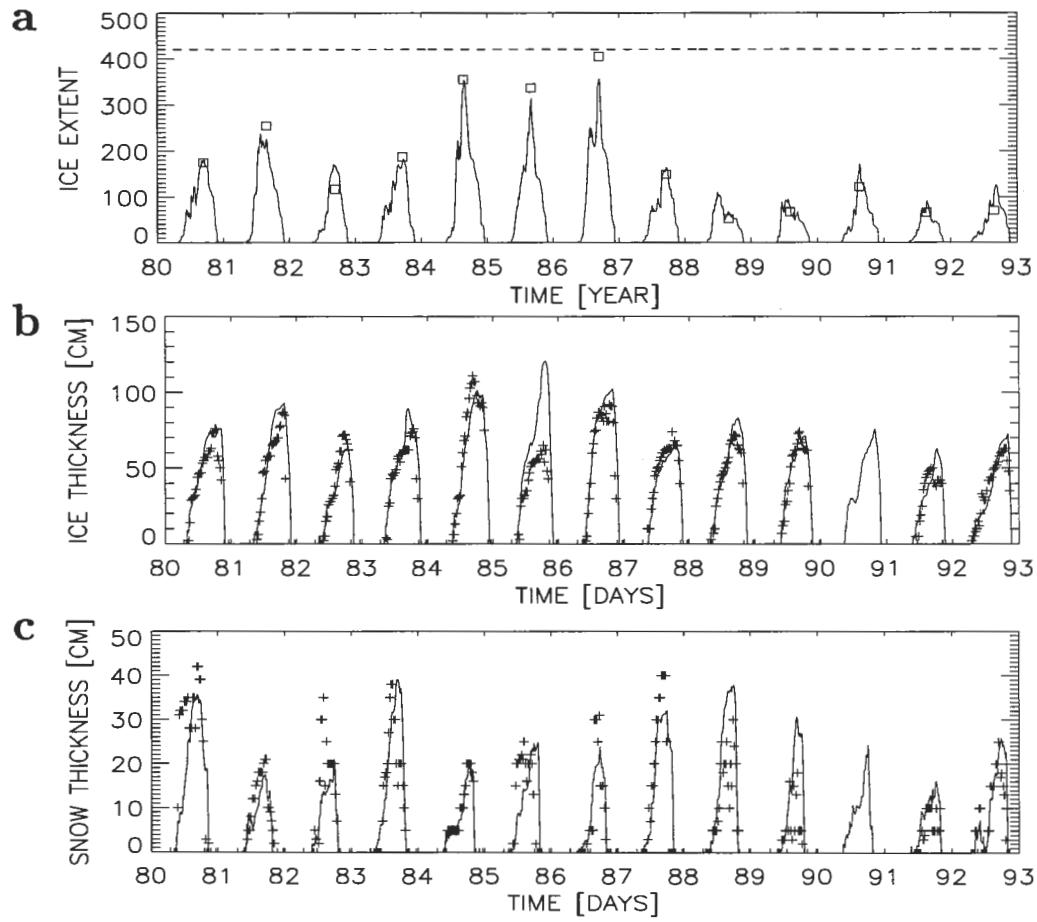

Figure 27: *(a) Simulated ice covered area (in $10^9\,m^2$) for the period July 1980 until June 1993. Tickmarks denote July 1 of the corresponding year. Squares denote observed maximum ice extent (adopted from Omstedt and Nyberg, 1996). In the lower panels simulated ice (b) and snow (c) thickness (in cm) at the monitoring station Kemi-Ajos (Bothnian Bay) are shown. Plus signs denote observations from Finnish Marine Research (1982), Kalliosaari and Seinä (1987), Seinä and Kalliosaari (1991), Seinä and Peltola (1991) and Seinä et al. (1996). For winter 1990/91 data are not available for this paper. The position of Kemi-Ajos is shown in Figure 1.*

In Figure 28 the corresponding results of the Richardson number dependent mixing are shown. Ice extent is much larger. During three winters, 1984/85, 1985/86, 1986/87, the sea surface of the model domain is covered by ice completely. In addition, ice and snow thickness at Kemi are increased too. As discussed in Section 10 ice thickness is very much dependent on the ice-ocean heat flux which is parameterized only crudely. Probably a better parameterization or a better vertical resolution of near surface processes might show an even larger sensitivity of ice and snow thickness against the used mixing scheme. For the moment this is an open question.

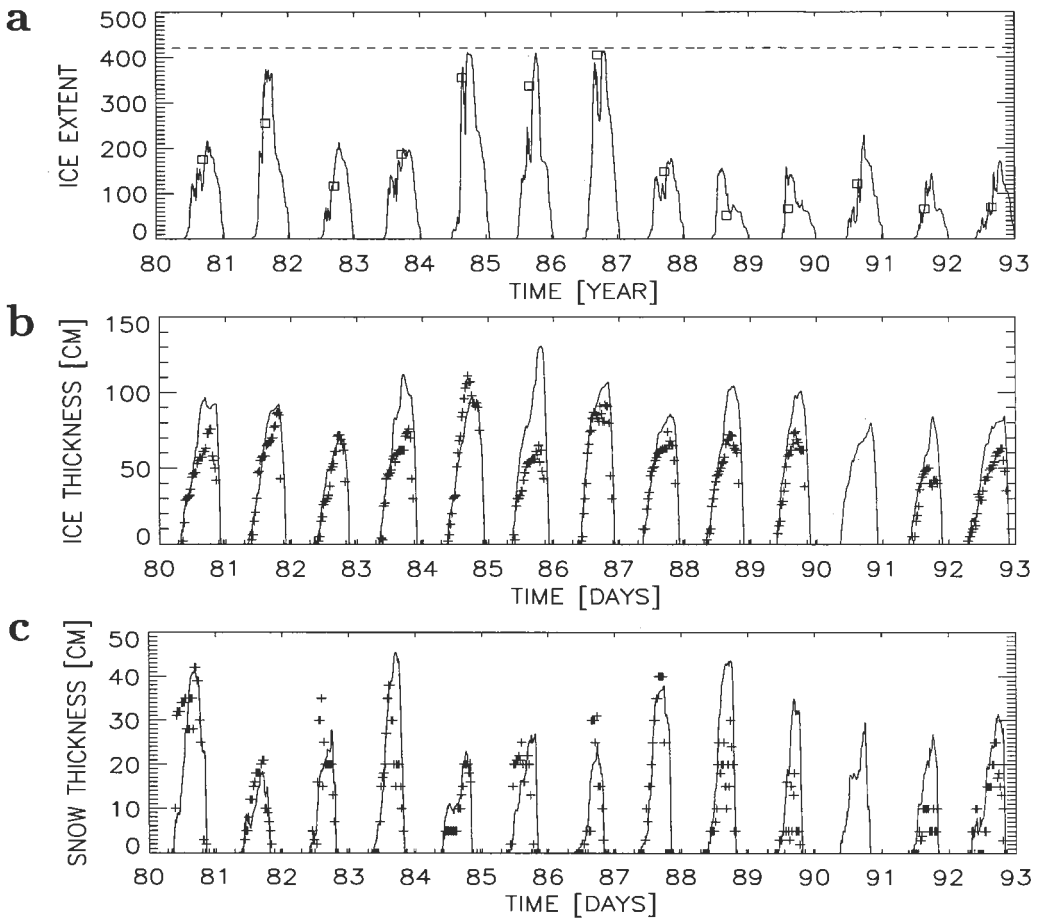

Figure 28: *As Figure 27 but simulated with Richardson number dependent viscosity and diffusivity.*

12.4 Mean sea surface temperatures

13-year mean SSTs of the period May 27 1980 until May 26 1993 for both mixing schemes are shown in Figure 29. The differences are in the range between -1 and $+0.8\,°C$. Coastal SSTs are colder with the Richardson approach but warmer in the centers of the southern Gotland Basin, Bothnian Sea and Bothnian Bay. Also the central Gulf of Finland is slightly warmer. The differences are smaller than those of simulations of the reference experiment with and without advection as shown in Fig.20 but of the same order of magnitude. The effect of underestimated mixed layer depths on the mean SST is almost as dramatic as the effect of advection. The seasonal change of heat content in the upper water column is much smaller in case of the Richardson number dependent mixing scheme than in case of the $k-\epsilon$ model. A change of $1\,°C$ in mean SST is quite important for the Baltic Sea heat budget resulting in heat flux differences of more than $10\,W\,m^{-2}$ as shown in the next section.

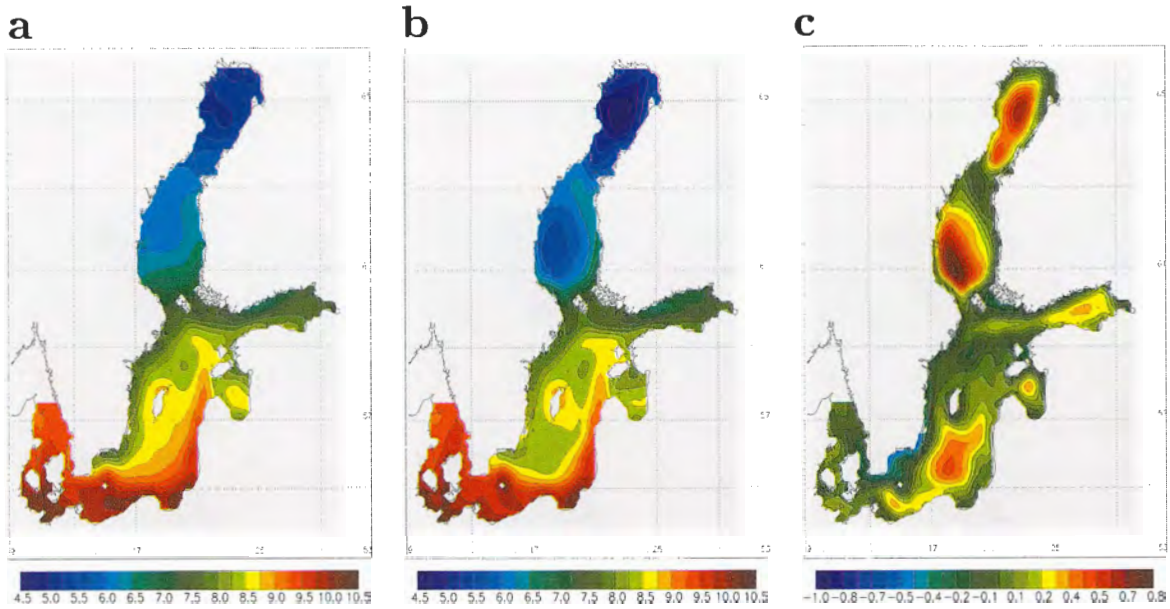

Figure 29: *Mean sea surface temperature (in °C) for the period May 27 1980 until May 26 1993: (a) Richardson number dependent friction, (b) $k - \epsilon$ turbulence model and (c) the difference between (a) and (b).*

12.5 Mean heat fluxes between atmosphere and ice/ocean

The total heat flux (Q_a) from the atmosphere into the coupled ice-ocean system consists of 10 components: shortwave (Q_{SW}), incoming ($Q_{LW\downarrow}$) and outgoing ($Q_{LW\uparrow}$) longwave radiation, sensible (Q_S) and latent (Q_L) heat flux into the ocean and into the sea ice:

$$Q_a = Q_a|_{noice}\,(1 - A) + Q_a|_{ice}\,A \tag{62}$$

with

$$Q_a|_{noice} = Q_{SW}|_{noice} + Q_{LW\downarrow}|_{noice} - Q_{LW\uparrow}|_{noice} + Q_S|_{noice} + Q_L|_{noice}\,, \tag{63}$$

and a corresponding formula for the ice case:

$$Q_a|_{ice} = Q_{SW}|_{ice} + Q_{LW\downarrow}|_{ice} - Q_{LW\uparrow}|_{ice} + Q_S|_{ice} + Q_L|_{ice}\,. \tag{64}$$

The used bulk formulae are given in Appendix A and B. During the summation the fluxes into the sea ice must be multiplied with ice concentration A and the fluxes into the ocean with $1 - A$. Thus, atmosphere-ocean heat fluxes in leads are taken into account. Net longwave radiation is given by $Q_{LW} = Q_{LW\downarrow} - Q_{LW\uparrow}$.

For the comparison with older reports (Meier et al., 1999; Meier, 1999a) the reader has to keep in mind that the bulk formulae for heat fluxes have been changed to get better agreement with observations. The earlier used heat flux package by Meier et al. (1999), which followed mainly Omstedt and Nyberg (1995), resulted systematically in too low winter SSTs over the whole model domain and has been replaced consequently. In Meier (1999a) depicted heat fluxes were by a factor 2 too large (but not the heat

fluxes in the model) because the analysis software was erroneous.

In Figure 30 13-year mean net heat fluxes are shown. The differences between simu-

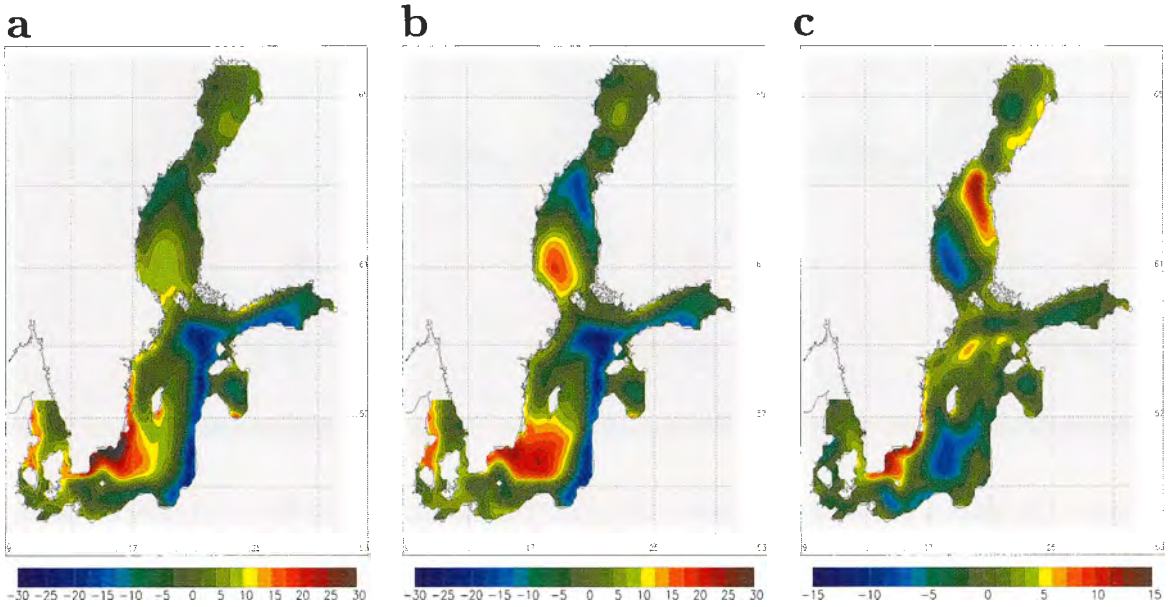

Figure 30: *Mean net heat flux (in $W\,m^2$) for the period May 27 1980 until May 26 1993: (a) Richardson number dependent friction, (b) $k-\epsilon$ turbulence model and (c) the difference between (a) and (b). Positive values indicate fluxes into ice or ocean.*

lations with Richardson number dependent friction and $k-\epsilon$ turbulence model are in the range between -15 and $+15\,W\,m^{-2}$. These are smaller than the mean heat flux differences between experiments with and without sea ice which are up to $47\,W\,m^{-2}$ (cf. Fig.23a by Meier, 1999a) but larger than the differences between experiments with and without ice dynamics which are in the range between -4 and $+5\,W\,m^{-2}$ (cf. Fig.23b by Meier, 1999a). The Richardson number dependent mixing scheme results in higher net heat fluxes into the Baltic close to the Swedish coast in Bornholm and Gotland Basin and in the northern central Gotland Basin. The net heat flux difference is also positive in the north-eastern Bothnian Sea and close to the Finnish coast in the south-eastern Bothnian Bay. Negative differences $> -7\,W\,m^{-2}$ are observed in the southern central Gotland Basin and in the south-western Bothnian Sea with higher net heat fluxes into the Baltic simulated with the $k-\epsilon$ model.

In Figures 31 and 32 the components of net heat flux Q_{SW}, Q_{LW}, Q_S and Q_L are depicted. Thereby, each heat flux is composed of two components. For example the shortwave radiation is calculated according to

$$Q_{SW} = Q_{SW}|_{noice}\,(1-A) + Q_{SW}|_{ice}\,A\,, \tag{65}$$

whereby the second term is much smaller than the first one. Shortwave radiation is always positive of course and is mainly distributed in latitudinal direction. Net longwave radiation, sensible and latent heat are always negative and show similar patterns

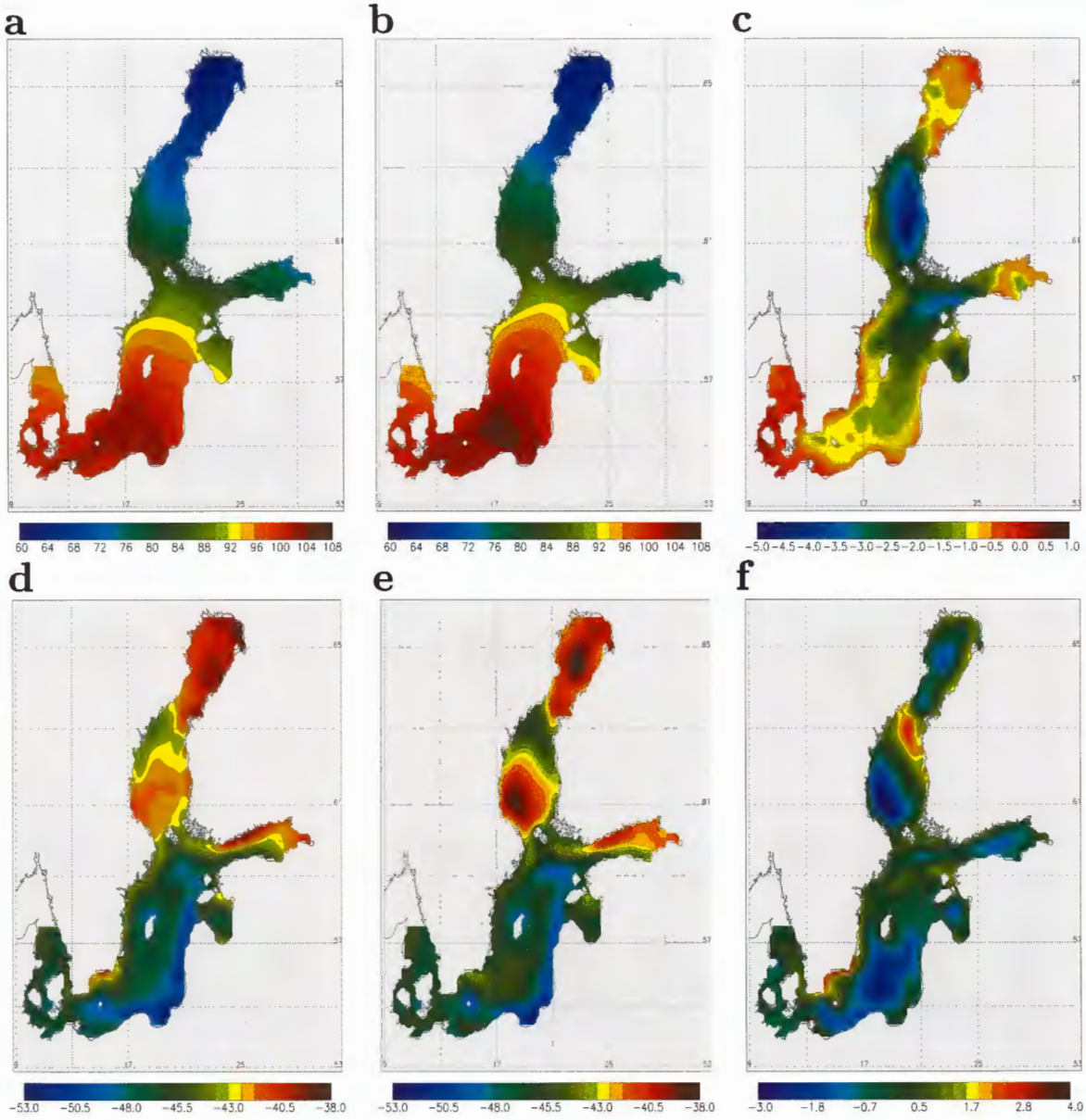

Figure 31: *As Fig.30 but for shortwave (a,b,c) and longwave radiation (d,e,f). Note the different color bars.*

than the net heat flux but with local deviations. The same is true for the differences.

In Table 4 the horizontally integrated values of the heat flux components are listed and compared for the two experiments.

The net differences are quite small (largest for sensible heat with about $2\,W\,m^{-2}$). The two mixing schemes redistribute heat fluxes in horizontal direction differently but the total net heat uptake of about $1\,W\,m^{-2}$ is not altered. This is true also for each of the heat flux components. The result that the heat budget of the Baltic Sea within the 3D model is almost closed (small heat transport out of the Danish Straits) is quite

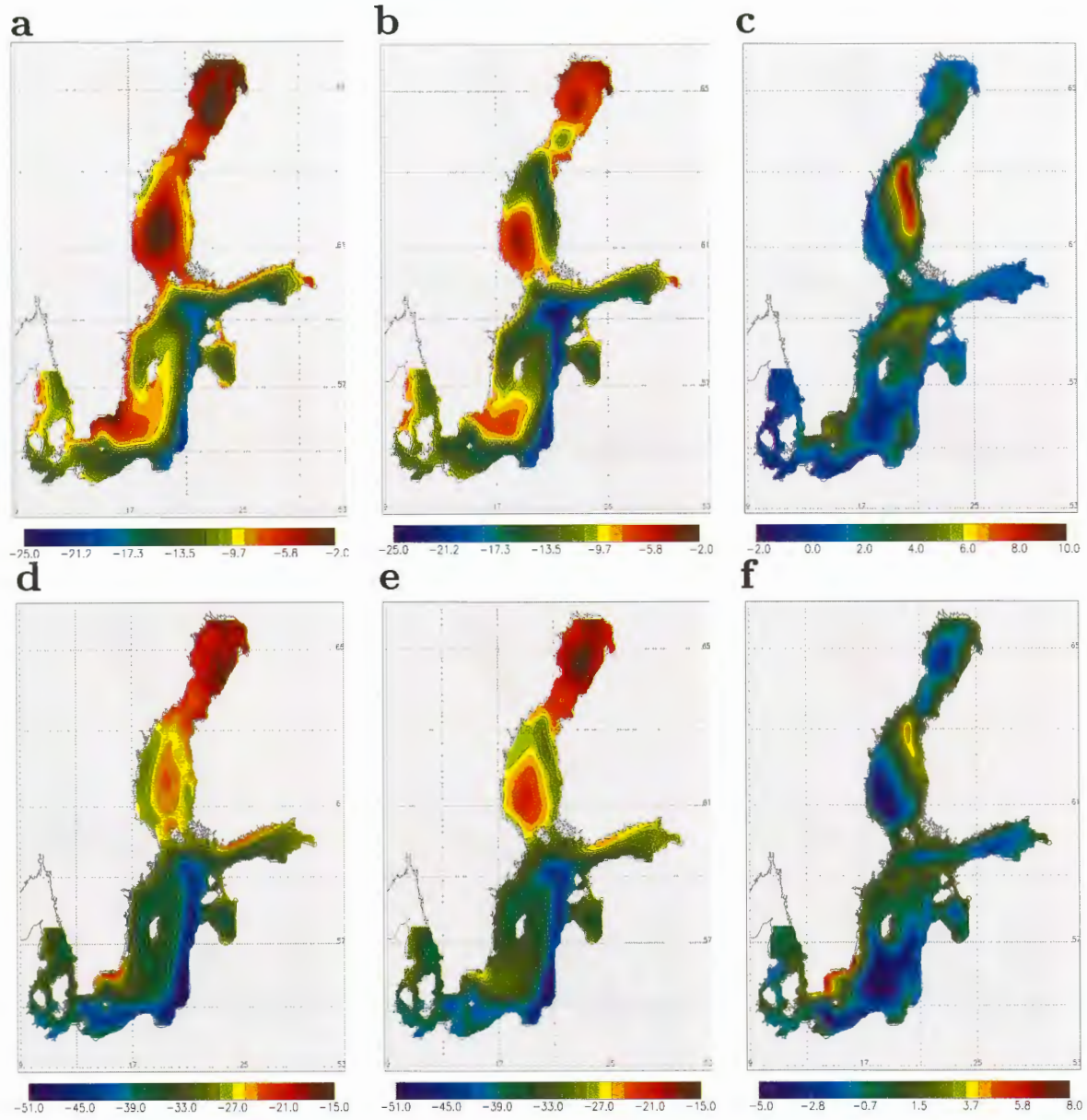

Figure 32: *As Fig.30 but for sensible (a,b,c) and latent heat (d,e,f).Note the different color bars.*

	Q_a	Q_{SW}	Q_{LW}	Q_S	Q_L
$k-\epsilon$	1.0	90.7	-45.1	-12.0	-32.7
Ri	1.4	89.3	-45.2	-9.8	-32.9

Table 4: *13-year mean heat fluxes (in $W\,m^{-2}$) for the period May 27 1980 until May 26 1993 for simulations with $k-\epsilon$ model with reduced dissipation and with Richardson number dependent friction.*

robust with respect to changes in the mixing parameterization, although these changes affect mixed layer depths tremendously. Also Omstedt and Rutgersson (2000) found that the Baltic Sea is almost in thermodynamical equilibrium with the atmosphere

as a long-term mean. Using for the Baltic Sea a completely different process-oriented model consisting of 13 horizontal boxes they calculated a net heat uptake at the water surface of $1\,W\,m^{-2}$ too (note that the signs by Omstedt and Rutgersson (2000) are reversed compared to this report).

12.6 Mean seasonal cycle of surface heat fluxes

Simulated mean seasonal cycles for surface heat fluxes into the atmosphere and out of the sea ice/snow are shown in Figure 33. The budgets are calculated according to

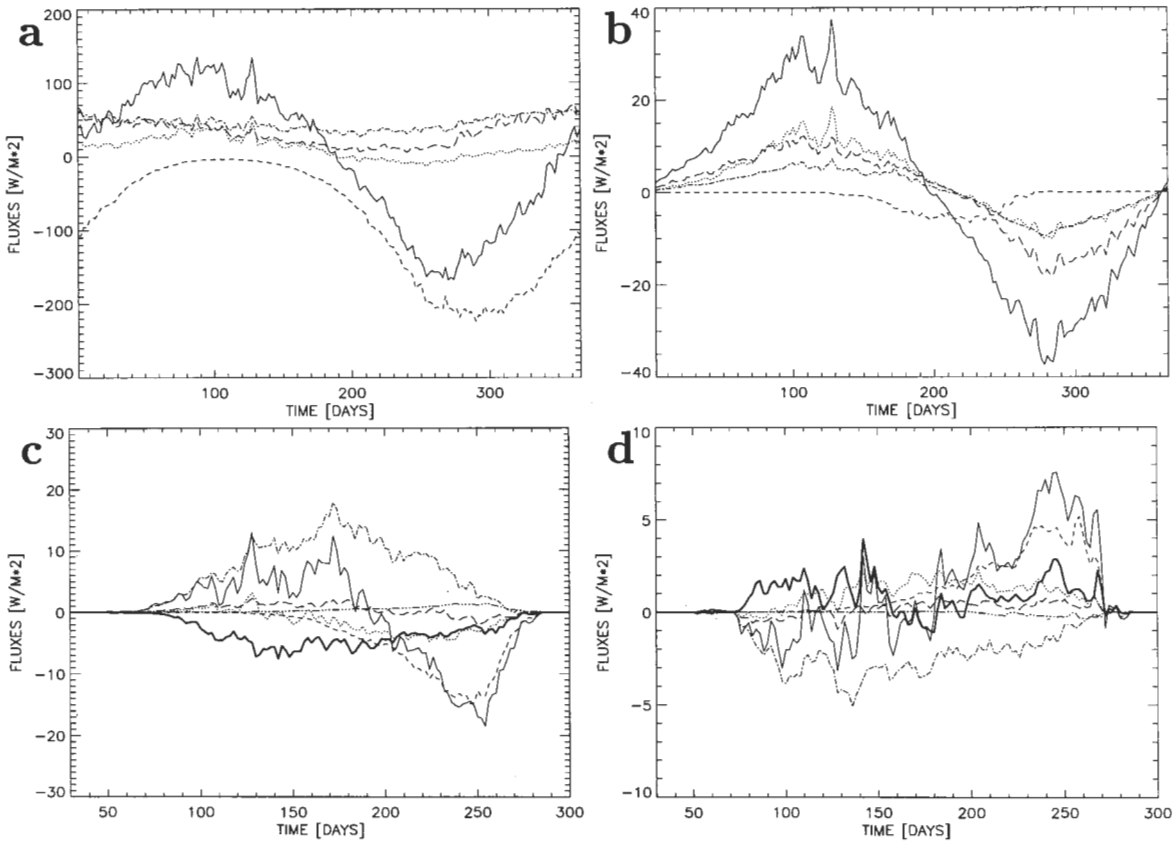

Figure 33: *(a) Mean seasonal cycle of surface fluxes (in $W\,m^{-2}$) into the atmosphere from September until August of the following year using the $k-\epsilon$ model. Positive values indicate heat fluxes into the atmosphere (solid: net heat flux, dashed: shortwave radiation, dashed-dotted: longwave radiation, dotted: sensible heat, long-dashed: latent heat). In (b) the difference between simulations using the $k-\epsilon$ model and Richardson number dependent friction is depicted. (c) and (d) are the same as (a) and (b), respectively, but show mean fluxes into the ice/snow system. Positive values indicate heat fluxes out of the ice/snow. In addition to (a) or (b) the ice-ocean heat flux (bold solid, always negative) and the shortwave radiation penetrating the sea ice (dashed-dotted with 3 dots, always positive) is shown. Note that the time axis is reduced (start after 30 days at October 1).*

(62) and (64), respectively. The amplitude of the seasonal cycle of the net heat fluxes

into the atmosphere is about $40\,W\,m^{-2}$ larger with $k-\epsilon$ model than with Richardson approach. In winter the difference is mainly explained by sensible and latent heat and to less extent by longwave radiation and in summer mainly by latent heat and to less extent by sensible heat and longwave radiation.

For the net heat flux into the ice/snow lateral freezing is neglected. The bottom heat flux between ice and ocean must be always negative (into the ice) because model SST is limited by freezing point temperature. Thus, the sea ice gains always heat from the ocean. During ice growth in winter net longwave radiation is large causing a net heat flux out of the ice (Fig.33c). In spring the shortwave radiation gets more and more important. Thus, net heat flux is directed into the ice causing ice melt. As there is more ice with Richardson number dependent friction, the net heat flux out of the ice/snow phase is smaller with $k-\epsilon$ model during freezing in early winter by up to $-3\,W\,m^{-2}$ and the net heat flux into the ice/snow phase is smaller during melting in spring by up to $7\,W\,m^{-2}$ (Fig.33d). Thus, the amplitude of the seasonal cycle is smaller with $k-\epsilon$ model than with Richardson approach. The bottom heat flux between ice and ocean is less negative (smaller into the ice) with the $k-\epsilon$ model with differences up to $2\,W\,m^{-2}$. Shortwave radiation (larger/more negative with the Richardson approach mainly in spring, maximum difference: $5\,W\,m^{-2}$) and longwave radiation (larger/more positive with the Richardson approach mainly in early winter, maximum difference: $-5\,W\,m^{-2}$) contribute to the net heat flux into the ice/snow system most.

13 Summary and conclusions

For the Baltic Sea different mixing schemes to be embedded in 3D circulation models have been compared and discussed: local parameterizations, e.g., the Richardson number dependent friction according to Pacanowski and Philander (1981) or the scheme according to Kochergin (1987), a reduced Kraus-Turner type model (Niiler and Kraus, 1977) and a turbulence model consisting of the prognostic equation for turbulent kinetic energy (TKE) together with a diagnostic equation for the turbulent length scale according to Gaspar et al. (1990). These earlier investigated mixing parameterizations led to serious shortcomings predicting the seasonal thermocline. Hence, a second-order moment turbulence closure model, the $k-\epsilon$ model, has been tested.

The $k-\epsilon$ turbulence model has been successfully embedded into two 3D circulation models of the Baltic Sea with different horizontal resolution. Mixed layer depths and SSTs are simulated realisticly using standard parameters which are adopted from 1D studies (Rodi, 1980). To obtain satisfactory results the turbulent Prandtl number is Richardson number dependent according to Blanke and Delecluse (1993). This setup has been named the standard $k-\epsilon$ model.

To replace the controversial equation for dissipation the performance of a hierarchy of k-models have been tested and compared with the $k-\epsilon$ model.

Minor important for performance of the $k-\epsilon$ model but more consistent is the utilization of flux boundary conditions to include the effect of a turbulence enhanced layer due to breaking surface gravity waves (Craig and Banner, 1994) and the modification of the dissipation term in both turbulent equations as suggested by Mellor (2000) for the Mellor-Yamada turbulence scheme. Breaking of internal waves is parameterized resulting in additional deep water mixing. Two approaches for deep water mixing have been implemented within the $k-\epsilon$ model and have been tested successfully in multi-year simulations.

The conclusions of the report are summarized as followed:

- Local schemes like Richardson number dependent friction are not sufficient to parameterize mixing in 3D models of the Baltic Sea. Vertical diffusion of TKE needs to be taken into account.

- A k-model with appropriate chosen length scales is more or less equivalent to the standard $k-\epsilon$ model but is only slightly more efficient concerning computational costs than the $k-\epsilon$ model and tends to numerical instabilities. Although additional central memory is necessary for the prognostic variable ϵ, this can today not be considered as limitation because state-of-the-art circulation models are based on massively parallel computer codes developed for hundreds of processor elements with corresponding memory (Meier et al., 2000). The comparison of k- and $k-\epsilon$ models shows that the dissipation equation fulfills important length

scale limitations which are postulates of the here presented k-model of Willebrand (1994). In spite of the controversial discussion about physical soundness, the dissipation equation is regarded as pragmatic approach to calculate adequate turbulent length scales.

- Using flux boundary conditions together with the analytical solution from Craig and Banner (1994), a turbulence enhanced surface layer due to breaking of surface gravity waves is taken into account. The difference between the new flux boundary conditions and the traditional Dirichlet approach is relatively small except in strong gale and storm situations. Flux boundary conditions are preferable because they avoid an artificial sink of TKE at the surface.

- Mellor's modification to reduce dissipation in stratified fluids (Mellor, 2000) applied to the $k-\epsilon$ model improves simulated surface mixed layers. Mixed layer depths depend on the critical Richardson number which is regarded as tuning parameter. With appropriate chosen tuning parameter it is possible to overcome the generic problem of too shallow mixed layer depths completely. However, in that case salinity profiles are affected disadvantageously (erosion of the halocline). Hence, the tuning have to be done carefully.

- Theoretically improved stability functions according to Canuto et al. (2000) reduce performance of the $k-\epsilon$ model in the present Baltic Sea application. Mixed layer depths are underestimated.

- Two approaches for deep water mixing are presented. The first method adds an additional term to eddy viscosity and diffusivity (Stigebrandt, 1987), which is inversely proportional to the Brunt-Väisälä frequency, and the second method utilizes appropriate limits for TKE and dissipation. The differences between both approaches are small (but not zero) and can be neglected. Further investigations are necessary to address more sophisticated wind dependent parameterizations for deep water mixing.

- The present ice-ocean heat flux parameterization in RCO does not include the effect, that in case of melting a fresh molecular sub-surface layer develops reducing interfacial salinity, and needs to be improved consequently. However, sensitivity experiments point to minor importance of this effect in the northern Baltic Sea than in the Arctic Ocean where surface salinity is much higher. Further investigations are necessary using higher vertical resolution of $k-\epsilon$ under sea ice, more ice levels and different ice classes.

- In the literature most results with mixed layer models are obtained using 1D column models assuming horizontal homogeneity. The dynamics of current velocity

is reduced to Ekman physics. As the Baltic Sea is shallow and limited horizontally by coasts, the approach of horizontal homogeneity does not hold in general. In the prognostic equation for TKE in k- or $k-\epsilon$ models vertical shear is the most important source of TKE below the turbulence enhanced surface layer. This production term gives different results in 1D and 3D models. In addition, Ekman pumping/suction and re-stratification due to horizontal advection is missing in 1D simulations. Hence, for the performance of the mixing scheme the choice of the ocean circulation model (1D or 3D, horizontal grid resolution), in which the 1D turbulence model is embedded, is quite important and improvements of the $k-\epsilon$ model tested in 1D studies can not be adopted automatically to the $k-\epsilon$ model embedded in 3D Baltic Sea models.

- The use of local Richardson number dependent mixing compared to the $k-\epsilon$ model within RCO affects the climatological mean state of the Baltic Sea tremendously. Examples are shown for vertical profiles of temperature and salinity, SST, ice extent and heat fluxes between atmosphere and ocean.

- The performance of coarse resolution 3D Baltic Sea models, to simulate overflow of high-saline Kattegat water into the Baltic Sea, depends on the used mixing scheme.

To answer the question, why the 1D $k-\epsilon$ turbulence model is used within RCO, it should be mentioned that the implemented scheme fulfills the following requirements:

- better performance than other (tested) approaches compared to data,
- easy implementation in the massively parallel OCCAM code (more difficult if horizontal advection of k and ϵ is considered too),
- satisfactory computational performance on different computer platforms,
- numerically robust.

Acknowledgments

This work has been funded partly by the European Union within the projects BASYS (Baltic Sea System Study, grant MAS3-CT96-0058) and the concerted action CARTUM (Comparative Analysis and Rationalization of Second-Moment Turbulence Models, grant MAS3-CT98-0172) and partly by the SWECLIM program. The latter is financed by MISTRA (Foundation for Strategic Environmental Research) and by SMHI (Swedish Meteorological and Hydrological Institute, Norrköping/Sweden). The testing and running of RCO have been done on the CRAY-T3E at NSC (Swedish National Supercomputer Centre, Linköping/Sweden). Special thanks are given to Nils Kajrup for providing oceanographic profile data from the Swedish Ocean Archive SHARK (Svenskt HavsARKiv, SMHI) and to Anders Omstedt for support during a very early stage of this work between summer 1996 and autumn 1997 within the BASYS project. Very helpful comments on an earlier draft have been made by Helmut Baumert and Andreas Oschlies.

Appendix A: Bulk formulae in case of open water

Wind stress is parameterized according to Large and Pond (1981):

$$\vec{\tau} = c_{aw}^{d}\, \rho_a \left|\vec{U}_{10}\right| \vec{U}_{10} \tag{66}$$

with

$$c_{aw}^{d} \times 10^3 = \begin{cases} 1.2 & : \quad 0 < \left|\vec{U}_{10}\right| \leq 11\, m/s \\ 0.49 + 0.065 \left|\vec{U}_{10}\right| & : \quad 11 < \left|\vec{U}_{10}\right| \leq 22\, m/s \end{cases} \tag{67}$$

$\vec{U}_{10}$ denotes wind speed in $10\,m$ height and ρ_a air density.

The shortwave energy flux through the open water surface is

$$Q_{SW} = Q_{SW}^{0}\,(1 - \alpha_w) \tag{68}$$

with incoming solar radiation Q_{SW}^{0} and sea surface albedo α_w which is calculated from Fresnel's formula. According to Bodin (1979) Q_{SW}^{0} can be calculated from

$$Q_{SW}^{0} = T_u\, S_0\, \cos\theta\, (T_r - A_w)(1 - C_a\, F_a) \tag{69}$$

with the atmospherical turbidity $T_u = 0.95$, the solar constant $S_0 = 1.368{\cdot}10^3\, J\, m^{-2}\, s^{-1}$, the zenith angle θ and total cloudiness C_a. T_r and A_w are transmission and absorption functions and F_a is a cloud function:

$$T_r = 1.041 - 0.16\, \cos\theta^{-0.5} \tag{70}$$

$$F_a = 0.55 + 0.01\, \cos\theta^{-1} \tag{71}$$

$$A_w = 0.077\, m^{0.3}\, \cos\theta^{-0.3}, \tag{72}$$

with the optical path length m. The daily cycle is included in the model.

Sensible and latent heat fluxes are parameterized according to Large and Pond (1982). The sensible heat flux Q_S is given by

$$Q_S = \rho_a\, c_{pa}\, c_{aw}^{s} \left|\vec{U}_{10}\right| (T_a - T_w) \tag{73}$$

with specific heat capacity of air c_{pa}, air temperature in 2 m height T_a and water temperature of the first model layer T_w. The transfer coefficient c_{aw}^{s} (Stanton number) is given by

$$c_{aw}^{s} \times 10^3 = \begin{cases} 1.13 & : \quad (T_a - T_w) < 0 \quad \text{unstable} \\ 0.66 & : \quad (T_a - T_w) \geq 0 \quad \text{stable} \end{cases} \tag{74}$$

The latent heat flux Q_L is determined by

$$Q_L = L_{aw}\, E \tag{75}$$

with L_{aw} latent heat of vaporization. Evaporation E is calculated according to

$$E = \rho_a\, c_{aw}^{l} \left|\vec{U}_{10}\right| (q_a - q_w) \tag{76}$$

with q_a and q_w specific humidity in $2\,m$ height of the atmosphere and close to the water surface, respectively. $c^l_{aw} = 1.15$ is the corresponding transfer coefficient (Dalton number).

The longwave incoming ($Q_{LW\downarrow}$) and outgoing radiation ($Q_{LW\uparrow}$) are calculated according to Maykut and Church (1973) and from Stefan Boltzmann's law, respectively:

$$Q_{LW\downarrow} - Q_{LW\uparrow} = \sigma_s\, a_1\, (1 + a_2\, C_a^{2.75})\, T_a^4 - \sigma_s\, T_w^4 \tag{77}$$

with Stefan Boltzmann's constant σ_s and the empirical constants $a_1 = 0.7829$ and $a_2 = 0.2232$.

The total heat flux through the sea surface Q_a is then given by the sum

$$Q_a = Q_{SW} + Q_{LW\downarrow} - Q_{LW\uparrow} + Q_S + Q_L\,. \tag{78}$$

The salt flux S_F is given to

$$S_F = -(P - E)\, S \tag{79}$$

with precipitation P and salinity S of the uppermost ocean box.

Appendix B: Bulk formulae in case of sea ice

Wind stress to the ice is parameterized as in case of open water. The flux of momentum between sea ice of concentration A and the ocean is given by

$$\vec{\tau} = (1 - A)\,\vec{\tau}|_{noice} + A\,\rho_w\,c^d_{wi}\,|\vec{u}_i - \vec{u}_w|\,(\vec{u}_i - \vec{u}_w) \tag{80}$$

with the ice-ocean drag coefficient $c^d_{wi} = 3.5 \cdot 10^{-3}$, water density ρ_w, ice velocity $\vec{u}_i$ and current velocity $\vec{u}_w$.

The bulk formulae of Appendix A are used for the ice case as well with only minor changes:

In Eq.(68) ice or snow albedo $\alpha_{(i,s)}$ is used instead of sea surface albedo and in Eq.(69) the cloud cover correction of Laevastu (1960) is utilized. One fraction of the incoming solar radiation penetrates the ice heating the ocean (cf. Sahlberg, 1988):

$$Q^{ib}_{SW} = \begin{cases} Q^0_{SW}\,(1-\alpha_s)\,f_{sol}\,e^{-\kappa_s h_s - \kappa_i h_i} & \text{if } h_s > 10\ cm\,, \\ Q^0_{SW}\,(1-\alpha_s)\,f_{sol}\,e^{-\kappa_i h_i} & \text{if } 0 < h_s \leq 10\ cm\,, \\ Q^0_{SW}\,(1-\alpha_i)\,f_{sol}\,e^{-\kappa_i h_i} & \text{if } h_s = 0\,. \end{cases} \tag{81}$$

$\kappa_i = 1.5\,m^{-1}$ and $\kappa_s = 15\,m^{-1}$ are bulk extinction coefficients and $f_{sol} = 0.1$ a penetration factor. h_i and h_s are ice and snow thickness, respectively.

The latent heat flux over sea ice is calculated using latent heat of sublimation instead of vaporization. In all formulae the prognostic variable for ice or snow surface temperature is used instead of sea surface temperature.

The total atmosphere-ocean heat flux is given by

$$Q_a = Q_a|_{noice}(1 - A) + Q_{bottom}\,A\,. \tag{82}$$

Q_{bottom} is the heat flux between ice and ocean:

$$Q_{bottom} = \rho_w\,c_{pw}\,c^h_{wi}\,|\vec{u}_w - \vec{u}_i|\,(T_w - T_{fp}) \tag{83}$$

where c_{pw} is the specific heat of sea water and c^h_{wi} the bulk heat transfer coefficient. T_{fp} is the salinity (S) dependent, freezing point temperature according to Millero (1978)

$$T_{fp} = -0.0575\,S + 1.710523 \cdot 10^{-3}\,S^{3/2} - 2.154996 \cdot 10^{-4}\,S^2\,. \tag{84}$$

Omstedt and Wettlaufer (1992) suggested to use $c^h_{wi} = 2.8 \cdot 10^{-4}$ in order to get reasonable results. Velocity differences in Eq.(83) have to be limited to ensure minimal heat flux under fast ice (Haapala and Leppäranta, 1996): $\Delta u_{min} = 0.001\ ms^{-1}$.

During the freezing process brine is released into the ocean. The total atmosphere-ocean freshwater flux is summarized in:

$$S_F = S_F|_{noice}\,(1 - A) + \frac{V_{new}}{\Delta t_e}\,\frac{\rho_i}{\rho_w}\,S \tag{85}$$

with Δt_e timestep of the ice model, ρ_i sea ice density and V_{new} volume per unit area of new ice (see Meier et al., 1999).

References

Axell, L.B., On the variability of Baltic Sea deepwater mixing, *J. Geophys. Res.*, 103, 21667-21682, 1998.

Baumert, H., and H. Peters, Second-moment closures and length scales for weakly stratified turbulent shear flows, *J. Geophys. Res.*, accepted, 2000.

Beckmann, A., and R. Döscher, A method for improved representation of dense water spreading over topography in geopotential-coordinate models, *J. Phys. Oceanogr.*, 27, 581-591, 1997.

Bergström, S., and B. Carlsson, River runoff to the Baltic Sea: 1950-1990, *Ambio*, 23, 280-287, 1994.

Blackadar, A.K., The vertical distribution of wind and turbulent exchange in a neutral atmosphere, *J. Geophys. Res.*, 67, 3095-3102, 1962.

Blanke, B., and P. Delecluse, Variability of the Tropical Atlantic Ocean simulated by a general circulation model with two different mixed layer physics, *J. Phys. Oceanogr.*, 23, 1363-1388, 1993.

Bodin, S., A predictive numerical model of the atmospheric boundary layer based on the turbulent energy equation, *Report Meteorology and Climatology, SMHI, Norrköping, Sweden*, 13, 139 pp, 1979.

Bryan, K., A numerical method for the study of the circulation of the World Ocean, *J. Comput. Phys.*, 4, 347-376, 1969.

Bryan, K., and M.D. Cox, An approximate equation of state for numerical models of ocean circulation, *J. Phys. Oceanogr.*, 2, 510-514, 1972.

Burchard, H., and H. Baumert, On the performance of a mixed-layer model based on the $k-\epsilon$ turbulence closure. *J. Geophys. Res.*, 100, 8523-8540, 1995.

Burchard, H., and K. Bolding, The role of stability functions in eddy viscosity turbulence models, *J. Phys. Oceanogr.*, submitted, 2000.

Burchard, H., and O. Petersen, Models of turbulence in the marine environment - A comparative study of two-equation turbulence models, *J. Marine Systems*, 21, 29-53, 1999.

Burchard, H., O. Petersen, and T.P. Rippeth, Comparing the performance of the Mellor-Yamada and the $k-\epsilon$ two-equation turbulence models, *J. Geophys. Res.*, 103, 10543-10554, 1998.

Canuto, V.M., A. Howard, Y. Cheng, and M.S. Dubovikov, Ocean turbulence I: one-point closure model. Momentum and heat vertical diffusivities, *J. Phys. Oceanogr.*, submitted, 2000.

Charnock, H., Wind stress on a water surface, *Quart. J. Roy. Meteor. Soc.*, 81, 639-640, 1955.

Cox, M.D., A primitive equation 3-dimensional model of the ocean, *GFDL Ocean Group Tech. Rep.*, 1, GFDL, Princeton University, U.S.A., 1984.

Craig, P.D., Velocity profiles and surface roughness under breaking waves, *J. Geophys. Res.*, 101, 1265-1277, 1996.

Craig, P.D., and M.L. Banner, Modelling wave-enhanced turbulence in the ocean surface layer, *J. Phys. Oceanogr.*, 24, 2546-2559, 1994.

Dahlström, B., Determination of areal precipitation for the Baltic Sea, In: *Baltic Sea Environment Proceedings*, 16, 174 pp, 1986.

Deleersnijder, E., and P. Luyten, On the pratical advantages of the quasi-equilibrium version of the Mellor and Yamada level 2.5 turbulence closure applied to marine modelling, *Appl. Math. Modelling*, 18, 281-287, 1994.

Dengg, J., Mixed layer concept of KTMIX. Documentation, AOS Program, Princeton, 24 pp, 1995.

Dera, J., Marine Physics, Elsevier, Amsterdam, 516 pp, 1992.

Dickey, T.D., and G.L. Mellor, Decaying turbulence in neutral and stratified fluids, *J. Fluid Mech.*, 99, 13-31, 1980.

Ekman, M., and J. Mäkinen, Mean sea surface topography in the Baltic sea and its transition area to the North Sea: A geodetic solution and comparison with oceanographic models, *J. Geophys. Res.*, 101 (C5), 11993-11999, 1996.

Ezer, T., On the seasonal mixed-layer simulated by a basin-scale ocean model and the Mellor-Yamada turbulence scheme, personal communication, 2000.

Fennel, W., T. Seifert and B. Kayser, Rossby radii and phase speeds in the Baltic Sea, *Contin. Shelf Res.*, 11, 23-36, 1991.

Finnish Marine Research (anonymous), Ice winters 1976-1980 along the Finnish coast, *Finnish Marine Research*, 249, p.46, 1982.

Galperin, B., L.H. Kantha, S. Hassid, and A. Rosati, A quasi-equilibrium turbulent energy model for geophysical flows, *J. Atmos. Sci.*, 45, 55-62, 1988.

Gargett, A.E., Vertical eddy diffusivity in the ocean interior, *J. Mar. Res.*, 42, 359-393, 1984.

Gaspar, P., Modeling the seasonal cycle of the upper ocean, *J. Phys. Oceanogr.*, 18, 161-180, 1988.

Gaspar, P., Y. Grégoris and J.-M. Lefevre, A simple eddy kinetic energy model for simulations of the oceanic vertical mixing: Tests at station Papa and long-term upper ocean study site, *J. Geophys. Res.*, 95 (C9), 16179-16193, 1990.

Gill, A.E., Atmosphere-ocean dynamics, Academic Press, London, 662 pp, 1982.

Haapala, J., On the modelling of ice thickness redistribution, *J. Glaciology*, in press, 2000.

Haapala, J., and M. Leppäranta, Simulating the Baltic Sea ice season with a coupled ice-ocean model, *Tellus*, 48A, 622-643, 1996.

Hasse, L., Parameterization of the dissipation term in second order closure modelling of the planetary boundary layer under conditions of forced convection, *Beitr. Phys. Atmos.*, 51, 166-173, 1977.

Hasse, L., Turbulence closure in boundary-layer theory - An invitation to debate, *Boundary-Layer Meteorol.*, 65, 249-254, 1993.

Hibler, W. D., A dynamic thermodynamic sea ice model, *J. Phys. Oceanogr.*, 9, 817-846, 1979.

Hunke, E.C., and J. K. Dukowicz, An elastic-viscous-plastic model for sea ice dynamics, *J. Phys. Oceanogr.*, 27, 1849-1867, 1997.

Hunke, E.C., and Y. Zhang, A Comparison of Sea Ice Dynamics Models at High Resolution, *Monthly Weather Review*, 127, 396-408, 1999.

Jakobsen, F., The major inflow to the Baltic Sea during January 1993, *J. Mar. Systems*, 6, 227-240, 1995.

Jerlov, N.G., Optical oceanography, Elsevier, 194 pp, 1968.

Kalliosaari, S., and A. Seinä, Ice winters 1981-85 along the Finnish coast, *Finnish Marine Research*, 254, 1-63, 1987.

Karger, U., Küsteneinfluß auf mittlere Bodenwindgeschwindigkeiten über der Ostsee, Diplomarbeit, Inst. f. Meeresk., Kiel, Germany, 82 pp, 1995.

Kato, H., and O.M. Phillips, On the penetration of a turbulent layer into stratified fluid, *J. Fluid Mech.*, 37, 643-655, 1969.

Killworth, P.D., D. Stainforth, D.J. Webb and S.M. Paterson, The development of a free-surface Bryan-Cox-Semtner ocean model, *J. Phys. Oceanogr.*, 21, 1333-1348, 1991.

Kochergin, V.P., Three-dimensional prognostic models, In: *Three-Dimensional Coastal Ocean Models, Coastal Estuarine Sci.*, Vol. 4, edited by N.S. Heaps, AGU, Washington D.C., USA, 201-208, 1987.

Kolmogorov, A.N., The equation of turbulent motion in an incompressible fluid, *Izv. Akad. Nauk SSSR, Ser. Fiz.*, 6, 56-58, 1942.

Laevastu, T., Factors affecting the temperature of the surface layer of the sea, *Commentat. Phys. Math.*, 25, 8-134, 1960.

Large, W.G., and S. Pond, Open ocean momentum flux measurements in moderate to strong winds, *J. Phys. Oceanogr.*, 11, 324-336, 1981.

Large, W.G., and S. Pond, Sensible and latent heat flux measurements over the ocean, *J. Phys. Oceanogr.*, 12, 464-482, 1982.

Lehmann, A., Ein dreidimensionales baroklines wirbelauflösendes Modell der Ostsee, *Ber. Inst. f. Meeresk., Kiel, Germany*, 231, 104 pp, 1992.

Lehmann, A., A three-dimensional baroclinic eddy-resolving model of the Baltic Sea, *Tellus*, 47A, 1013-1031, 1995.

Lueck, R., and R. Reid, On the production and dissipation of mechanical energy in the ocean, *J. Geophys. Res.*, 89 (C3), 3439-3445, 1984.

Luyten, P.J., E. Deleersnijder, J. Ozeri, and K.G. Ruddick, Presentation of a family of turbulence closure models for stratified shallow water flows and preliminary application to the Rhine outflow region, *Contin. Shelf Res.*, 16, 101-130, 1996.

Ly, L.N., Numerical studies of the surface-wave effects on the upper turbulent layer in the ocean, *Tellus*, 42, 557-567, 1990.

Matthäus, W., H.-U. Lass and R. Tiesel, The major Baltic inflow in January 1993, *ICES Statutory Meeting, Dublin, Ireland, ICES C.M. 1993/C:51*, 1993.

Maykut, G.A., and P. Church, Radiation climate of Barrow, Alaska, 1962-1966, *J. Appl. Meteorol.*, 12, 620-628, 1973.

McPhee, M.G., G.A. Maykut, and J.H. Morison, Dynamics and thermodynamics of the ice/ocean system in the marginal ice zone of the Greenland Sea, *J. Geophys. Res.*, 92(C7), 7017-7031, 1987.

Meier, H.E.M., A regional model of the western Baltic Sea with open boundary conditions and data assimilation (in German), *Ber. Inst. f. Meereskunde, Kiel, Germany*, 284, 117 pp, 1996.

Meier, H.E.M., Embedding a $k - \epsilon$ turbulence model into a three-dimensional model of the western Baltic Sea, Manuscript presented at the 1^{st} BASYS annual science meeting, 29.09.-01.10.1997, Warnemünde/Germany, 13 pp, 1997.

Meier, H.E.M., First results of multi-year simulations using a 3D Baltic Sea model, *Reports Oceanography, SMHI, Norrköping, Sweden*, 27, 48 pp, 1999a.

Meier, H.E.M., The Baltic Sea as a lake, *SWECLIM Newsletter, SMHI, Norrköping, Sweden*, 6, 27-31, 1999b.

Meier, H.E.M., and W. Krauss, Data assimilation into a numerical model of the Baltic Sea using the adjoint method, In: *Proceedings of the* 19^{th} *Conference of the Baltic Oceanographers*, Sopot, Poland, 447-458, 1994.

Meier, H.E.M., and T. Faxén, Performance analysis of a multiprocessor coupled ice-ocean model for the Baltic Sea, submitted, 2000.

Meier, H.E.M., R. Döscher, and T. Faxén, A multiprocessor coupled ice-ocean model for the Baltic Sea, submitted, 2000.

Meier, H.E.M., R. Döscher, A.C. Coward, J. Nycander, and K. Döös, RCO - Rossby Centre regional Ocean climate model: model description (version 1.0) and first results from the hindcast period 1992/93, *Reports Oceanography, SMHI, Norrköping, Sweden*, 26, 102 pp, 1999.

Mellor, G.L., One-dimensional, ocean surface layer modeling, a problem and a solution, personal communication, 2000.

Mellor, G.L., and T. Yamada, A hierarchy of turbulence closure models for planetary boundary layers, *J. Atmos. Sci.*, 31, 1791-1806, 1974.

Mellor, G.L., and T. Yamada, Development of a turbulence closure model for geophysical fluid problems, *Rev. Geophys. Space Phys.*, 20, 851-875, 1982.

Mesinger, F., and A. Arakawa, Numerical methods used in atmospheric models, Vol. 1, *GARP Publications Series, WMO, Geneva*, 17, 64 pp, 1976.

Millero, F.J., Freezing point of sea water, Eigth report of the joint panel of oceanographic tables and standards, *UNESCO Technical Papers in marine science*, 28, UNESCO, Paris, France, 1978.

Millero, F.J., and K. Kremling, The densities of Baltic Sea waters, *Deep Sea Res.*, 23, 1129-1138, 1976.

Munk, W.H., and E.R. Anderson, Notes on a theory of the thermocline, *J. Mar. Res.*, 3, 276-295, 1948.

Niiler, P.P., and E.B. Kraus, One-dimensional models of the upper ocean. In: *Modeling and prediction of the upper layers of the ocean*, edited by E.B. Kraus, Pergamon, New York, USA, 143-172, 1977.

Omstedt, A., A coupled one-dimensional sea ice-ocean model applied to a semi-enclosed basin, *Tellus*, 42A, 568-582, 1990.

Omstedt, A., and L. Nyberg, A coupled ice-ocean model supporting winter navigation in the Baltic Sea. Part 2. Thermodynamics and meteorological coupling, *Reports Oceanography, SMHI, Norrköping, Sweden*, 21, 39 pp, 1995.

Omstedt, A., and L. Nyberg, Response of Baltic Sea ice to seasonal, interannual forcing and climate change, *Tellus*, 48 A, 644-662, 1996.

Omstedt, A., and A. Rutgersson, Closing the water and heat cycles of the Baltic Sea, *Meteorol. Z.*, 9, 57-64, 2000.

Omstedt, A., and J.S. Wettlaufer, Ice growth and oceanic heat flux, models and measurements, *J. Geophys. Res.*, 97, 9383-9390, 1992.

Omstedt, A., J. Sahlberg, and U. Svensson, Measured and numerically-simulated autumn cooling in the Bay of Bothnia, *Tellus*, 35A, 231-240, 1983.

Oschlies, A., and V. Garçon, An eddy-permitting coupled physical-biological model of the North Atlantic. Part I: Sensitivity to advection numerics and mixed layer physics, *Global Biogeochem. Cycles*, 13, 135 - 160, 1999.

Pacanowski, R.C., and S.G.H. Philander, Parameterization of vertical mixing in numerical models of tropical oceans, *J. Phys. Oceanogr.*, 11, 1443-1451, 1981.

Paulson, C.A., and J.J. Simpson, Irradiance measurements in the upper ocean, *J. Phys. Oceanogr.*, 7, 952-956, 1977.

Pohlmann, T., Predicting the thermocline in a circulation model of the North Sea. Part I: Model description, calibration and verification. *Cont. Shelf Res.*, 16, 131-146, 1996.

Pollard, R.T., and R.C. Millard, Comparison between observed and simulated wind-generated inertial oscillations, *Deep Sea Res.*, 17, 813-821, 1970.

Rodi, W., Turbulence models and their application in hydraulics - a state-of-the-art review, *Int. Assoc. for Hydraul. Res.*, Delft, Netherlands, 104 pp, 1980.

Sahlberg, J., Modelling of the thermal regime of a lake during winter season, *Cold Region Science and Technology*, 15, 151-159, 1988.

Saloranta, T.M., Modeling the evolution of snow, snow ice and ice in the Baltic Sea, *Tellus*, 52A, 93-108, 2000.

Schmidt, M., T. Seifert, H.U. Lass and W. Fennel, Patterns of salt propagation in the southwestern Baltic Sea, *Dt. Hydrogr. Z.*, 50, 345-364, 1998.

Schrum, C., F. Janssen and U. Hübner, Recent climate modelling in North Sea and Baltic Sea, Part A: Model description and validation, *Ber. Zentrum f. Meeres- u. Klimaforschung, Hamburg, Germany*, 37, 60 pp, 2000.

Seifert, T., and B. Kayser, A high resolution spherical grid topography of the Baltic Sea, *Meereswiss. Ber., Warnemünde*, 9, 73-88, 1995.

Seinä, A., and S. Kalliosaari, Ice winters 1986-1990 along the Finnish coast, *Finnish Marine Research*, 259, 3-61, 1991.

Seinä, A., and J. Peltola, Duration of the ice season and statistics of fast ice thickness along the Finnish coast 1961-1990, *Finnish Marine Research*, 258, 1991.

Seinä, A., H. Grönvall, S. Kalliosaari, and J. Vainio, Ice season 1991-1995 along the Finnish coast, *Meri, Report Series of the Finnish Institute of Marine Research*, 27, 3-76, 1996.

Semtner, A.J., A general circulation model for the World Ocean, *Tech. Rep., Department of Meteorology, University of California, Los Angeles*, 9, 99 pp, 1974.

Semtner, A.J., A model for the thermodynamic growth of sea ice in numerical investigations of climate, *J. Phys. Oceanogr.*, 6, 379-389, 1976.

Stacey, M.W., and S. Pond, On the Mellor-Yamada turbulence closure scheme: the surface boundary condition for q^2, *J. Phys. Oceanogr.*, 27, 2081-2086, 1997.

Stevens, D.P., On open boundary conditions for three dimensional primitive equation ocean circulation models, *Geophys. Astrophys. Fluid Dynamics*, 51, 103-133, 1990.

Stevens, D.P., The open boundary condition in the United Kingdom fine-resolution Antarctic model, *J. Phys. Oceanogr.*, 21, 1494-1499, 1991.

Stigebrandt, A., A model of the vertical circulation of the Baltic deep water, *J. Phys. Oceanogr.*, 17, 1772-1785, 1987.

Svensson, U., A mathematical model of the seasonal thermocline, *Rep. 1002, Dep. of Water Resour. Eng., Univ. of Lund, Lund, Sweden*, 187 pp, 1978.

UNESCO, Tenth report of the joint panel on oceanographic tables and standards, *UNESCO Technical Papers in Marine Sci.*, 36, UNESCO, Paris, France, 1981.

Webb, D.J., The vertical advection of momentum in Bryan-Cox-Semtner Ocean General Circulation models, *J. Phys. Oceanogr.*, 25, 3186-3195, 1995.

Webb, D.J., A.C. Coward, B.A. de Cuevas and C.S. Gwilliam, A multiprocessor ocean circulation model using message passing, *J. Atmos. Oceanic Technol.*, 14, 175-183, 1997.

Webb, D.J., B.A. de Cuevas and C.S. Richmond, Improved advection schemes for ocean models, *J. Atmos. Oceanic Technol.*, 15, 1171-1187, 1998.

Welander, P., Two-layer exchange in an estuary basin, with special reference to the Baltic Sea, *J. Phys. Oceanogr.*, 4, 542-556, 1974.

Wells, N.C., A coupled ocean-atmosphere experiment: The ocean response, *Quart. J. Roy. Meteor. Soc.*, 105, 355-370, 1979.

Wettlaufer, J.S., Heat flux at the ice-ocean interface, *J. Geophys. Res.*, 96 (C4), 7215-7236, 1991.

Willebrand, J., Theorie der Turbulenz, Manuscript of the turbulence lecture, summer term '94, University of Kiel, Kiel/Germany, 1994.

List of Figures

List of Tables

SMHIs publications

SMHI publishes six report series. Three of these, the R-series, are intended for international readers and are in most cases written in English. For the others the Swedish language is used.

Names of the Series	**Published since**
RMK (Report Meteorology och Climatology)	1974
RH (Report Hydrology)	1990
RO (Report Oceanography)	1986
METEOROLOGI	1985
HYDROLOGI	1985
OCEANOGRAFI	1985

Earlier issues published in RO

1 Lars Gidhagen, Lennart Funkquist and Ray Murthy (1986)
Calculations of horizontal exchange coefficients using Eulerian time series current meter data from the Baltic Sea.

2 Thomas Thompson (1986)
Ymer-80, satellites, arctic sea ice and weather.

3 Stig Carlberg et al (1986)
Program för miljökvalitetsövervakning - PMK.

4 Jan-Erik Lundqvist och Anders Omstedt (1987)
Isförhållandena i Sveriges södra och västra farvatten.

5 Stig Carlberg, Sven Engström, Stig Fonselius, Håkan Palmén, Eva-Gun Thelén, Lotta Fyrberg och Bengt Yhlen (1987)
Program för miljökvalitetsövervakning - PMK. Utsjöprogram under 1986.

6 Jorge C. Valderama (1987)
Results of a five year survey of the distribution of UREA in the Baltic sea.

7 Stig Carlberg, Sven Engström, Stig Fonselius, Håkan Palmén, Eva-Gun Thelén, Lotta Fyrberg, Bengt Yhlen och Danuta Zagradkin (1988).
Program för miljökvalitetsövervakning - PMK. Utsjöprogram under 1987.

8 Bertil Håkansson (1988)
Ice reconnaissance and forecasts in Storfjorden, Svalbard.

9 Stig Carlberg, Sven Engström, Stig Fonselius, Håkan Palmén, Eva-Gun Thelén, Lotta Fyrberg, Bengt Yhlen, Danuta Zagradkin, Bo Juhlin och Jan Szaron (1989)
Program för miljökvalitetsövervakning - PMK. Utsjöprogram under 1988.

10 L. Fransson, B. Håkansson, A. Omstedt och L. Stehn (1989)
Sea ice properties studied from the icebreaker Tor during BEPERS-88.

11 Stig Carlberg, Sven Engström, Stig Fonselius, Håkan Palmén, Lotta Fyrberg, Bengt Yhlen, Bo Juhlin och Jan Szaron (1990)
Program för miljökvalitetsövervakning - PMK. Utsjöprogram under 1989.

12 Anders Omstedt (1990)
Real-time modelling and forecasting of temperatures in the Baltic Sea.

13 Lars Andersson, Stig Carlberg, Elisabet Fogelqvist, Stig Fonselius, Håkan Palmén, Eva-Gun Thelén, Lotta Fyrberg, Bengt Yhlen och Danuta Zagradkin (1991)
Program för miljökvalitetsövervakning - PMK. Utsjöprogram under 1990.

14 Lars Andersson, Stig Carlberg, Lars Edler, Elisabet Fogelqvist, Stig Fonselius, Lotta Fyrberg, Marie Larsson, Håkan Palmén, Björn Sjöberg, Danuta Zagradkin, och Bengt Yhlen (1992)
Haven runt Sverige 1991. Rapport från SMHI, Oceanografiska Laboratoriet, inklusive PMK - utsjöprogrammet. (The conditions of the seas around Sweden. Report from the activities in 1991, including PMK - The National Swedish Programme for Monitoring of Environmental Quality Open Sea Programme.)

15 Ray Murthy, Bertil Håkansson and Pekka Alenius (ed.) (1993)
The Gulf of Bothnia Year-1991 - Physical transport experiments.

16 Lars Andersson, Lars Edler and Björn Sjöberg (1993)
The conditions of the seas around Sweden. Report from activities in 1992.

17 Anders Omstedt, Leif Nyberg and Matti Leppäranta (1994)
A coupled ice-ocean model supporting winter navigation in the Baltic Sea.
Part 1. Ice dynamics and water levels.

18 Lennart Funkquist (1993)
An operational Baltic Sea circulation model. Part 1. Barotropic version.

19 Eleonor Marmefelt (1994)
Currents in the Gulf of Bothnia. During the Field Year of 1991.

20 Lars Andersson, Björn Sjöberg and Mikaell Krysell (1994)
The conditions of the seas around Sweden. Report from the activities in 1993.

21 Anders Omstedt and Leif Nyberg (1995)
A coupled ice-ocean model supporting winter navigation in the Baltic Sea.
Part 2. Thermodynamics and meteorological coupling.

22 Lennart Funkquist and Eckhard Kleine (1995)
Application of the BSH model to Kattegat and Skagerrak.

23 Tarmo Köuts and Bertil Håkansson (1995)
Observations of water exchange, currents, sea levels and nutrients in the Gulf of Riga.

24 Urban Svensson (1998)
PROBE An Instruction Manual.

25 Maria Lundin (1999)
Time Series Analysis of SAR Sea Ice Backscatter Variability and its Dependence on Weather Conditions.

26 Markus Meier[1], Ralf Döscher[1], Andrew, C. Coward[2], Jonas Nycander[3] and Kristofer Döös[3] (1999). RCO – Rossby Centre regional Ocean climate model: model description (version 1.0) and first results from the hindcast period 1992/93.
[1] Rossby Centre, SMHI [2] James Rennell Division, Southampton Oceanography Centre, [3] Department of Meteorology, Stockholm University

27 H, E, Markus Meier (1999)
First results of multi-year simulations using a 3D Baltic Sea model.

Swedish Meteorological and Hydrological Institute
SE 601 76 Norrköping, Sweden.
Tel +46 11-495 80 00 · Fax +46 11-495 80 01

ISSN 0283-1112